MAIN GROUP SUPRAMOLECULAR COORDINATION CHEMISTRY: DESIGN STRATEGIES AND DYNAMIC ASSEMBLIES

by

MELANIE A. PITT

A DISSERTATION

Presented to the Department of Chemistry
and the Graduate School of the University of Oregon
in partial fulfillment of the requirements
for the degree of
Doctor of Philosophy

June 2009

University of Oregon Graduate School

Confirmation of Approval and Acceptance of Dissertation prepared by:

Melanie Pitt

Title:

"Main Group Supramolecular Coordination Chemistry: Design Strategies and Dynamic Assemblies"

This dissertation has been accepted and approved in partial fulfillment of the requirements for the Doctor of Philosophy degree in the Department of Chemistry by:

Kenneth Doxsee, Chairperson, Chemistry
Darren Johnson, Advisor, Chemistry
David Tyler, Member, Chemistry
Victoria DeRose, Member, Chemistry
Stephen Remington, Outside Member, Physics

and Richard Linton, Vice President for Research and Graduate Studies/Dean of the Graduate School for the University of Oregon.

June 13, 2009

Original approval signatures are on file with the Graduate School and the University of Oregon Libraries.

An Abstract of the Dissertation of

Melanie A. Pitt for the degree of Doctor of Philosophy
in the Department of Chemistry to be taken June 2009

Title: MAIN GROUP SUPRAMOLECULAR COORDINATION CHEMISTRY: DESIGN STRATEGIES AND DYNAMIC ASSEMBLIES

Approved: _____
Darren W. Johnson

Main group supramolecular chemistry is a rapidly expanding field that combines the tools of coordination chemistry with the unusual and frequently unexpected coordination preferences exhibited by the main group elements. Application of established supramolecular design principles to those elements provides access to novel structure types and the possibility of new functionality introduced by the rich chemistry of the main group.

Chapter I is a general review of the field of main group supramolecular chemistry, focusing in particular on the aspects of coordination chemistry and rational design strategies that have been thus far used to prepare polynuclear "metal"-ligand assemblies. Chapter II is a discussion of work toward supramolecular assemblies based on the coordination preferences of lead(II), in

particular focusing on the 2-mercaptoacetamide and arylthiolate functionalities to target four-coordinate and three-coordinate geometries, respectively. Several possible avenues for further pursuing this research are suggested, with designs for ligands that may provide a more fruitful approach to the coordination of lead(II). Chapter III deals with the preparation of $As_2\mathbf{L}_3$ assemblies based on flexible ligand scaffolds. These assemblies exhibit structural changes in response to temperature and solvent, which may provide some insight into the subtle shape requirements involved in supramolecular guest binding. Chapter IV continues this work with an examination of how ligand structure affects mechanical coupling of stereochemistry between metal centers when the chelate ring is completed by a secondary bonding interaction such as the As-π contact. Finally, Chapter V presents a crystallographic and synthetic study of the nature of the interaction between pnictogens and arene rings. This interaction is ubiquitous in the coordination chemistry performed in the Johnson laboratory; understanding the role these interactions play in determining the final structure of supramolecular assemblies is vital to the preparation of more complex structures. Chapter VI presents a set of conclusions and outlook for future work on lead(II) supramolecular assemblies and the dynamic assemblies prepared from flexible organic scaffolds.

This dissertation contains previously published and coauthored material.

CURRICULUM VITAE

NAME OF AUTHOR: Melanie A. Pitt

PLACE OF BIRTH: Indianapolis, Indiana

DATE OF BIRTH: April 1980

GRADUATE AND UNDERGRADUATE SCHOOLS ATTENDED:

University of Oregon, Eugene
Indiana University, Bloomington

DEGREES AWARDED:

Doctor of Philosophy, Chemistry, 2009, University of Oregon
Master of Science, Chemistry, 2005, University of Oregon
Bachelor of Science, Chemistry, 2003, Indiana University

AREAS OF SPECIAL INTEREST:

Main group coordination chemistry
Supramolecular chemistry

PROFESSIONAL EXPERIENCE:

Graduate Research Assistant, University of Oregon, 2003–2008
Graduate Teaching Fellow, University of Oregon, 2003–2007
Graduate Research Fellow, Pacific Northwest National Laboratory, 2004

GRANTS, AWARDS AND HONORS:

National Science Foundation IGERT Fellowship, 2004-2007
Pacific Northwest National Laboratory Doctoral Fellowship, 2004

PUBLICATIONS:

Pitt, Melanie A., Zakharov, Lev N., Thompson, Ward H., Vanka Kumar, Laird, Brian B., and Johnson, Darren W., "Multiple Weak Supramolecular Interactions Stabilize A Surprisingly "Twisted" $As_2\mathbf{L}_3$ Assembly," *Chemical Communications,* **2008**, 10.1039/b806958a.

Cangelosi, Virginia C., Fontenot, Sean F., Pitt, Melanie A., and Johnson, Darren W. "Host-Guest Interactions In A Series Of Self-Assembled $As_2\mathbf{L}_2Cl_2$ Macrocycles," *Journal of the Chemical Society, Dalton Transactions.* **2008**, 3447.

Pitt, Melanie A. and Johnson, Darren W. "Main Group Supramolecular Chemistry," *Chemical Society Reviews*, **2007**, *36*, 1441.

Johnson, Darren W., Pitt, Melanie A., and Harris, James M., "Adsorbent With Multiple Layers," US Patent Application 20070181502.

Carter, Timothy G., Rather-Healey, Elizabeth, Pitt, Melanie A. and Johnson, Darren W., "Secondary Bonding Interactions Observed In Two Arsenic Thiolate Complexes," *Inorganic Chemistry,* **2005**

ACKNOWLEDGMENTS

My sincere thanks go out to my advisor, Darren W. Johnson, for the past several years of interesting chemistry, insightful discussions, and barbecue-related debates. I also thank my committee chair, Professor Kenneth N. Doxsee, as well as my other committee members, Professors David R. Tyler, Victoria J. DeRose, and James R. Remington for insight and guidance. The funding and equipment provided by the University of Oregon is gratefully acknowledged, as is financial support from the National Science Foundation's IGERT fellowship.

The other members of the Johnson laboratory have provided me with what I can only describe as priceless. In addition to their scientific and intellectual contributions and despite the inevitable ups and downs that come with research, there is very real friendship and camaraderie in the group. There have been too many past and present members to thank each individually, but I must single out Tim Carter, Zack Mensinger, and Dr. Randall Hicks for their support and assistance at a particularly trying time in my life. It will not be forgotten.

Finally, I thank those on the outside: my friends, my family, especially my parents Jane and Randy Pitt, and the Wolfe family for welcoming me as one of their own. Especially Michelle. Most of all, however, I thank my wonderful partner Christopher Wolfe for more love, support, and friendship than any person could ever hope for.

For everyone who helped me on my way here.

TABLE OF CONTENTS

Chapter Page

I. INTRODUCTION: MAIN GROUP SUPRAMOLECULAR CHEMISTRY 1

Introduction 1

Scope of Review 2

Coordination Geometries of Main Group Elements 3

Group 12 – Zinc, Cadmium, and Mercury 5

Group 13 – Aluminum and Gallium 12

Group 14 – Germanium, Tin, and Lead 19

Group 15 – Arsenic, Antimony, and Bismuth 27

Groups 16 and 17 – Chalcogens and Halides 33

Host-Guest Chemistry of Supramolecular Main Group Complexes 35

Conclusions 40

II. LIGAND DESIGN FOR MAIN GROUP SUPRAMOLECULAR ASSEMBLIES 42

Health and Environmental Concerns Associated with the Main Group Elements 42

Supramolecular Design Principles and Application to Main Group Chemistry 44

Secondary Bonding Interactions 46

Ligand Design for Pb(II) and Hg(II) 47

Design and Synthesis of 2-Mercaptoacetamide Ligands 50

Chapter Page

Trigonal Pyramidal Coordination of Pb(II) 54

Future Directions for Research in Supramolecular Lead(II) Chemistry 60

Experimental Details 65

General Information 65

Synthesis of 2-Mercaptoacetamides and Derivatives 65

Synthesis of Thiophenolate Complexes of Pb(II) 69

Synthesis of Bifunctional Thiophenol Derivatives 70

Crystallographic Details 73

III. MULTIPLE WEAK SUPRAMOLECULAR INTERACTIONS STABILIZE SURPRISINGLY TWISTED $AS_2\mathbf{L}_3$ ASSEMBLIES: SOLID STATE DISTORTION AND TEMPERATURE SENSITIVE CONFORMATIONAL CHANGES IN SOLUTION 74

Introduction 74

Diphenylmethane in Supramolecular Chemistry 76

Synthesis of an $As_2\mathbf{L}_3$ Assembly Bridged by Diphenylmethane 79

DFT Calculations Support Distorted Structure 83

$As_2\mathbf{L}^2_3$ and Solution Stability 84

Conformational Equilibrium Based on Intramolecular CH•••π Interactions 85

Edge-to-Face Aromatic Interactions 87

Open-Closed Equilibrium Based on Edge-to-Face Interactions 90

Chapter Page

Summary and Conclusions....92

Experimental Details....94

General Information....94

Ligand Syntheses....94

Synthesis of $As_2\mathbf{L}_3$ Assemblies....96

Crystallographic Data....97

2-Dimensional NMR Spectra....98

Variable Temperature NMR Spectra....100

Thermodynamic Parameters....101

DFT Calculations....106

IV. ARSENIC-π INTERACTIONS INFLUENCE MECHANICAL COUPLING IN A SERIES OF SUPRAMOLECULAR ASSEMBLIES....110

Introduction: Mechanical Coupling in Supramolecular Chemistry....110

Stereochemical Descriptions of $As_2\mathbf{L}_3$ and Other Supramolecular Assemblies....113

Ligand Scaffolds and Effects on Helicity....116

Structural Effects of Pnictogen•••Arene Interactions....118

Conclusions: The Arene-CH_2SH Group as a Chelating Moiety....120

Experimental Details....121

General Information....121

Chapter Page

General Method for Synthesis of $As_2\mathbf{L}_3$ Assemblies 121

Crystallographic Data 122

V. DESIGN CONSIDERATIONS FOR THE GROUP 15 ELEMENTS: THE PNICTOGEN•••π INTERACTION AS A COMPLEMENTARY COMPONENT IN SUPRAMOLECULAR ASSEMBLY DESIGN 124

Introduction 124

Pnictogen•••Arene Interactions Observed in Mononuclear Complexes 125

Pnictogen•••Arene Interactions in a Supramolecular Context 127

Factors Contributing to Pnictogen•••Arene Interactions 129

Charge Transfer Model for the Pnictogen•••Arene Interaction 129

Structural Survey 130

Trends Observed in Pnictogen•••Arene Interactions 131

Are Interaction Distances and Angles Correlated? 136

How Does the Pnictogen•••π Interaction Influence Self-Assembly? 138

Effects of Competing π-Stacking Interactions 138

Macrobicyclic Effects and Steric Strain 140

Geometric Consequences of Chelate Ring Size 140

Conclusions 142

Experimental Details 144

Chapter Page

General Information 144

Ligand and Complex Syntheses 144

Crystal Structures Included in Survey 146

VI. CONCLUSIONS AND OUTLOOK FOR FUTURE WORK 147

Supramolecular Design for Lead(II) and Mercury(II) 147

Extended Supramolecular Assemblies of As(III) 148

Mechanical Coupling and Design Strategies for Higher-Order As_mL_n Assemblies 149

Proposed Design Requirements for Higher-Order As_mL_n Assemblies 150

Pnictogen•••π Interactions as Supramolecular Design Elements 150

APPENDIX: SPREADSHEET FOR THERMODYNAMIC PARAMETERS EXTRACTED FROM VARIABLE TEMPERATURE NMR DATA 152

REFERENCES 160

LIST OF FIGURES

Figure Page

1.1. Coordination geometries commonly observed in main group coordination complexes. 4

1.2 $Hg_2\mathbf{L}_2Cl_2$ macrocycle where **L** = adenine-*N*1 oxide. 8

1.3 Formation of an $Hg_2\mathbf{L}_2Cl_2$ macrocycle whose structure depends strongly on the geometry of an intramolecular hydrogen bond. 8

1.4 Expanded dinuclear Hg(II) macrocycle with diphenylfluorene-derived spacer 9

1.5 A planar, trinuclear Hg(II) macrocycle bridged by *ortho*-substituted perfluorophenyl ligands 11

1.6 Synthesis of mercuracarborands with and without halide templates. 11

1.7 $Al_4\mathbf{L}_4$ molecular square with tetrahedral aluminum(III) centers bridged by 2-hydroxybenzoxazole ligands 14

1.8 Aluminum-based helicate prepared from a hydroxypyridinone ligand 15

1.9 Guest-dependent formation of helix or tetrahedron from a bis-catecholamide ligand. 17

1.10 Phthalocyaninato ligand and its dinuclear Tl(I) complex 18

1.11 A bifunctional ligand containing catecholate and phosphine donors assembles with tin(IV) to form a C_{3h} symmetric heterometallic structure 21

1.12 A pyrazine carboxylate ligand forms a trinuclear macrocycle with tin(IV) 23

1.13 A pyridine dicarboxylate ligand assembles with organotin precursors to form a trinuclear macrocycle with a repeating capsular structure 24

1.14 A pyridine/pyrimidine $Pb_{16}\mathbf{L}_8$ grid assembly. 25

Figure Page

1.15 Unexpected structures formed with pentatopic and tritopic pyridine/pyrimidine ligands....26

1.16. Formation of $As_2\mathbf{L}_3$ mesocate and $As_2\mathbf{L}_2Cl_2$ macrocycles....29

1.17 Antimony atoms are interspersed with alternating Na(I) cations and coordinated THF molecules....32

1.18 Supramolecular triangle based on coordination of dicarboxylates to organotellurane centers....34

1.19 A molecular square based on coordination of biphenyl bridges to *cis*-square planar iodinium cations....35

1.20 Mechanism for guest exchange from $M_4\mathbf{L}_6$ host structures showing host distortion....37

1.21 Partial encapsulation of an amphilic guest molecule....38

1.22 Halide sandwich complexes of hexamethyl-[9]mercuracarborand-3....39

2.1 Examples of low coordination number Pb(II) complexes with oxygen and sulfur donors....50

2.2 2-Mercaptoacetamide ligands designed for Pb(II) coordination....52

2.3 Crystal structure of dibenzyl-2-mercaptoacetamide **4**....53

2.4 Example of incorrect assignment of lead(II) coordination sphere in the solid state....55

2.5 Infinite chain structure obtained from biphasic reaction of thiophenol and $Pb(OAc)_2$....57

2.6 Tris-pyrazyl Pb(II) complex model of ALAD active site....58

2.7 Proposed designs for the next-generation ligands for Pb(II)....61

Figure Page

2.8 Aryldithiolate ligand design with substituents to block thiolate bridging interactions....62

2.9 Diphenylmethane spaced 2-mercaptoacetamide ligand....63

3.1 Examples of supramolecular hosts containing diphenylmethane....78

3.2 Predicted three-dimensional structure of $As_2\mathbf{L}^2_3$ based on molecular mechanics (MM3) calculations. 80

3.3 Three-dimensional structure of $As_2\mathbf{L}^2_3$ 82

3.4 Overlays of DFT optimized geometry for $As_2\mathbf{L}^2_3$ mesocate with crystal structure and optimized helicate geometries.. 84

3.5 VT-NMR of $As_2\mathbf{L}^2_3$ in CD_2Cl_2 87

3.6 Examples of edge-to-face aromatic interactions....89

3.7 gHMBC of $As_2\mathbf{L}^2_3$ (CD_2Cl_2, 500 MHz, -20 °C)....98

3.8 gHMQC of $As_2\mathbf{L}^2_3$ (CD_2Cl_2, 500 MHz, -20 °C)....99

3.9 Variable temperature ^1H NMR of $As_2\mathbf{L}^2_3$ in $CDCl_3$ 100

3.10 Variable temperature ^1H NMR of $As_2\mathbf{L}^2_3$ in $CDCl_2CDCl_2$....100

3.11 Chemical shift of H3 in $As_2\mathbf{L}^2_3$ as a function of temperature in CD_2Cl_2....101

3.12 Observed and calculated chemical shifts for H3 of $As_2\mathbf{L}^2_3$ in $CDCl_3$ 102

3.13 Observed and calculated chemical shifts for H3 of $As_2\mathbf{L}^2_3$ in $CDCl_2CDCl_2$....103

4.1 The new dome of the German Reichstag building in Berlin displays a prominent pair of right-handed helices....111

4.2 Crystal structures of new $As_2\mathbf{L}_3$ assemblies shown as the ΔΔ isomer....118

Figure Page

5.1 Examples of structures from the CSD with particularly short pnictogen•••arene distances. 127

5.2 Examples of supramolecular assemblies featuring pnictogen•••arene interactions 128

5.3 A charge transfer model for the pnictogen•••arene interaction in supramolecular assemblies 130

5.4 Schematic for measurement of pnictogen•••arene interaction distances and interaction angles 131

5.5 Scatter plot of interaction distance/angle pairs. 137

5.6 Macrocyclic effects and pnictogen•••arene interactions. 139

5.7 Effect of increased "chelate" ring size on an *anti*-$As_2\mathbf{L}_2Cl_2$ macrocycle. 141

LIST OF TABLES

Table Page

3.1 Thermodynamic parameters for the closed-open equilibrium of $As_2\mathbf{L}^2_3$ in CD_2Cl_2, $CDCl_3$, and $CDCl_2CDCl_2$ based on the chemical shift change associated with H3 92

3.2 Observed chemical shift of H3 and derived values for P_c, $\hat{\delta}$, and K for $As_2\mathbf{L}^2_3$ in CD_2Cl_2. 104

3.3 Observed chemical shift of H3 and derived values for P_c, $\hat{\delta}$, and K for $As_2\mathbf{L}^2_3$ in $CDCl_3$. 104

3.4 Observed chemical shift of H3 and derived values for P_c, $\hat{\delta}$, and K for $As_2\mathbf{L}^2_3$ in $CDCl_2CDCl_2$. 105

3.5 Atomic coordinates for (Δ,Δ)-$As_2\mathbf{L}^2_3$ DFT geometry. 106

3.6 Atomic coordinates for (Δ,Λ)-$As_2\mathbf{L}^2_3$ DFT geometry 108

4.1 Stereochemical outcomes for $As_2\mathbf{L}_3$ assemblies 119

5.1 Mean interaction distances and angles for pnictogen•••π interactions 134

5.2 Arsenic-containing crystal structures included in structural survey 146

5.3 Antimony-containing crystal structures included in structural survey 146

5.4 Bismuth-containing crystal structures included in structural survey 146

LIST OF CHARTS

Chart Page

2.1 Frequency of coordination numbers found in Pb(II) complexes.....50

5.1 Mean pnictogen•••π distances observed in the CSD. 133

5.2 Mean angles for pnictogen•••π interactions observed in the CSD.....134

5.3 Angular preferences for pnictogen•••arene interactions as observed in the CSD 135

LIST OF SCHEMES

Scheme Page

2.1 Two methods for synthesis of 2-mercaptoacetamide ligands.....52

2.2 Synthesis of $Pb(SPh)_3$ salts.....56

2.3 Synthesis of aryldithiolate ligands.....59

3.1 Synthesis of $As_2\mathbf{L}^2_3$.....79

4.1 General self-assembly reaction forming $As_2\mathbf{L}_3$ helicates and mesocates from bis(mercaptomethyl)arene ligands and illustration of local stereochemistry of arsenic(III) centers.....114

CHAPTER I

MAIN GROUP SUPRAMOLECULAR CHEMISTRY

This chapter is a general survey of the field of main group supramolecular chemistry, with a focus on the structural diversity that can be attained when main group elements are incorporated into supramolecular designs. The material in this chapter has been published in *Chemical Society Reviews*[1,*] and written by myself with editorial input from D.W. Johnson.

Introduction

The field of supramolecular chemistry has produced numerous examples of chemically interesting and aesthetically pleasing self-assembled structures using metals as directing elements.[2-6] The self-assembly process that guides the formation of these thermodynamically stable architectures is thought to have many advantages over traditional stepwise synthesis in accessing large and ordered structures.[2] Most of these assemblies leverage the predictable and well-characterized coordination preferences of the transition metals — typically octahedral, square planar or tetrahedral. A growing area of interest, however, lies in

---

* Dedicated to Professor Kenneth N. Raymond on the occasion of his 65th birthday.

the exploration of main group metals as directing elements in order to access structure types previously unattainable through traditional means.[6] The main group elements possess unique coordination preferences and electronic properties observed rarely in the rest of the periodic table, presenting unique opportunities for the preparation of novel structures with new and interesting characteristics.[3-5] This tutorial review highlights examples of self-assembled supramolecular structures comprising main group elements with a focus on the unusual coordination geometries often observed in these assemblies.

Scope of Review

The main group elements are typically defined as the set of s and p block elements, plus zinc, cadmium, and mercury.[4] For the purposes of this review, we mainly consider the heavier p block elements, and we focus on supramolecular structures containing main group metal centers bearing unusual coordination geometries. Some notable examples of main group supramolecular complexes found in tetrahedral or octahedral coordination environments are also included. To limit the scope of this tutorial review, we highlight key representative examples of the complexes found from Groups 12-17. Complexes in Group 12 are particularly challenging to separate into "main group" versus transition metal-type complexes, as zinc tends to behave more as a transition metal in terms of reactivity and coordination and is often covered thoroughly in general supramolecular reviews.

Mercury, however, tends to display the unusual coordination geometries common to the main group elements and will be discussed in "Group 12 – Zinc, Cadmium, and Mercury." Finally, structures containing Group 1 and 2 elements are not covered, and the reader is referred to recent reviews.[7-9]

The types of structures reviewed include discrete, polynuclear complexes without bonds between the main group metal centers. We also exclude organometallic main group complexes and those in which the multiple main group elements are bridged by simple halogen or chalcogen ions to form dimers or larger complexes. This review focuses on discrete self-assembled metal-ligand complexes where the main group ion is a directing element for the self-assembly reaction. Throughout the review, we are careful to note where the properties and coordination geometries of the main group elements depart from those expressed by the transition metals. Given the unusual coordination preferences of the main group, we first classify these coordination spheres, followed by a more detailed discussion of the individual supramolecular structures.

Coordination Geometries of Main Group Elements

The set of coordination geometries most commonly observed with transition metal complexes is relatively small and limited compared with the main group metals. Ligand distributions far removed from the typical tetrahedral and octahedral arrangements are frequently observed in complexes containing elements

from Groups 13-15; these unusual structures are intimately linked with the unique electronic properties of these elements.[3] The heavier main group elements such as lead(II) and thallium(I) are stabilized in unexpectedly low oxidation states due to relativistic stabilization of s orbitals. The presence of this "inert pair" of electrons often results in some of the more unusual hemidirected coordination spheres observed in main group complexes.

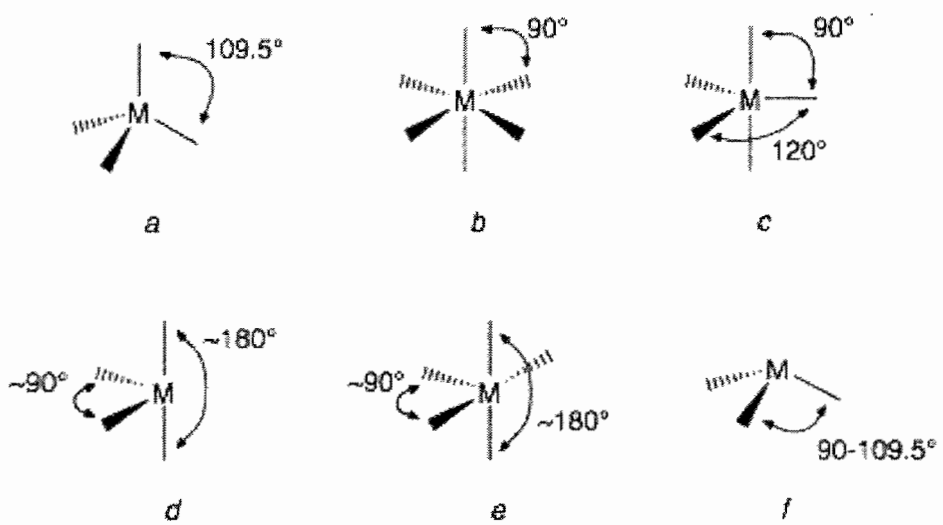

Figure 1.1. Coordination geometries commonly observed in main group coordination complexes. The bond angles shown correspond to the idealized coordination geometries. Depending on the nature of the bonding in each case, the precise angles may vary. This is quite pronounced in the trigonal pyramidal geometry *f*, where increasing p character in the bonding can reduce the bond angles to near 90°.

Tetrahedral and octahedral ligand distributions are frequently observed with the trivalent Group 13 elements, such as aluminum, gallium, and indium. A selection of the coordination geometries of particular relevance is illustrated in Figure 1.1, in which *a* and *b* indicate the more common tetrahedral and octahedral coordination spheres, respectively. Less common are the trigonal bipyramidal (*c*), disphenoidal (*d*), square pyramidal (*e*), and trigonal pyramidal (*f*) coordination geometries.

Coordination geometries common to the heavier p-block elements often exhibit stereoactive lone pairs, but these preferences are less predictable. Particularly common are trigonal pyramidal (observed often with the pnictogens), square pyramidal, and disphenoidal (observed frequently in Pb(II) complexes) coordination geometries about the metal center.

Group 12 – Zinc, Cadmium, and Mercury

The Group 12 elements are a somewhat special case when considering the chemistry of the main group elements. Zinc in particular resembles a transition metal in both reactivity and coordination preferences and has been used extensively in the preparation of supramolecular structures. The literature on this topic is certainly too broad to be considered here and has been discussed in many general supramolecular reviews.[10,11,2] Cadmium displays similar properties and coordination preferences to zinc, although it does possess a preference for softer Lewis base donors, similar to its softer main group brethren. In particular, trigonal

planar coordination of three cysteine thiolates is used to assemble tripeptide bundles about a Cd(II) center.[12]

Mercury(II)-containing supramolecular structures, however, tend to have much more in common with main group elements, in part because of their propensity to form structures with low-coordinate linear or other distorted coordination geometries. This fact has been used to direct the formation of a variety of macrocyclic structures, some of which exhibit novel guest binding properties.

Mercury(II) is not often included in the design of well-ordered, discrete supramolecular complexes. In the few examples of supramolecular mercury complexes, the Hg(II) ion typically adopts either two-coordinate, linear geometries or a distorted tetrahedral, nearly disphenoidal type of geometry. An example of the disphenoidal geometry occurs when mercury(II) is coordinated to adenine-N1-oxide in an $Hg_2\mathbf{L}_2$ macrocyclic structure (Figure 1.2).[13] While distorted from ideality, one can clearly observe the nearly linear (155°) arrangement of the Cl-Hg-Cl triad, as well as a much sharper angle (96.7°) between the oxygen and nitrogen donors.

An elegant example of mercury(II)-directed self-assembly combines both the lability of Hg-N bonds as well as the directional preferences of hydrogen bonds to influence the structure.[14] The twofold symmetric dipyridyl ligands shown in Figure 1.3 contain both a metal-coordination site and a pair of hydrogen bond donor/acceptors. The nature of the structure formed depends exquisitely on the

presence or absence of one methylene group between the pyridine and the amide linkage or between the central phenylene ring and the amide linkage – without these methylene groups, an $Hg_2\mathbf{L}_2\mathbf{X}_2$ (**X** = Cl, Br, I) macrocycle forms, while with the methylene groups, polymers and sheets form. In the structure lacking the methylene linkages, two intramolecular hydrogen bonds stabilize the macrocycle. Both tetrahydrofuran (THF) and dichloroethane (DCE) have been found in the cavity. The Hg(II) atoms in the structure are separated by 12.77 Å, while the distance between the aromatic rings of the two ligands measures approximately 7.68 Å when DCE is encapsulated. Another pyridine-containing Hg macrocycle has been prepared with a much larger ester-linked diphenylfluorene backbone and bridging two *meta*-substituted pyridine rings (Figure 1.4).[15] The cavity formed in this macrocycle is significantly larger than the previously described macrocycle; the Hg atoms are separated by 16.68 Å and the distance between the two central, quaternary carbon centers is 15.04 Å. The crystal structure of this macrocycle reveals several disordered water molecules in the cavity.

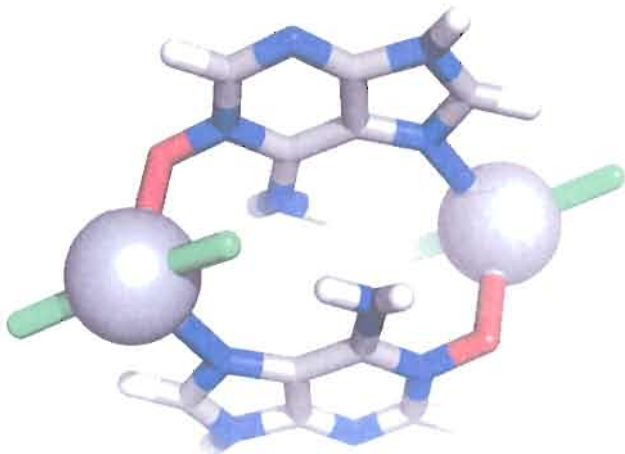

Figure 1.2. $Hg_2L_2Cl_2$ macrocycle where L = adenine-*N*1 oxide. Hg(II) atoms are separated by 7.43 Å. The Cl-Hg-Cl triad is nearly linear (155°), while the N-Hg-O triad lies at a sharper angle (96.7°). In most cases, spheres represent the main group element directing assembly formation. Unless otherwise noted, gray = carbon, white = hydrogen, blue = nitrogen, red = oxygen, and green = chlorine. Gray spheres = Hg(II).

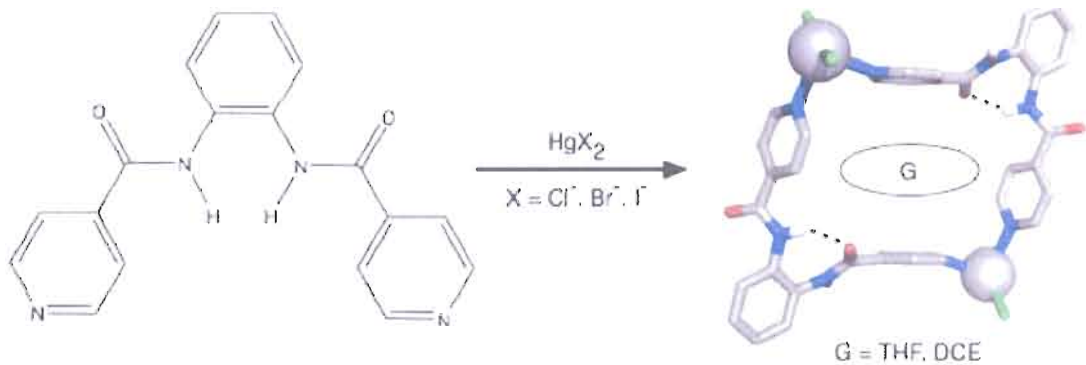

Figure 1.3. Formation of an $Hg_2L_2Cl_2$ macrocycle whose structure depends strongly on the geometry of an intramolecular hydrogen bond. The hydrogen bonds are represented as dashed lines. Hg(II) cations are separated by 12.77 Å, while the two pyridyl rings interacting with the guest are separated by 7.68 Å. The Cl-Hg-Cl triad is again nearly linear, while a more bent arrangement is observed for the N-Hg-N triad.

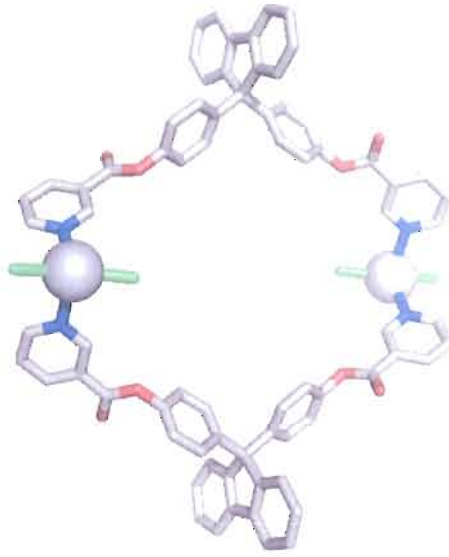

Figure 1.4. Expanded dinuclear Hg(II) macrocycle with diphenylfluorene-derived spacer. The larger fluorene based ligands provide a much larger cavity; disordered water molecules have been removed for clarity. The Hg(II) centers are separated by 16.68 Å, while the distance between the quaternary fluorene carbons is 15.04 Å.

The tendency of Hg(II) to form linear coordination complexes has been used to prepare a series of trinuclear macrocycles.[16] While these structures fall into the realm of organometallic chemistry by virtue of the Hg-carbon bonds that connect the components, these complexes are a striking example of main group elements as integral parts of a macromolecular assembly. In this case, the ligand is an ortho substituted tetrafluorophenyl ring, with Hg(II)-C bonds occupying these two ortho positions. The linearly coordinated Hg(II) ions form the edges of an equilateral

triangle capped by the *ortho* substituted ligands, with an average Hg•••Hg distance of 3.63 Å. The $Hg_3\mathbf{L}_3$ macrocycle has been successfully cocrystallized with a wide variety of organic compounds that generally do not penetrate the cavity of the macrocycle, but rather are complexed to the exterior of the macrocycles. A representative example of an $Hg_3\mathbf{L}_3$ structure is shown in Figure 1.5.

Icosahedral carboranes such as *closo*-1,2-$C_2B_{10}H_{12}$ (*ortho*) and *closo*-1,7-$C_2B_{10}H_{12}$ (*meta*) have also been used to great effect in the preparation of tri- and tetranuclear macrocycles of mercury(II), also referred to as mercuracarborands or "anti-crown" reagents (due to their anion binding properties).[17] The formation of tri- versus tetranuclear structures is dependent on the presence of an anion template – when halide salts of Hg(II) are employed, a planar, tetranuclear macrocycle ([12]mercuracarborand-4) is obtained. A variety of structures form based on the size of the halide template. For example, when $HgCl_2$ is the Hg(II) source, the chloride is coordinated to all four mercury atoms in a square-planar fashion inside the macrocycle. Bromide and iodide, however, are both too large to fit inside the macrocycle and are therefore coordinated to the Hg(II) ions out of the plane of the tetranuclear macrocycle. If Hg(II) salts such as acetate are used instead, the template effect is lost and a trinuclear macrocycle forms (Figure 1.6). These triangles exhibit a rich host-guest chemistry of their own, including the formation of

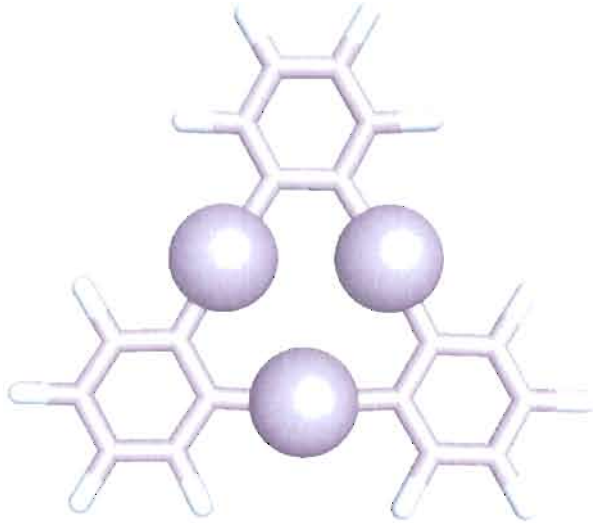

Figure 1.5. A planar, trinuclear Hg(II) macrocycle bridged by *ortho*-substituted perfluorophenyl ligands. The average Hg(II)•••Hg(II) distance is 3.63 Å and the Hg(II) centers form an equilateral triangle. Light blue = fluorine.

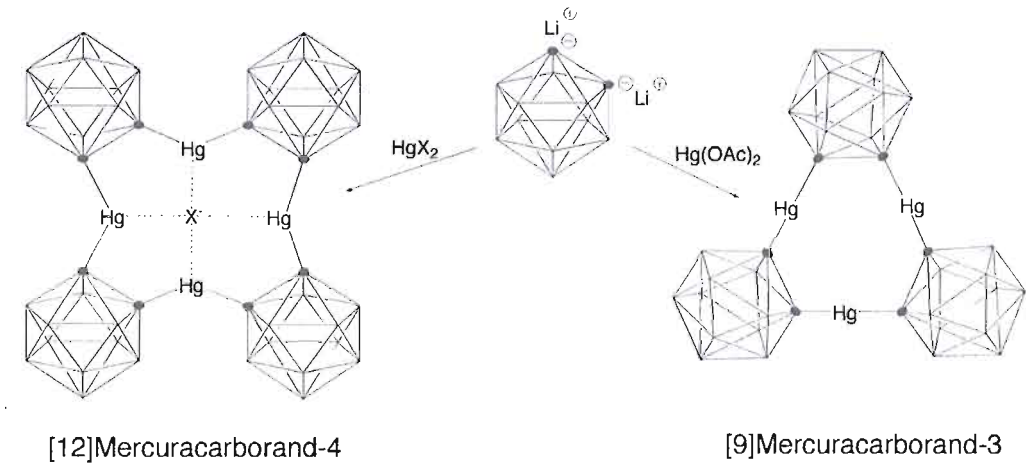

Figure 1.6. Synthesis of mercuracarborands with and without halide templates. A tetranuclear macrocycle (left, [12]-mercuracarborand-4) forms in the presence of a halide template. Without the template (right, [9]-mercuracarborand-3), a trinuclear macrocycle is formed. Vertices of polyhedra represent boron, while solid dots represent carbon. Hydrogens are omitted for clarity.

sandwich-type structures with both iodide and benzene in the solid state. (See "Host-Guest Chemistry of Supramolecular Main Group Complexes").

Hg(II) also forms a variety of supramolecular complexes with amino acid derived ligands. Cysteine, for example, assembles with Hg(II) to form an M_4L_4 supramolecular square where each terminal thiolate group bridges two metal cations.[18]

While Hg(II) often adopts the aforementioned linear coordination sphere, a trigonal tris-thiolato structure can be enforced by use of a de novo designed peptide sequence to assemble tripeptide bundles similar to those reported with Cd(II).[12]

Group 13 – Aluminum and Gallium

The Group 13 metals have recently emerged as important building blocks in the fabrication of self-assembled supramolecular structures. Aluminum, gallium, and indium are generally found as trivalent cations and consequently have a preference for harder donor ligands based on oxygen and nitrogen and tend to take on predictable tetrahedral and octahedral coordination geometries. Multibranched chelating ligands based on β-diketonates, catecholates, hydroxamates, and other such groups have been used to great effect in the rational synthesis of supramolecular structures.

An interesting example of an $Al_4\mathbf{L}_4$ square structure has been prepared from 2-hydroxybenzoxazole and trimethylaluminum, where each Al(III) loses one methyl group and is coordinated by two ligands.[19] The resulting tetrahedral aluminum center comprises each corner of the square, and it is bridged by coordination of a hydroxyl oxygen on one ligand and an oxazole nitrogen on a second ligand (Figure 1.7). Most supramolecular structures with a square topology such as this are formed from *cis*-square planar coordination to metal centers – in this case, the tetrahedral geometry around the corner units induces a bent structure analogous to cyclobutane.

A representative example of the many metallohelicates prepared from trivalent main group metals is shown in Figure 1.8. The bis(hydroxipyridinone) ligand shown on the left forms an $Al_2\mathbf{L}_3$ helicate as a racemic mixture of Δ,Δ and Λ,Λ isomers. This molecule encapsulates one guest water molecule in the center of its cavity in the crystalline state; in solution, the complex converts slowly from the chiral enantiomers to an achiral Δ,Λ *meso* structure. When this ligand is treated with Ga(lll), however, the Δ,Λ mesocate is observed in the crystalline state. In solution, the structure rapidly interconverts between the achiral and chiral forms as a result of a fast Bailar twist at the metal centers. This rather uncommon example of the same ligand driving the formation of two different isomers is thought to be caused by the relatively small size of Al(III) compared with Ga(III). The small Al(III)

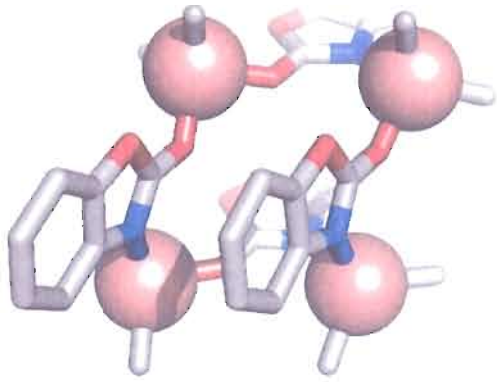

Figure 1.7. Al_4L_4 molecular square with tetrahedral aluminum(III) centers bridged by 2-hydroxybenzoxazole ligands. The unusual tetrahedral coordination mode observed in the tetranuclear square complex induces a distorted shape akin to that observed in cyclobutane. Light pink = Al(III).

center should make the trigonal prismatic intermediate in a Bailar twist much less stable as a result of interligand repulsions, and thus the *meso* and helical isomers interconvert slowly.[20]

Following the pioneering work of Saalfrank in preparing the first M_4L_6 coordination cluster,[21] many groups have presented spectacular examples of related tetrahedral assemblies. The use of gallium(III) has played a crucial role in this research, as it maintains a predictable octahedral coordination geometry with hard donor ligands (such as catecholates) and the complexes are diamagnetic, enabling study by NMR spectroscopy. In this case, it is clear that main group elements can serve as effective models to study supramolecular systems when transition metals

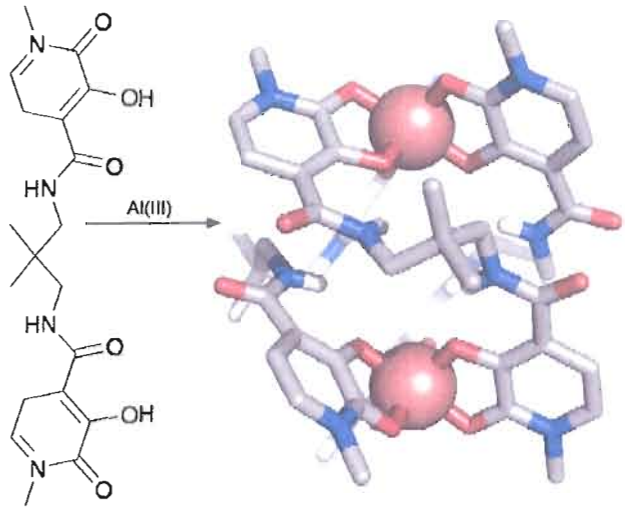

Figure 1.8. Aluminum-based helicate prepared from a hydroxypyridinone ligand. The hydroxypyridinone ligand (left) forms the homochiral $Al_2\mathbf{L}_3$ helicate (right). The Al(III) centers are separated by 7.13 Å. Upon encapsulation of a water molecule, the helicate converts to a heterochiral *meso*-helicate.

have properties (such as paramagnetism in iron catecholates) that are not conducive to the use of certain spectroscopic or characterization techniques.

Rather than survey the entire field of supramolecular gallium coordination clusters, the reader is directed to a thorough recent review on this topic.[22] A few representative examples based on catecholate and β-diketonate ligands are reviewed here. It should be noted that many structures analogous to those prepared with Ga(III) have also been observed using In(III) instead.

In particular, dicatecholamide ligands linked with an anthracene backbone are known to form either an $M_2\mathbf{L}_3$ helicate or an $M_4\mathbf{L}_6$ tetrahedron depending on the presence or absence of a suitable cationic guest (Figure 1.9). In this case, the use of the more labile Ga(III) cluster rather than a substitutionally-inert Ti(IV) analog was the key to allow study of this interconversion process on a reasonable timescale. Phenyl, naphthyl, and pyrenyl groups have also been used to great effect as ligand spacers in preparation of these tetrahedral structure types. A large series of coordination tetrahedra based on chelation of catecholamide donors to aluminum, gallium and other main group ions has also been recently reported by Raymond and coworkers.[23] These certainly fall under the purview of main group supramolecular chemistry; however, all the coordination modes in these structures are octahedral, so we defer discussion of these structures to "Host–Guest Chemistry of Supramolecular Main Group Complexes," where their rich host-guest chemistry is discussed in depth.

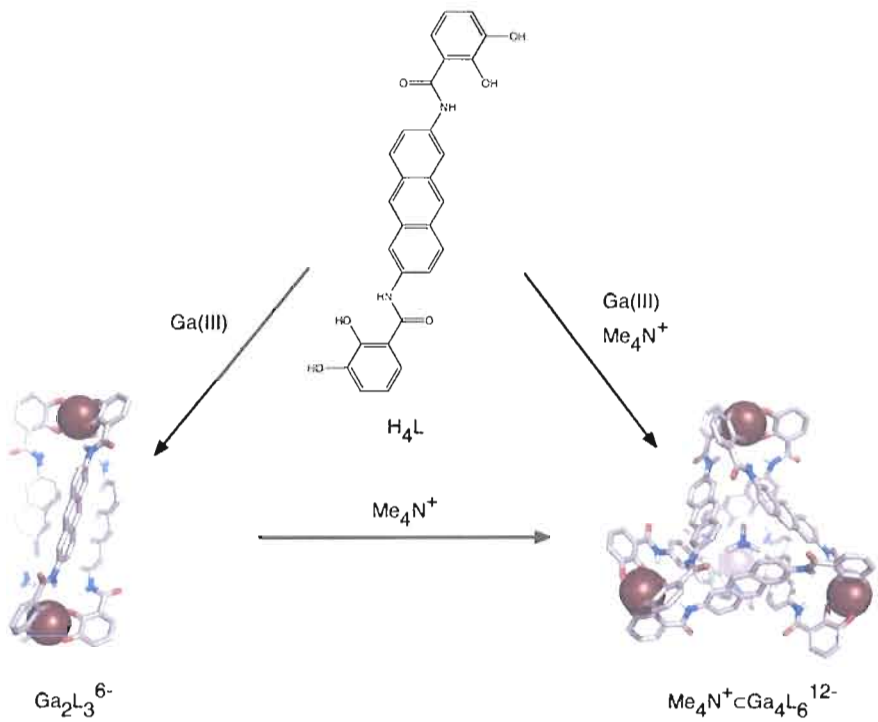

Figure 1.9. Guest-dependent formation of helix or tetrahedron from bis(catecholamide) ligand (H_4L). Addition of an appropriate guest (in this case, tetramethylammonium) to the helicate drives the assembly to a tetrahedral structure. Dark red = Ga(III).

Thallium diverges sharply from the other Group 13 elements in that it prefers a monovalent oxidation state and exhibits a much wider variety of coordination modes. Structural studies have indicated that many Tl(I) complexes display a stereochemically active lone pair which leads to hemidirected coordination geometries such as trigonal pyramidal. Tl(I) participates in a wide variety of secondary bonding interactions in the solid state, including at least one example of a Tl(I) •••Tl(I) interactions.

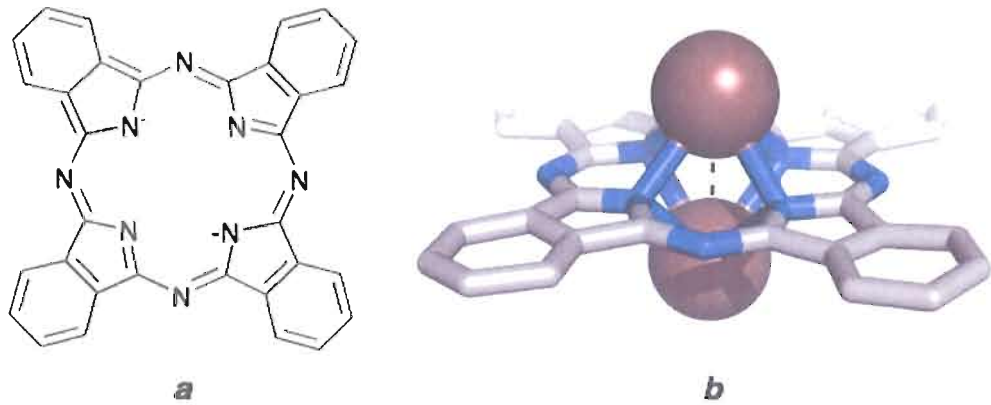

Figure 1.10. Phthalocyaninato ligand and its dinuclear Tl(I) complex. Each Tl(I) is coordinated to four nitrogen donors to the phthalocyaninato ligand (*a*) in a square pyramidal fashion; a weak Tl(I)•••Tl(I) interaction (dashed line) is observed in the complex (*b*) where the distance between the two metal centers is 3.69 Å. Red-brown = Tl(I).

A dinuclear complex containing two Tl(I) centers coordinated to a phthalocyaninato macrocycle contains several interesting features (Figure 1.10).[24,25] Each Tl(I) center is coordinated to four ring nitrogens and has a stereoactive lone pair, leading to a very uncommon square pyramidal coordination geometry. Furthermore, a weak Tl(I)•••Tl(I) interaction (dashed line) is observed through the center of the macrocycle, where the two Tl(I) centers are separated by 3.69 Å. This is slightly less than the sum of the van der Waals radii of two Tl atoms (3.92 Å). It is apparent from this and other structures that these weak interactions between main group ions may have important implications for the design and synthesis of main group supramolecular complexes. Their inclusion may allow for fine tuning of

desirable electronic and optical properties, and these interactions alone comprise a supramolecular interaction that can be exploited as a self-assembly motif.[26]

Group 14 – Germanium, Tin, and Lead

The heavier elements of Group 14 (Ge, Sn, and Pb) tend toward the formation of complexes where the central atom is in the (II) or (IV) oxidation state and bears a combination of O, N, and S-donor ligands. The coordination geometries found in these complexes tend to be variable and complex. While tetrahedral and octahedral complexes are certainly observed frequently, coordination numbers can range from two up to ten, and even twelve in rare cases.[27] A deeper understanding of the coordination chemistry of these elements is desirable, especially given their well-known toxic effects and health hazards. These elements also provide interesting opportunities for ligand design, due to the frequently observed stereochemically active lone pairs that cause hemidirected coordination geometries.

Germanium is generally found in coordination complexes as Ge(IV) and is known to coordinate strongly to hard oxygen donors such as catecholates. In contrast to the structures observed with chalcogen donors and metals such as Al(III), Ga(III), or In(III), Ge(IV) tends toward the formation of cage-type structures of the form $[Ge_4\mathbf{X}_{10}]^{4-}$ with **X** being a chalcogen donor such as sulfur or selenium.

$M_4\mathbf{L}_4$ and $M_4\mathbf{L}_6$ tetrahedral coordination assemblies analogous to those formed with Ga(III) (Figure 1.9) and Al(III) have been reported using Ge(IV) instead; these were prepared in order to elucidate the mechanism of guest exchange in the Group 13 assemblies, as Ge(IV) is much more inert to ligand substitution than its trivalent counterparts. $Ge_4\mathbf{L}_6$ was characterized by NMR and high-resolution mass spectral techniques rather than crystallographically due to the poor quality of crystals obtained. Had guest exchange occurred via a partial ligand dissociation mechanism, the rate of guest exchange should have slowed relative to the Ga(III) structure upon substitution of a tetravalent metal cation such as Ge(IV). As the rate of guest exchange was unaffected, the Ge(IV) structure helped to show that the exchange mechanism involved deformation of the host rather than by partial ligand dissociation.

Tin(IV) is also well known to form tris-chelate complexes with catecholate donors, leading to the design and synthesis of C_{3h} symmetric mesocates (achiral structures with both Δ and Λ centers) containing two tin ions bound to symmetry equivalent coordination sites and a second metal such as silver or palladium coordinated to the softer phosphine donors of the ligand (Figure 1.11). When the mesocate is prepared using silver(I), a Cs(I) guest appears to mediate the structure's formation – this guest is included in the cluster's cavity and is necessary for formation (the supramolecular structure does not form in its absence).[28] This

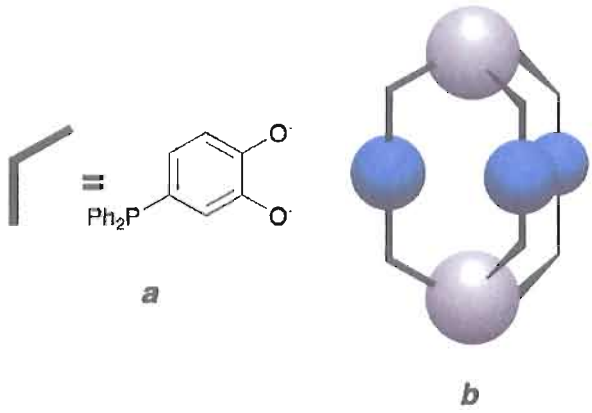

Figure 1.11. A bifunctional ligand containing catecholate and phosphine donors assembles with tin(IV) to form a C_{3h} symmetric heterometallic structure. The phosphine catecholate ligand (*a*) is represented as a heavy line. The assembly forms with either silver(I) or palladium(II) (*b*). Silver(I)/palladium(II) are represented as smaller blue spheres, while tin(IV) is shown as larger gray spheres.

approach takes into account the hard/soft coordination preferences of both metals and allows the formation of heterometallic supramolecular structures with great site specificity.

A variety of tin-containing macrocyclic triangles derived from organotin precursors have been reported using bifunctional bridging ligands. A more thorough review of these multinuclear organotin structures has been prepared by Haiduc.[26]

Pyrazine carboxylic acids have also been shown by Ma and coworkers to drive the self-assembly of a trinuclear Sn(IV) macrocycle (Figure 1.12).[3] These structures bear tin(IV) in a distorted octahedral geometry where the metal center is coordinated by a chelate ring containing both an oxygen and nitrogen on one ligand,

as well as a carboxylate oxygen on a second ligand. Each chelating portion of the ligand is oriented at a 60° angle to the chelating group of the next ligand, which supports the formation of an equilateral triangle. It is interesting to note that the **R** groups on the organotin precursor have a strong effect on the crystal packing of the triangle: when **R** is a methyl group, all the triangles exist in an extremely close-packed structure, whereas when **R** is the much bulkier di-*n*-butyl group, the triangles spread out and segregate into overlapping regions of alkyl and aromatic groups in the crystalline lattice.

Many other examples of tin-containing supramolecular triangles have been prepared; a few representative examples are discussed below. The contributions of Höpfl and coworkers illustrate the effects of solvent on the formation of larger tin-containing architectures,[29] especially in the formation of a spherical hydrogen-bonded capsule which forms an extended three-dimensional structure in the solid state. In this structure (Figure 1.13), a pyridine dicarboxylate ligand (*a*) assembles with organotin precursors to form a triangle (*b*), which then forms a repeating capsular structure in the solid state (*c*), where each triangular face is shared to form a large, porous structure sustained by the presence of 36 hydrogen bonds per repeating unit.

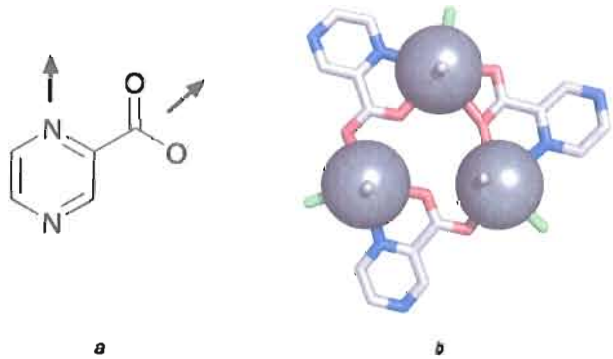

Figure 1.12. A pyrazine carboxylate ligand forms a trinuclear macrocycle with tin(IV). The pyrazine carboxylate ligand with chelate vectors oriented at 60° (*a*) assembles with an organic tin(IV) precursor (SnR_4) to form an equilateral triangle (*b*). Sn(IV) centers are separated by 5.35 Å. Dark gray = Sn(IV).

Lead(II) has appeared in several supramolecular assemblies, presumably a result of its reasonably predictable coordination preferences with certain types of ligand donors, especially those containing pyridyl nitrogens. The large size of the Pb(II) ion also provides opportunities for the synthesis of expanded structures with less steric strain than an analogous transition metal complex. Pb(II) is generally observed in distorted tetrahedral or octahedral coordination environments with a prominent stereochemically active lone pair.

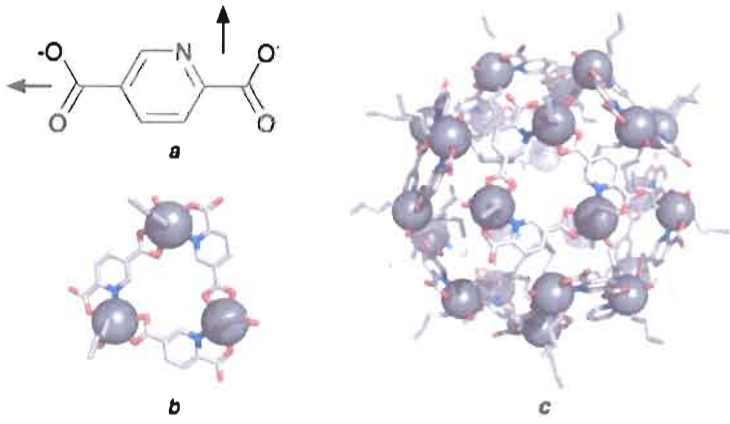

Figure 1.13. A pyridine dicarboxylate ligand assembles with organotin precursors to form a trinuclear macrocycle with a repeating capsular structure. The pyridine carboxylate ligand (*a*) assembles with organotin precursors to form a trinuclear macrocycle (*b*). The extended solid-state structure of this assembly forms a repeating capsular structure (*c*).

Lehn and coworkers have reported a series of grid-type architectures self-assembled from linear pyridine/pyrimidine ligands and Pb(II) ions. This strategy is well illustrated in a spectacular example of a self-assembled grid-type structure containing eight tetratopic, tridentate pyridine based ligands and sixteen Pb(II) ions, constituting a [4 x 4] grid, shown in top-down and side-on views in Figure 1.14.[30] The self-assembly of this twenty four component system containing 96 coordinate bonds overcomes enormous energetic barriers and effectively highlights the power of self-assembly in the fabrication of grid-type architectures. The structure also contains 16 closely coordinated triflate anions and 8 waters; there are a further 16 triflate anions and one additional water molecule located in secondary coordination with the structure. The ligands in the structure are bent such that the overall form

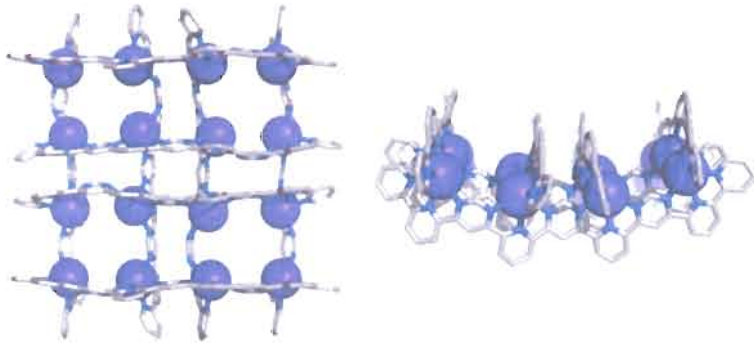

Figure 1.14. A pyridine/pyrimidine $Pb_{16}L_8$ grid assembly. Note the "saddle"-type structure. Triflate anions and coordinated water molecules have been removed for clarity. Left: top view, right: side view. π•••π stacking distance between ligands is 3.62 Å; average Pb(II)•••Pb(II) distance is ~6.5 Å. Dark purple = Pb(II).

is that of a saddle. The short (3.62 Å) π-stacking distances clearly contribute to the stability of this assembly. The lead(II) atoms are coordinated in a hemidirected fashion with between 7 and 9 donors depending on the number of anions associated with each.

Similar pyridine/pyrimidine ligands have induced the formation of [3 x 3] and [3 x 2] grids. Attempts to prepare even larger grids from ligands containing five chelating sites on each ligand led to the surprising formation of a dinuclear helix, with one ligand wrapped around two Pb(II) centers separated by 3.94 Å. In the absence of Pb(II), the ligand was observed to exist in an extended, linear conformation – the helix was observed only when Pb(II) was coordinated, shown in Figure 1.15. The specific folding and unfolding of an organic precursor in the

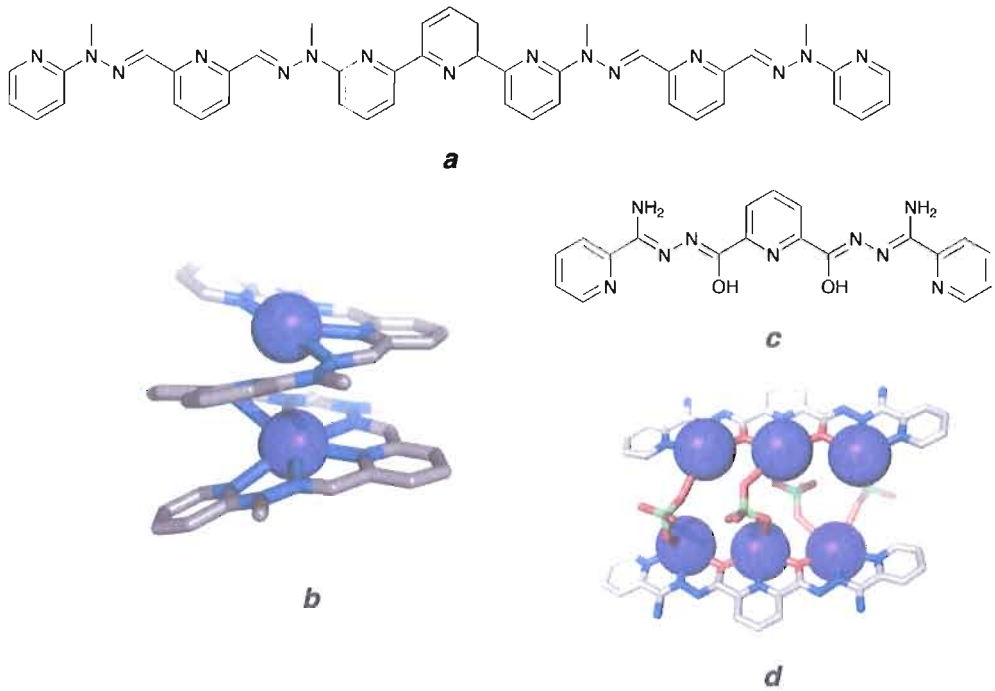

Figure 1.15. Unexpected structures formed with pentatopic and tritopic pyridine/pyrimidine ligands. A pentatopic pyridine/pyrimidine ligand (*a*) yielded the dinuclear Pb_2**L** helix (*b*). The tritopic ligand (*c*) yields two strands of Pb_3**L** bridged by four perchlorate anions (*d*).

presence of a metal template could have promising implications for the design of functional materials that mimic biological systems.[30]

An alternate approach to preparing supramolecular structures containing Pb(II) has focused on using ligands which bear a negative charge to balance the divalent lead(II) cation, reducing the presence of coordinating counterions. While the use of alkoxydiazine groups on the chelating site did not lead to the expected formation of a [3 x 3] grid structure, a rather fascinating hexanuclear lead(II)

structure formed where three lead ions were found coordinated to each of two ligand strands. (Figure 1.15, *c* and *d*.) The grids were then linked in the solid state by bridging perchlorate anions.[31]

Group 15 – Arsenic, Antimony, and Bismuth

The heavier members of Group 15, also known as the pnictogens, are particularly interesting as design elements for supramolecular main group chemistry, owing to a rare preference for a tripodal trigonal pyramidal coordination geometry found infrequently in transition metal complexes. This coordination mode is particularly attractive as a design element, as the coordination vectors involved produce the vertex of a convex polyhedron. This convergent arrangement of ligands in these complexes should favor formation of discrete species without the requirement for blocking ligands often used in other supramolecular design strategies. When observed in their preferred coordination sphere, an additional stereochemically active lone pair of electrons is available: the pnictogens are well known to act as both Lewis acids and bases. In particular, the Lewis acidity of these elements increases markedly as one moves down the group: Bi(III) predominantly behaves as a Lewis acid (due to the lone pair primarily inhabiting a low energy s-orbital), while nitrogen behaves primarily as a Lewis base. This fact may contribute to the possibility for further reactivity of the pnictogen after being incorporated into a supramolecular structure. Finally, these elements are frequently involved in a

variety of the weak secondary interactions that form the basis of supramolecular chemistry.[32] As the field of supramolecular pnictogen chemistry is extremely broad, we present several representative examples of the many complex types known in the literature, with relevant reviews noted as appropriate.

The tripodal coordination mode found in many arsenic-thiolate complexes has led to the facile synthesis of both $As_2\mathbf{L}_3$ triple mesocates[33] and a pair of $As_2\mathbf{L}_2Cl_2$ macrocycles[34] from 1,4-bis(mercaptomethyl)benzene and As(III) (Figure 1.16). These structures are stabilized by interactions between the arsenic lone pair and the π system of the central aromatic ring and are in fact so robust that extended heating under ambient atmosphere in the presence of competing metal ions, trifluoromethanesulfonic acid, and *p*-toluenesulfonic acid fail to cause dissociation of the assembly. Despite the remarkably robust nature of the assembly, proton NMR experiments indicate the rapid interconversion of the two macrocycles in solution. Analogous $Sb_2\mathbf{L}_3$ and an $Sb_2\mathbf{L}_2Cl_2$ macrocycle have also been reported using the same ligand.[35]

Tartrate salts are well known to form a variety of interesting structures with both As(III) and Sb(III). A dinuclear, double stranded macrocycle forms with As(III) coordinated by two hydroxylate and two carboxylate groups from each ligand, leading to a disphenoidal 4-coordinate geometry around the arsenic center, with the stereoactive lone pair maintained.[36] As tartaric acid bears two chiral carbon centers

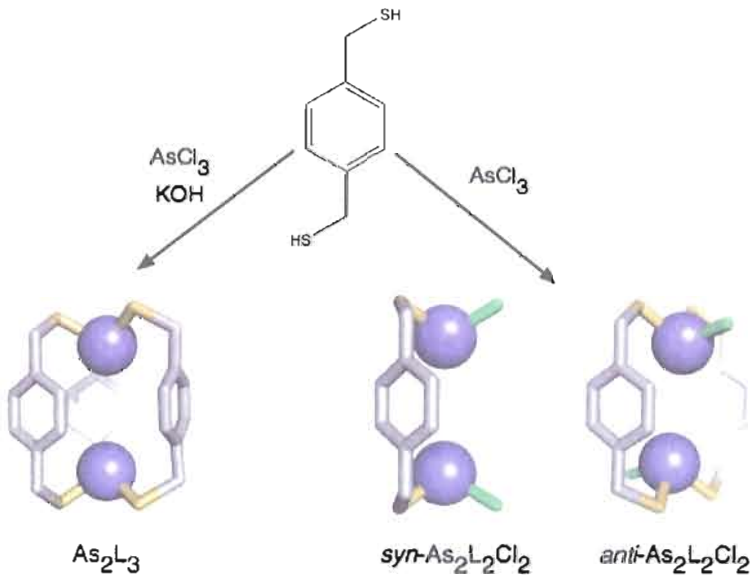

Figure 1.16. Formation of As_2L_3 mesocate and $As_2L_2Cl_2$ macrocycles. 1,4-bis(mercaptomethyl)benzene leads to the formation of either an M_2L_3 mesocate in the presence of base or a mixture of *syn* and *anti* $As_2L_2Cl_2$ macrocycles in the absence of base. Yellow = sulfur and light purple = As(III).

(*R,R*, *S,S*, and *R,S* are possible), any metal complexes arising from this ligand will have several possibilities for their overall stereochemistry. Steric arguments have been used to explain the much greater stability of assemblies containing enantiomerically pure tartrate ligands – the physical interactions between As(III) centers by way of the bridging ligand causes the chirality at one metal center to depend strongly on the other.

Antimony tartrate salts are also quite well known. Potassium antimony(III) tartrate has a long history as a pharmaceutical and is in fact one of the few

supramolecular complexes in widespread medical use,[37] mainly in the treatment of parasites such as schistosomiasis. Interestingly, this complex was long believed to exist as a monomer until modern X-ray crystallography techniques revealed that this species is a self-assembled dinuclear macrocycle. As was observed with As(III), the Sb(III) centers are coordinated to two hydroxylate and two carboxylate oxygen donors, leading again to a disphenoidal coordination sphere. Furthermore, these Sb(III) tartrate complexes are only known to form from (*R*,*R*) or (*S*,*S*) combinations; a mixed macrocycle containing both tartrate enantiomers does not form. *Meso*-tartrate complexes containing the (*R*,*S*) isomer of tartrate are also unknown. Even more interestingly, when Sb(III) and As(III) are combined and added to the tartrate salt, mixed macrocycles containing one of each metal center form, which reinforces the idea that these macrocycles form through genuine self-assembly processes and concomitant rearrangement of weak metal-ligand bonds.[38]

The pnictogens are also known to assemble with a variety of organic and inorganic components to form cyclic oligomers. One example (Figure 1.17) involves the formation of an Sb_6Na_6 alternating ring, supported by the presence of 3-methylcatecholate and coordinated THF molecules.[39] As(III) and Sb(III) complexes also both can assemble with Group 13 elements such as Ga to form cyclic oligomers.[40,41] Alternating structures of these types may lead to use as interesting precursors for the preparation of semiconductor materials. The ring-like structures

are often prepared through reactions that include salt or alkane elimination, as well as dehalosilylation reactions.

As Bi(III) compounds are often challenging to handle due to undesirable properties such as the ease of formation of insoluble oxide salts, its supramolecular chemistry is not nearly as well-developed as is that of As(III) and Sb(III). However, due to its unique position in the periodic table as the heaviest nonradioactive element, it has some important differences in coordination and reactivity from the rest of the Group 15 elements. A large atomic radius and the availability of expanded orbitals leads to a more variable coordination sphere; coordination numbers as high as 9 and 10 have been observed. Because of this fact, for example, tartrate complexes of Bi(III) (used in medicine to treat syphilis) tend to form polymeric structures with coordination number five (instead of four as observed with the lighter pnictogens) in order to satisfy its greater coordination demands.

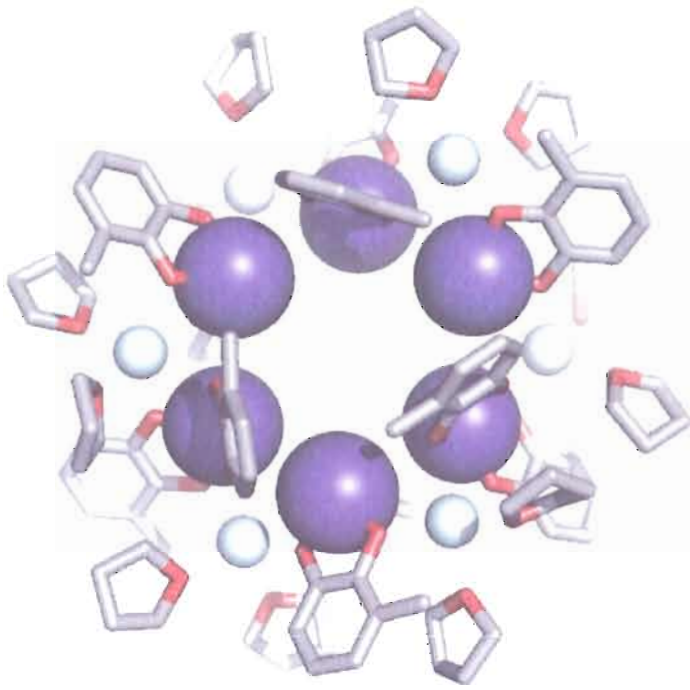

Figure 1.17. Antimony atoms are interspersed with alternating Na(I) cations and coordinated THF molecules. Sb(III) is shown as larger purple spheres, while Na(I) is shown as smaller light blue spheres.

A few notable examples that illustrate the intriguing coordination chemistry of Bi(III) are discussed here. Thiosalicylic acid and Bi(III) form an octanuclear complex where a ring of six Bi(III) centers are supported by coordination to six oxygens and one sulfur atom, while two additional bismuth atoms lie above and below the ring's center and are bound by three sulfur and three oxygen atoms. The "empty spaces" of the coordination spheres on the two Bi(III) atoms point into the cavity formed by the ring, possibly forming a secondary Bi•••Bi interaction.[42]

Finally, it has been shown that the high coordination number preferences of Bi(III) can be sidestepped by the use of a multidentate capping ligand that leaves only a few coordination sites available for the coordination of bridging ligands. This approach has been used to prepare a dinuclear Bi(III) macrocycle – triazacyclononanes are used to cap the Bi(III) centers through their nitrogen groups, while the carboxylate group bridges to the second Bi(III) center.[43]

Group 16 and 17 – Chalcogens and Halides

In general, elements of Group 16 and 17 have not found widespread use as building blocks for supramolecular architectures. The heavier chalcogens in Group 16 such as selenium and tellurium do provide some notable exceptions. These elements are commonly found in the (II) or (IV) oxidation states and their secondary interactions with the halogens have been well-documented in model systems.[44] Tellurium(IV) has also been shown to form a trinuclear $Te_3\mathbf{L}_3$ macrocycle (**L** = 1,2-benzenedicarboxylate) with two *p*-tolyl supporting ligands (Figure 1.18).[45] The Te(IV) cations are arranged in an equilateral triangular fashion with an average Te(IV)•••Te(IV) distance of 6.30 Å. The coordination geometry around each Te(IV) center is slightly distorted from an ideal disphenoidal structure: the O-Te-O bond angle averages 168.3°, while the C-Te-C angle averages 98.5°. While this structure may be categorized as organometallic due to the presence of Te-C bonds, the assembly of the dicarboxylate ligands supports the macrocyclic structure itself.

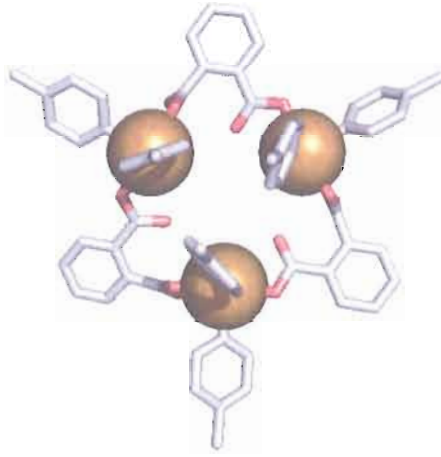

Figure 1.18. Supramolecular triangle based on coordination of dicarboxylates to organotellurane centers. The average distance between Te(IV) centers is 6.30 Å. Orange = Te(IV).

In a particularly elegant example of synthetic fabrication, Stang and co-workers prepared a molecular square $[I_4\mathbf{L}_4]^{4+}$ containing iodinium cations in a *cis*-square-planar arrangement and a linear biphenyl group as the organic linker.[46] As direct crystallographic observation was not possible with this assembly, based on ESI-MS and NMR data, an energy-minimized model was prepared (Figure 1.19).

While this molecular square should perhaps not be considered a true supramolecular or self-assembled structure due to the stepwise nature of its synthesis, it is nonetheless an excellent and illustrative example of a main group element being used to direct the formation of a nanoscale structure.

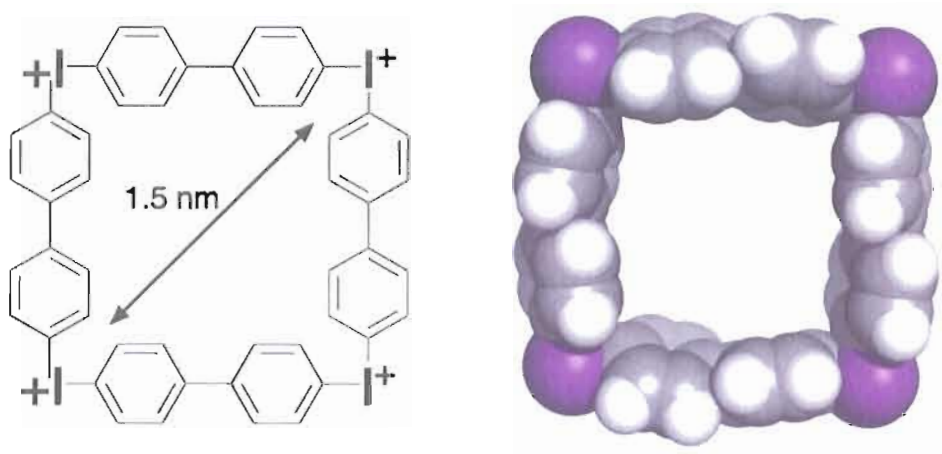

Figure 1.19. A molecular square based on coordination of biphenyl bridges to *cis*-square planar iodinium cations. A schematic view is shown on the left; a space filling molecular model is on the right. The diagonal distance across the square is approximately 1.5 nm. Purple = iodine.

It is clear from the few examples of Group 16 and 17 supramolecular structures that these elements provide interesting motifs for the construction of supramolecular assemblies; the unique manner in which these elements can bind to organic groups will likely expand the variety of structures containing main group elements in the future.

Host-Guest Chemistry of Supramolecular Main Group Complexes

As research in main group supramolecular chemistry is less developed than in transition metal-based supramolecular chemistry, likewise the host-guest chemistry of the main group congeners is less explored as well. Many of the

structures described have host cavities of insufficient size or inappropriate shape to contain common guest molecules. Additionally, the electronic properties of main group elements often vary substantially from those of the transition metals, which may affect the nature of the host structure's cavity in a manner precluding the entry of a guest molecule. A notable example is the $As_2\mathbf{L}_3$ structure described in "Group 15 – Arsenic, Antimony, and Bismuth": all efforts to bind small guests or metal ions (even protons) in the cluster cavity have failed. Without a more spacious cavity, this assembly appears to be devoid of host-guest chemistry.

In contrast, both the $Ga_4\mathbf{L}_6$ tetrahedra[23] prepared by Raymond and coworkers and the mercuracarborands prepared by Hawthorne[17] have exhibited a wide variety of rich host-guest chemistry which has led to a greater understanding of the solution phase behavior of supramolecular assemblies. A combination of NMR studies and computer calculations of tetrahedra containing a variety of metal centers has revealed the mechanism for guest exchange in these structures. Guests escape the cavity through a deformation of the host structure which permits guests to enter and exit through existing apertures, rather than via partial dissociation of one or more ligands from one of the metal center vertices (Figure 1.20). For example, guest exchange rates were comparable when the tetrahedra were assembled from Ge(IV) or Ga(III).

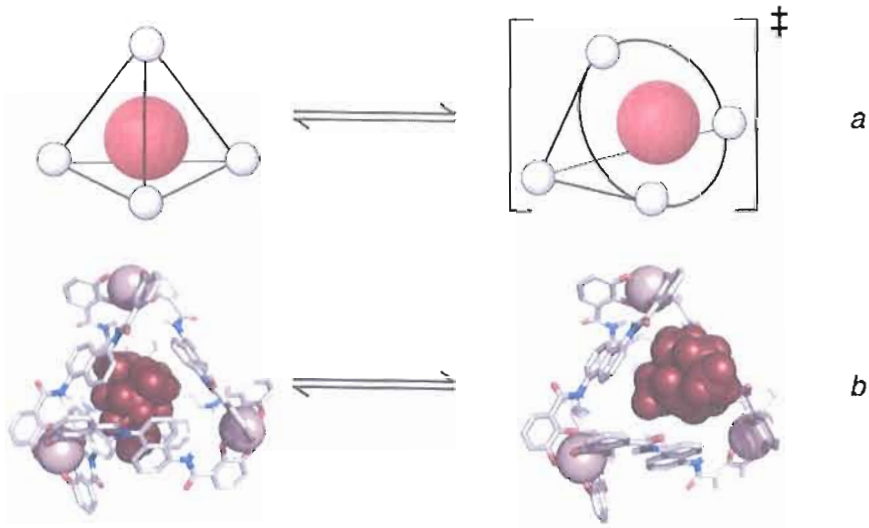

Figure 1.20. Mechanism for guest exchange from M_4L_6 host structures showing host distortion. (*a*) Cartoon representation. (*b*) Molecular model representation. The host is shown as a stick representation, while the guest is shown as a dark red space filling model.

Ge(IV) is more inert to ligand substitution than Ga(III); therefore, it could be inferred that partial ligand dissociation was not a significant factor in guest exchange. Molecular modeling corroborated this. It was shown that an aperture of sufficient size for ingress and egress of guest molecules could be formed through only deformation of the host structure. Furthermore, a cleverly designed amphiphilic guest containing a Ru(III) sandwich complex and an alkylsulfonate tail can enter through one host aperture without disrupting the structure, leaving the "tail" of the guest outside the cavity, as illustrated in Figure 1.21. This may have

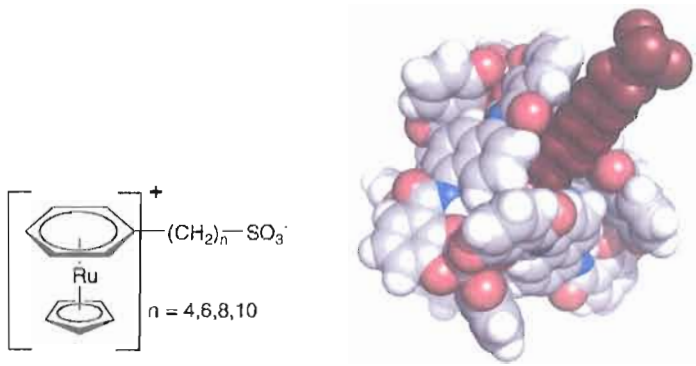

Figure 1.21. Partial encapsulation of an amphilic guest molecule. Ru(III) sandwich complex (*a*) with alkylsulfonate tail is encapsulated at the hydrophobic end; the hydrophilic sulfonate head group is exposed (*b*).

significant implications for applications in catalysis or synthesis of linear polymers in a stepwise fashion inside a properly designed nanoscale reaction vessel.

The mercuracarborands described previously also show rich anion-binding properties, especially with the halides.[17] For example, the formation of [12]mercuracarborand-4 requires the presence of a halide template; in its absence, the smaller and less strained [9]mercuracarborand-3 forms instead (Figure 1.6). Furthermore, it has been shown that the iodide guest may be removed from the tetranuclear host with silver acetate; the resulting empty macrocycle loses its planar structure and adopts a folded "butterfly" conformation. This now-empty host has been shown to complex both nitrate anions as well as $B_{10}H_{10}^{2-}$.

The trinuclear macrocyclic host has been involved in the formation of several interesting sandwich-type structures, such as a 2:1 carborand:benzene structure observed in the solid state. Hexamethyl-[9]mercuracarborand-3 also forms 2:1 complexes with halide ions (Figure 1.22). The halide is coordinated to six Hg(II) centers, forming what is thought to be three equivalent three-center, two-electron bonds between the anion and each macrocycle. This is supported by the decreasing distance between the trimer planes with decreasing guest size and the equidistant mercury-halide atoms that were less than the sum of the van der Waals radii.

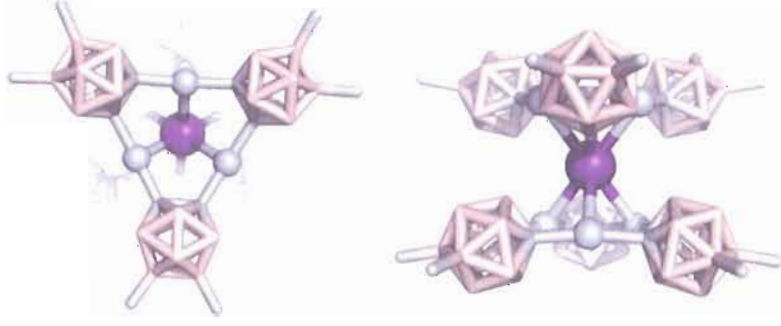

Figure 1.22. Halide sandwich complexes of hexamethyl-[9]mercuracarborand-3. View from top is shown at left; side view at right. The halide shown is iodide – similar complexes form from both chloride and bromide. The distance between Hg-macrocycle planes is I- (4.90 Å) > Br- (4.764 Å) > Cl- (4.672 Å). Pink polyhedra = parent carborand and purple spheres = halogen guest.

Conclusions

The main group elements have been used to prepare a wide variety of supramolecular, self-assembled structures. Many of these structures contain geometric elements which are either inaccessible or require use of blocking ligands when using transition metals as directing groups. While the main group elements have certainly not seen the widespread use in supramolecular chemistry enjoyed by the transition metals, it is clear that there is much utility to be found in this section of the periodic table, particularly in situations where the properties of a transition metal might preclude the use of a desired experimental technique. This has been particularly important in studying the solution state behavior of catecholamide-based supramolecular structures. The paramagnetism of iron(III) prevents study of these clusters by NMR. Gallium(III), on the other hand, served as an extremely effective model for these systems, allowing for more rigorous characterization of the supramolecular structures and dynamics. As more is understood about the supramolecular coordination chemistry of the main group elements, more and larger structures will continue to be prepared. We anticipate that these structures will see novel uses in the design and synthesis of functional materials and perhaps as synthons for materials for optics, electronics, and other emerging fields. One must also note that there are many challenges associated with work in the main group – coordination geometries are often unpredictable and can lead to unexpected difficulties with solubility or characterization. Crystalline samples of

these large structures are also at times difficult to prepare and one must rely on combinations of solution techniques to characterize products. Nevertheless, the stability imparted by self-assembly can lead to robust main group complexes. Given the interest in Bi-containing radiopharmaceuticals and other applications of main group chemistry, supramolecular structures such as those describes herein may find application in a broad range of fields.

CHAPTER II

LIGAND DESIGN FOR MAIN GROUP SUPRAMOLECULAR ASSEMBLIES

Supramolecular chemistry is frequently defined as "chemistry beyond the molecule" – that is to say very broadly, it is the study of noncovalent interactions between molecules. More specifically, the supramolecular chemist's goal is to use information stored in individual molecules to understand the myriad interactions that govern chemical and biological processes. Through careful selection of components, the supramolecular chemist is thus able to impose order in chemical systems and build successively larger assemblies and arrays that exhibit a wide range of functional properties through self-assembly processes that can sidestep lengthy covalent syntheses.

Health and Environmental Concerns Associated with the Main Group Elements

The main group elements are widely used in many applications. They are frequently a component of electronics, byproduct of mining activity, ETC. Their widespread usage has led to concerns over their toxicity – the pnictogen elements, especially As(III), are well-known to have deleterious effects on both human and environmental health, and lead poisoning is considered to be the most common disease of environment origin in children.[47] In fact, only recently was lead banned as

a component in children's toys.[48] It is therefore extremely important to gain a better understanding of the coordination chemistry of these elements, both for treatment of acute and chronic poisoning, as well as prevention through more effective sequestration of these contaminants. As shown in the previous chapter, the pnictogens have a strong preference for trigonal pyramidal coordination geometries, especially in the presence of thiolate ligands. In addition, these elements frequently interact with nearby arene rings, which can stabilize rather unusual structures.[33] The nature of this interaction is unclear and will be discussed in greater detail in Chapter V.

Lead(II) is another significant and dangerous environmental contaminant that has been used in many applications,[47,49,50] ranging from cosmetics to a gasoline additive; it is this widespread use that has made its presence the danger that it is today. There are many pathways by which lead contamination can enter the human body, ranging from skin contact in the case of organolead compounds to ingestion and inhalation in the case of lead carbonate based paints. The toxic effects of lead poisoning are also quite variable, from mild developmental impairment to acute psychotic episodes in the unfortunate case of several lead plant workers in the 1920's.[50] Lead is known to compete for calcium and zinc protein-binding sites, in particular ALAD heme biosynthetic pathway. Pb(II) has been found to bind preferentially over Zn(II) to models of ALAD; lead in fact binds over zinc by 500:1.[51]

In addition to the structural distortions found when Pb(II) substitutes for Zn(II)[52] (much of the structural change is related to the much larger volume occupied by lead)[53] the Lewis acidity of the metal center is reduced, contributing to the inhibition of the synthesis of porphobilinogen and the buildup of aminolevulinic acid. Pb(II) also binds to certain DNA sequences with unexpectedly high affinity – one striking example is that of the thrombin binding aptamer, which folds into a unimolecular structure based on formation of a guanine quartet around the Pb(II) center.[54] The structural implications of this unimolecular DNA folding suggest a pathway for genotoxic effects of Pb(II); in contrast, lead induces the hydrolysis of RNA.[55,56]

Supramolecular Design Principles and Application to Main Group Chemistry

Many of the supramolecular assemblies detailed in Chapter I suffer a significant drawback: their preparation frequently relies on serendipity. Introducing functionality into larger assemblies requires a well-defined framework in order to obtain predictable results; in application, this is frequently dubbed *rational design*, in which chemical building blocks contain information that guides their assembly into larger structures. In particular, this design strategy has been exemplified in supramolecular coordination chemistry by the elegant two-dimensional structures and polyhedra prepared by Raymond,[22,57] Fujita, and Stang.[2]

The "information" that is supplied by individual chemical units has many sources. It arises from the coordination preferences of metals. It can be found in the strong directionality of hydrogen bonds and even in the weak interactions between two or more arene rings in close proximity. Central to supramolecular chemistry, however, is the idea of "strength in numbers." Multiple weak noncovalent interactions can provide the driving force needed to cause the spontaneous self-assembly of multiple components to form assemblies otherwise completely inaccessible through traditional means. This include assemblies held together by "seams" of hydrogen bonds, the many structures that utilize the well-understood coordination preferences of the transition metals, and more recently structures that utilize the more unusual and less predictable coordination geometries accessible to the main group elements that has been reviewed in Chapter I.

While an overview of main group coordination preferences has been presented in Chapter I, certain elements within this set deserve a deeper examination. In particular, the "lower" pnictogens (As, Sb, and Bi) exhibit coordination preferences that simultaneously mirror the bonding preferences of the "higher" pnictogens (nitrogen and phosphorus), while also retaining a great deal of metallic character. Particularly, there is a marked preference for a trigonal pyramidal bonding pattern, and a prominent stereochemically active lone pair of

electrons. In contrast to the strong covalent character involved in nitrogen and phosphorus bonding, As – Bi exhibit bonding patterns that are closer to coordinate bonds in character. The kinetically labile nature of bonds to these lower pnictogens presents a unique opportunity to prepare analogs of existing organic macrocyclic and macrobicyclic cage compounds through a coordinative self-assembly pathway rather than a covalent synthesis. This approach provides the benefits of supramolecular assembly processes and allows access to an increased variety of structures. In addition, some of the heavier elements such as lead(II) and mercury(II) share many of the same coordination preferences despite their lower oxidation state and tendency toward the formation of oligomers in the solid state.

Secondary Bonding Interactions

Secondary or noncovalent bonding interactions comprise a huge segment of supramolecular chemistry and indeed macromolecular chemistry as a whole;[58] their key common feature is their relative weakness (compared to covalent bonds) and reversibility. The strongest of these interactions are those involving electrostatic attractions between oppositely charged ions – the crystalline lattice of salts exemplifies this type of interaction. These stronger interactions are also the most difficult to control, as they lack directional character beyond that gained through the preferred packing array in the lattice. Ion•••dipole interactions are also quite strong, but can be effectively used to guide the formation of specific assemblies.

Among the most widely used interaction in supramolecular chemistry is the hydrogen bond – a vast array of host assemblies have been prepared due to the strength, reversibility, and predictable geometries of hydrogen bonds. Cation•••π and π•••π interactions also play major structural roles in biological systems and supramolecular assemblies.

Although not as strong as primary metal-ligand interactions, secondary bonding interactions play an important role in the overall structure of metal-ligand assemblies. The main group elements in particular exhibit a wide variety of these interactions – the frequency at which they present stereoactive lone pairs and hemidirected primary coordination spheres provides many opportunities for additional, weaker interactions. The pnictogens display these secondary interactions with chalcogens (especially oxygen and sulfur),[59] halogens, hydrogen bond donors, and arenes in particular.

Ligand Design for Pb(II) and Hg(II)

In a nearly exhaustive review of the known coordination chemistry and biochemistry of lead(II), Claudio *et al.* have shown apparent trends in the crystal structures of lead complexes pertaining to coordination environment, coordination number, and chelate ring size.[49] The most common coordination numbers found in the Cambridge Structural Database are 4 and 6.[27] (See Chart 2.1 for the distribution of coordination numbers found in this study.) In the case of six-coordinate lead, an

octahedral, "holodirected' geometry is typically observed. In the case of the four-coordinate lead, a stereoactive lone pair is usually observed, with distinct geometric consequences. In hemidirected complexes, the $6s^2$ pair of electrons hybridizes with *p* orbitals, resulting in what appears to be a "hole" in the crystal structure. Four-coordinate Pb(II) therefore assumes a distorted trigonal bipyramidal or "sawhorse" coordination sphere.

The existence of the $6s^2$ lone pair in Pb(II) is of interest on its own. It is generally quite resistant to oxidation due to the stabilization afforded by relativistic contraction of the *s* orbitals; calculations show that this contraction can be as much as 25% in the 1*s* orbital.[60-62] In addition, Pyykkö showed that 2*s* orbitals and beyond contract by nearly the same magnitude.

A combined crystallographic and computational study of the coordination preferences of Pb(II)[27,49] found several distinct trends in the coordination preferences of lead(II):

- *Coordination number*: A bimodal distribution (Chart 2.1) was observed that found a preference for a coordination number of four, with a secondary preference for coordination number six.
- *Coordination sphere*: A hemidirected coordination sphere was preferred, in which ligands are unevenly distributed about the metal center that represents the prominent stereochemically active lone pair of electrons.
- *Donor atoms*: The most commonly observed donors to the lead(II) center were oxygen and sulfur.[63,64]

- *Chelate ring size*: Five and six membered chelate rings were frequently observed, with a preference for five membered rings.
- *Steric bulk of ligands*: Bulkier ligands tend to drive formation of holodirected complexes, while hemidirected complexes are more common with less sterically demanding ligands.

The computational study complementing this crystallographic survey found an interesting parallel between the idealized structure of four-coordinate complexes of lead(II) and the structures observed in the supramolecular complexes of mercury(II) as described in Chapter I. Indeed, two ligands tend to form a nearly linear L-Pb-L triad, while the second L-Pb-L triad forms a much sharper angle (near 90°). Several examples of four-coordinate oxygen and sulfur donor Pb(II) complexes have been reported.[63,64] Figure 2.1 shows two particular examples in which the orientation of both the bite angle between chelate groups and the angle between arene ring scaffolds varies based on the connectivity of the ligand framework. Furthermore, the computational studies suggest a strong preference for hemidirected coordination; in some cases, the hemidirected geometry is more stable than the holodirected by as much as 29 kcal/mol.

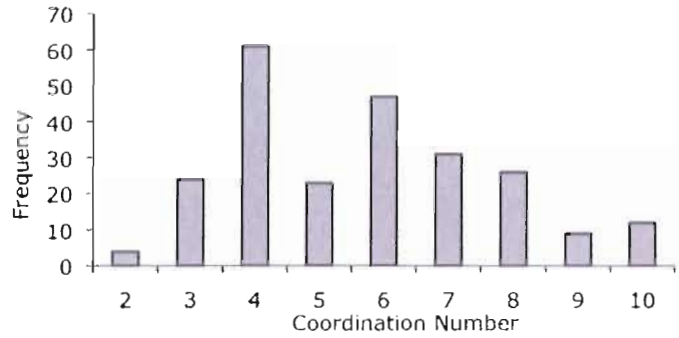

Chart 2.1. Frequency of coordination numbers found in Pb(II) complexes. Note the bimodal distribution centered at coordination numbers four and six. Complexes with coordination number five and below are generally hemidirected; complexes with coordination number six and above are generally holodirected.

Figure 2.1. Examples of low coordination number Pb(II) complexes with oxygen and sulfur donors. (*a*) Bis(thiomaltolato)lead(II)[65] orients the chelate groups at 81°, while the aryl rings themselves are oriented at 133° to one another. (*b*) A bis(thiohydroxamato)lead(II) structure[63,64] orients the chelate groups at 84°, while the aryl substituents are much closer to parallel at 22°.

Design and Synthesis of 2-Mercaptoacetamide Ligands

With these coordination preferences for Pb(II) in mind, we sought to design twofold symmetric ligands that would assemble to form either two- or three-stranded coordination assemblies. The preference for mixed oxygen/sulfur

coordination spheres and five-membered chelate rings led us to work with the 2-mercaptoacetamide ligand class. This ligand class was expected to provide the desired coordination number (4) and maintain the presence of the stereochemically active lone pair, which had been shown to be a definite preference of Pb(II) centers. Based on molecular models (CAChe, MM3) that suggested that a $Pb_2\mathbf{L}_2$ macrocycle was a feasible supramolecular structure, a bisfunctional 2-mercaptoacetamide ligand with a phenylene linkage was prepared (Figure 2.2 and Scheme 2.1).

Direct condensation of thioglycolic acid with aniline and *p*-phenylenediamine yielded ligands **1** and **2** in a single step. The monofunctional ligand **1** was prepared as a model compound for comparison with complexes prepared from the bifunctional ligands. When **2** was treated with a variety of Pb(II) sources under a broad series of conditions, only insoluble yellow solids were obtained. An alternate synthesis was developed to prepare ligand **3**, based on a durene spacer – the methyl groups were intended to increase the solubility of the ligand and any complexes. The insolubility problem persisted, which was attributed to the formation of a hydrogen bond network between the ligands. Ligand **4** with a tertiary amide instead of a secondary amide was thus prepared, eliminating the hydrogen bond donors. Indeed, this ligand was much more soluble than **3**; no discrete product could be formed when this was treated with Pb(II) sources.

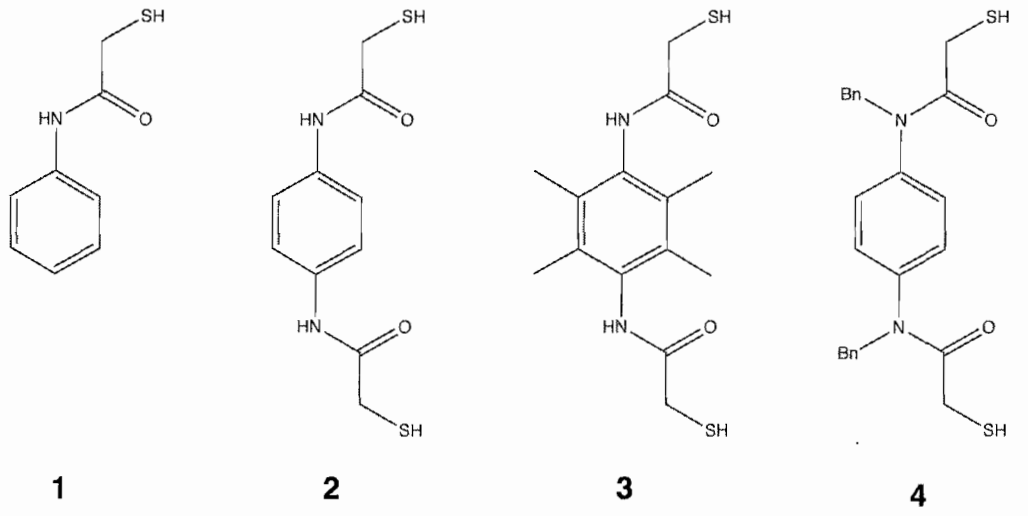

Figure 2.2. 2-Mercaptoacetamide ligands designed for Pb(II) coordination.

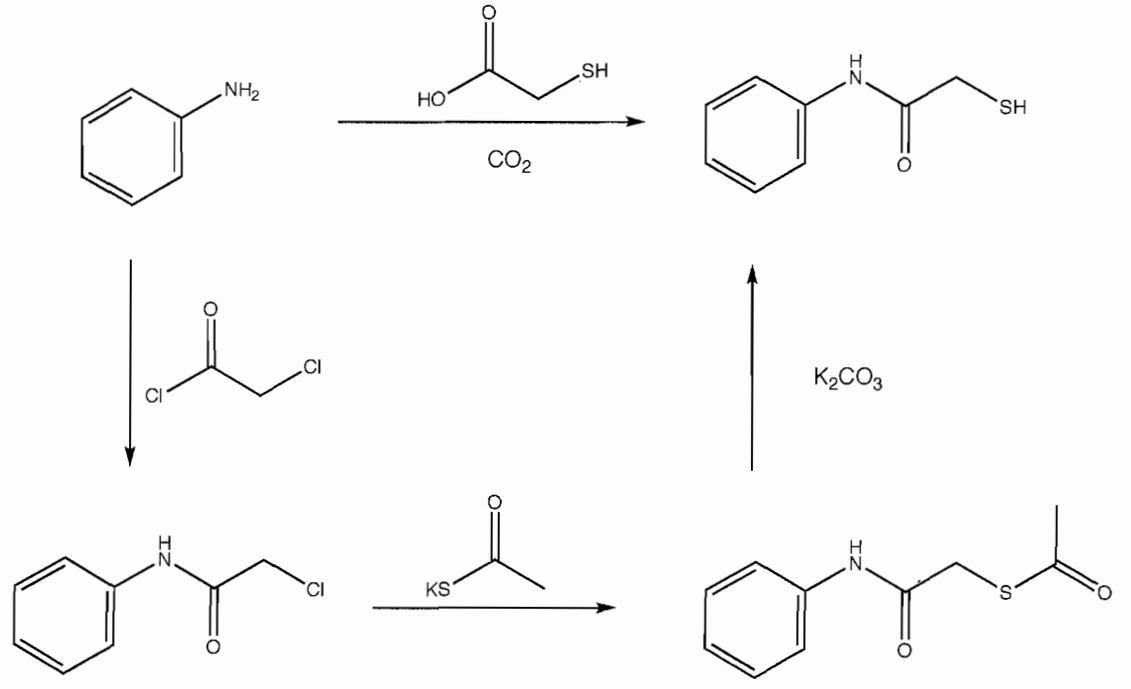

Scheme 2.1. Two methods for synthesis of 2-mercaptoacetamide ligands.

A possible explanation for the formation of insoluble coordination polymers comes from closer examination of ligand **4** (Figure 2.3) The crystal structure of this ligand indicated that the chelate groups prefer to take on a divergent, antiparallel orientation. This arrangement of chelate vectors is in opposition to design principles involved in the preparation of discrete supramolecular structures, which require convergent chelate vectors to form a closed structure. Instead, the divergent chelate groups presented by this ligand suggests that extended coordination networks are the most likely product upon addition of Pb(II) to phenylene-linked 2-mercaptoacetamide ligands.

Figure 2.3 Crystal structure of dibenzyl-2-mercaptoacetamide 4. The ligand presents divergent, *antiparallel* chelate vectors, indicating its unsuitability for formation of discrete supramolecular structures.

Trigonal Pyramidal Coordination of Pb(II)

Recent work suggests that lead(II) in particular has coordination preferences more similar to the pnictogens than previously thought. A thorough reexamination of lead(II)'s coordination chemistry[66] in both small molecules and larger biomolecules reveals that lead(II) has a similar preference for trigonal pyramidal coordination by three sulfur donors. In fact, many of the small molecule structures in the literature were incorrectly assigned to four-coordinate geometries due to the tendency of lead(II) compounds to form bridges, especially with thiolate donors. Surprisingly, lead(II) very rarely presents true four-coordinate geometries and even *avoids* this coordination sphere in many cases, remaining either three coordinate or taking on 5, 6, or 7 coordinate geometries. One particularly striking example of this incorrect structural assignment is shown in Figure 2.4. Originally presented as a discrete four coordinate complex, this structure was later examined in more depth and observed to be a dimer of pseudo six coordinate Pb(II) centers.[66] Each metal center bears three very short Pb-S bonds, and three longer Pb•••S contacts. These problems with structural characterization show clearly that the coordination chemistry of Pb(II), especially in the solid state, is even more poorly understood than previously thought.

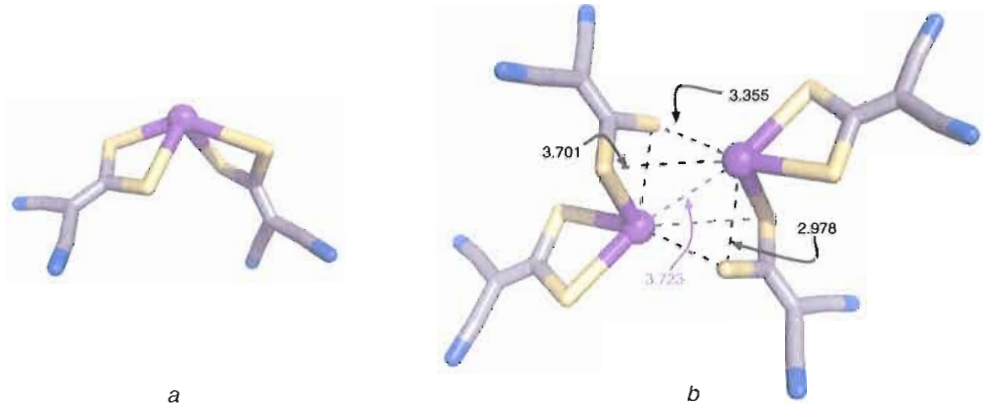

Figure 2.4. Example of incorrect assignment of lead(II) coordination spheres in the solid state. (*a*) Asymmetric unit of lead(II)-*iso*-maleonitriledithiolate dianion (Pb(*i*-mnt)$_2^{2-}$) with apparent four coordinate geometry. Tetraphenylarsonium cations are omitted for clarity. (*b*) Reexamination found that the structure is actually a dimer, where each Pb(II) atom is pseudo six-coordinate with three short bonds to sulfur and three longer contacts (black dashed lines). An additional long Pb•••Pb contact (purple dashed line) was also observed. Measurements are given in angstroms.

The coordination preferences observed by Godwin, *et al.* are supported by previous results found by Christou[67] and Parkin. Both lead(II) and mercury(II) form discrete coordination complexes with thiophenolate ligands and are soluble with tetraalkylammonium cations. Pb(II) forms a trigonal pyramidal complex in which additional coordination to the lead center is blocked by the arene rings of the ligands and the close association of the bulky counterion (Bu_4N^+) (Scheme 2.2). Hg(II) forms a trigonal planar complex, with similar close pairing of the ammonium cation.

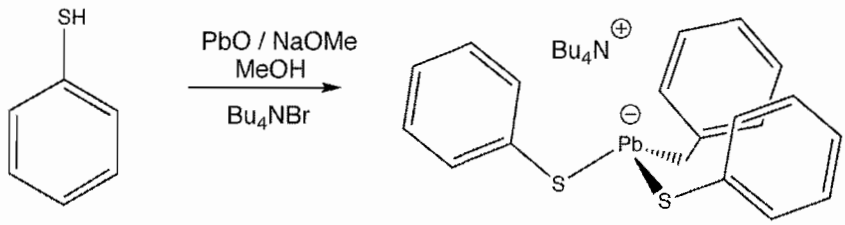

Scheme 2.2. Synthesis of $Pb(SPh)_3$ salts.

An alternate *neutral* structure, $Pb(SPh)_2$, forms from the biphasic reaction of thiophenol with lead(II) acetate when a base is omitted from the reaction (Figure 2.5). While the stoichiometry of the complex has two thiophenolate ligands per metal, each Pb(II) center is actually three coordinate – a repeating, infinite chain is formed by bridges between a sulfur on one ligand and a neighboring Pb(II) center. These chains pack in a parallel fashion, and the lone pairs of the lead centers alternate in being directed up or down with respect to the overall chain structure. This structure indicates that when the metal center is deprived of sulfur, the $Pb(SPh)_2$ units bridge to form a coordination polymer that satisifies the three-coordinate, trigonal pyramidal coordination preference of Pb(II). This simultaneously shows that coordination polymers are a very likely byproduct of bifunctional ligands added to Pb(II) and that the three-coordinate geometry is an important target in supramolecular assembly design. Other researchers have observed this type of chain structure a variety of ligands such as *p*-methylthiophenol[68] in a 1:2 M:L ratio. When the ligand bears sterically demanding

substituents (such as isopropyl) near the donor atom, a *trimer* forms instead of an infinite chain.[69] With a less demanding 2,6-dimethyl substitution, a decamer is formed with the form of a dimer of pentamersl;[70] other *n*-mers are possible depending on cocrystallized solvent. Electron deficient arylthiothiolates such as -SC_6F_5 produced an interpenetrated network of PbL_3 bridged by an additional Pb(II) center with linear coordination.[71] while 2,4,6-trifluoromethylthiophenol yields a pentamer.[72]

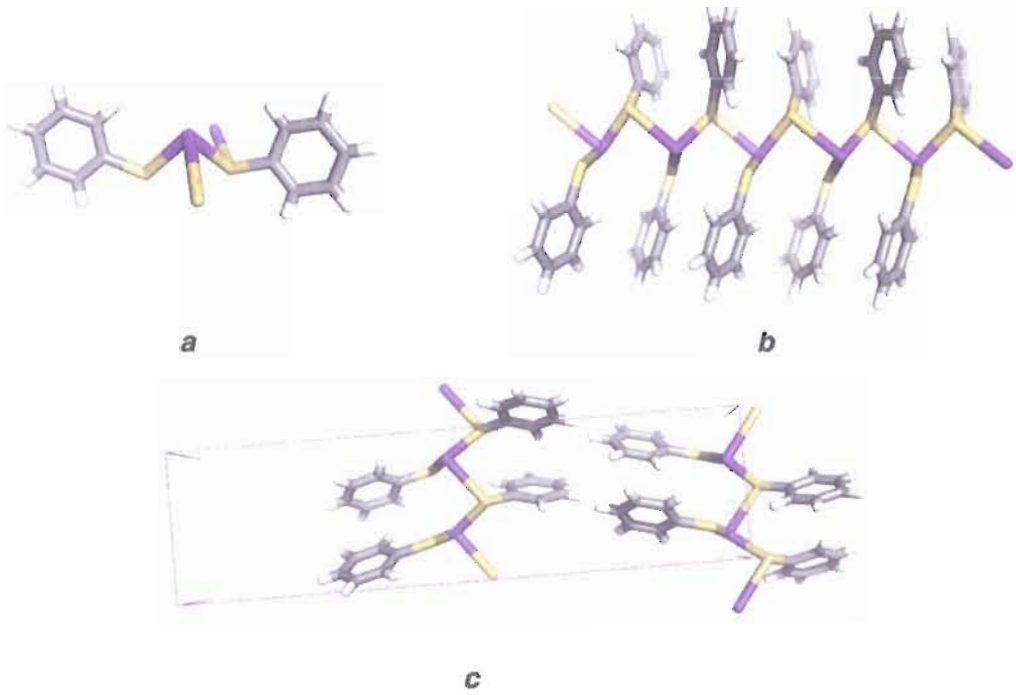

Figure 2.5. Infinite chain structure obtained from biphasic reaction of thiophenol and $Pb(OAc)_2$. The drive for trigonal pyramidal coordination is manifested in the formation of chains between individual units of $Pb(SPh)_2$. (*a*) The individual unit of $Pb(SPh)_2$, with attachment points for the repeating unit shown. (*b*) Chain structure formed by bridging of a thiol to a neighboring Pb(II) center. (*c*) Unit cell of $Pb(SPh)_2$ showing the interaction between two chains of the repeating unit.

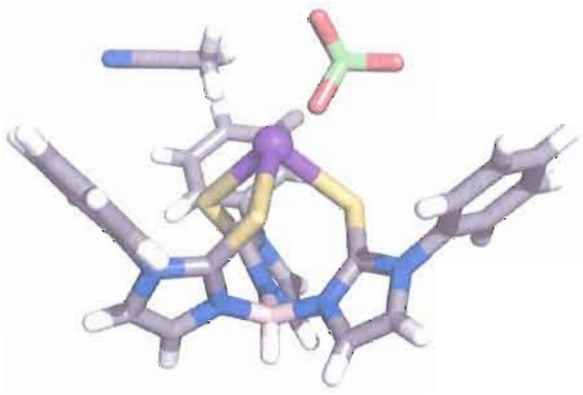

Figure 2.6. Tris-pyrazyl Pb(II) complex model of ALAD active site. The threefold axis provided by the B-H bridgehead preorganizes the ligand for trigonal pyramidal binding to metals.

Models for the active sites of proteins that are often biological targets of Pb(II) have been prepared by the Parkin group.[52] The trigonal coordination (Figure 2.6) by aryl thiolate ligands is again the major structural feature of these complexes, bearing out the theory that this is the predominant geometry found when lead(II) associates with cysteine-rich proteins.

Ligands incorporating aryl thiolate donors were thus designed as a way to accommodate the trigonal pyramidal coordination geometry of lead(II). In particular, 4,4'-dimercaptodiphenylmethane, 4,4'-dimercaptobenzophenone, and 4,4'-dimercaptodiphenyl ether were prepared (Scheme 2.3); molecular modeling

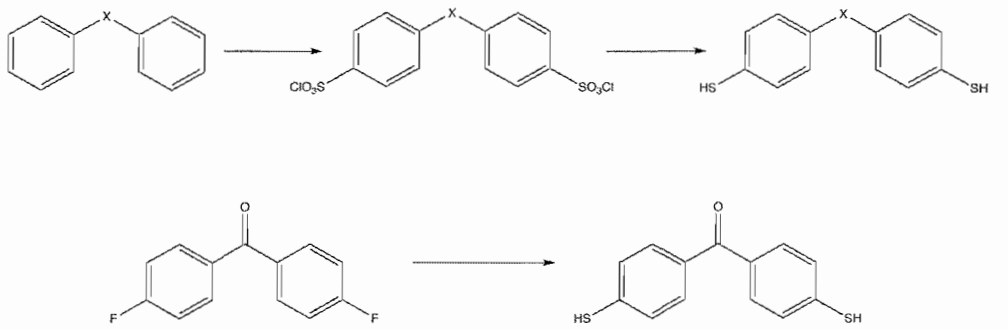

Scheme 2.3 Synthesis of aryldithiolate ligands. Conditions: *a.* Chlorosulfonic acid. *b.* Zinc, HCl. *c.* NaSH, DMF. X = $-CH_2-$ and –O-.

suggested that these ligands were capable of bridging two lead(II) centers to form $Pb_2\mathbf{L}_3$ assemblies.

Initial studies with this ligand class (4,4'-dimercaptobenzophenone in particular) suggest that they may hold promise for the preparation of supramolecular species from lead(II) sources. Solution ^1H NMR studies showed that upon addition of $Pb(NO_3)_2$ to a solution of ligand in chloroform, a new high-symmetry species gradually formed. All attempts to crystallize this structure yielded intractable, amorphous solid materials, preventing identification by X-ray crystallography. ^{207}Pb NMR experiments did provide some evidence of at least two species of lead in solution – one resonance was observed corresponding to the $Pb(NO_3)_2$ source, while a second resonance was observed downfield in the region typically associated with Pb-S complexes. This suggestion of a high-symmetry Pb-S species is intriguing, though not definitive: several stoichiometric combinations

could satisfy these criteria, including the desired $[Pb_2\mathbf{L}_3]^{2-}$ assembly, a neutral $Pb_2\mathbf{L}_2$ macrocycle, or a $[Pb_2\mathbf{L}]^{2+}$ complex. Given the intractability of this complex in the solid state, further characterization by solution-based methods such as mass spectrometry will be required.

Future Directions for Research in Supramolecular Lead(II) Chemistry

While these ligands again formed intractable polymers in the solid state, they do offer several points of departure for future work. One of the likely problems with this design is the outwardly directed lone pair. In the aryldithiolate ligand design, this represents a very large empty space in the coordination sphere, opening the metal center to bridging interactions with extra sulfur donors, likely causing the formation of coordination polymers. This is commonly observed in the extended structures of mononuclear lead(II) complexes – bridging secondary interactions are found in this "hole" in the primary coordination sphere.[66] Lead(II) is a very large cation,[53] and the potential to direct the lone pair into an assembly's interior is quite low based on the limited conformational freedom of the aryl dithiolate ligands prepared to date. One possible way to reconcile these problems is to move the point of attachment for the ligand spacer and allow the lone pairs to be directed outward, but with a "basket" of arene rings around the metal center to block additional ligands from coordinating the metal. In effect, the aryl thiolate moiety itself might

act to protect the lead center from undesirable secondary interactions that cause formation of coordination polymers (Figure 2.7).

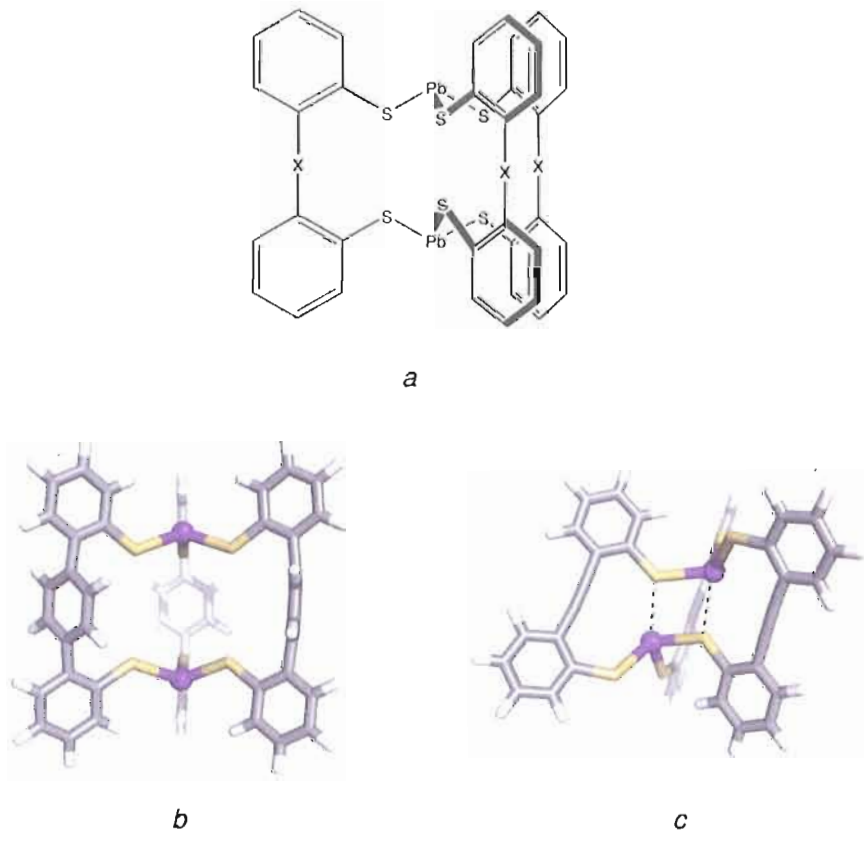

Figure 2.7. Proposed designs for next-generation ligands for Pb(II). These ligands are designed to simultaneously accommodate the three-coordinate sulfur donor environment that Pb(II) prefers, while minimizing the possibility of bridging interactions between the sulfur and neighboring metal centers. (*a*) Generalized structure of $Pb_2\mathbf{L}_3$ assembly in which the thiophenolate donor moiety acts to block additional bridging interactions involving either lead or sulfur. (*b*) Molecular model where the bridging group **X** = -(C_6H_4)-. (*c*) Molecular model in which **X** = -C≡C-. This choice of linker is short enough to allow the three-coordinate Pb(II) centers to accept a fourth long intramolecular contact (shown as dashed lines).

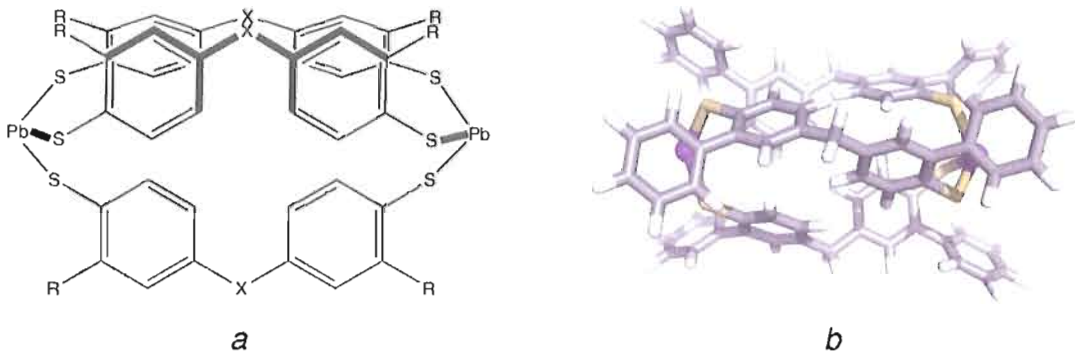

Figure 2.8. Aryldithiolate ligand design with substituents to block thiolate bridging interactions. (*a*) General schematic showing that this ligand class is likely to have exohedrally directed lone pairs, with location of **R** groups designated. **X** = -CH_2-, -O-, etc. (*b*) Molecular model where **R** = Ph.

Alternately, the aryldithiolate ligand scaffold may be retained, but additional steric bulk added *ortho* to the thiol position could be employed to the same effect. For example, a benzyl group appended to the 4,4'-dimercaptodiphenylmethane ligand *ortho* to the thiolate group as shown in Figure 2.8 could be very effective at preventing the thiolates from bridging multiple Pb(II) centers, therefore driving the formation of discrete supramolecular assemblies.

A second possibility for improved supramolecular ligand design for Pb(II) is that of a hybrid between the diphenylmethane linked arylthiolate ligands and the 2-mercaptoacetamide ligand class. The thiohydroxamato structure in Figure 2.9 exhibits chelate vectors oriented at 84° to one another. While this suggests that the

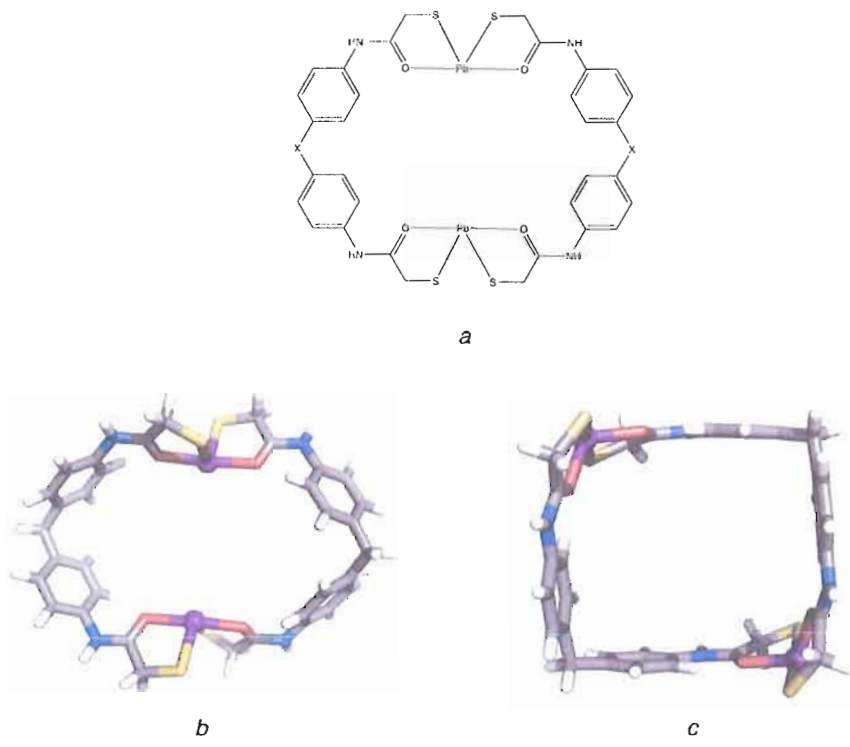

Figure 2.9. Diphenylmethane spaced 2-mercaptoacetamide ligand. X = -CH_2-, -O-, or –C(=O)-. (*a*) Schematic representation of a more conformationally mobile $Pb_2\mathbf{L}_2$ macrocycle based on the 2-mercaptoacetamide chelating functionality. (*b*) Molecular model (CAChe, MM3) of the macrocycle (**X** = -CH_2-) with lone pair oriented endohedrally. Note the O-Pb-O bond angle is nearly 180° and the S-Pb-S angle is much sharper. (*c*) Molecular model of the macrocycle with exohedrally directed lone pairs. This model forms a definite "square" shape and this time the S-Pb-S angle is near 180°, with a sharper O-Pb-O angle.

phenylene substituent on the ligand itself would be a poor supramolecular spacer due to steric strain, two 2-mercaptoacetanilides could be linked with a methylene spacer to create a ligand with somewhat more flexibility than the original designs. This approach has been used successfully in the preparation of diphenylmethane and diphenylethane spaced assemblies based on the coordination of benzylic

thiolates to As(III) centers, which will be discussed in more detail in Chapters III and IV.

As discussed in this chapter, we have encountered significant challenges in the preparation of supramolecular assemblies based on coordination to lead(II) centers. Many of these challenges arise from the very properties that make lead(II) an important target of study. Its unpredictable coordination geometries and propensity to be involved in coordination networks to satisfy its capricious preferences makes preparation and characterization of discrete complexes challenging; it has been noted in previous work that many alkyl and arylthiolate complexes of lead(II) exhibit low solubility in most common solvents, and attempts to recrystallize these complexes from hot solvents leads to decomposition of the product. Nevertheless, there is evidence that a predictable tris-thiolate coordination sphere is strongly preferred by the lead center and is likely one of the most biologically relevant coordination modes. Several new designs for ligands based on the lead(II) coordination preferences have been proposed, which may yet yield the elusive supramolecular assemblies.

Experimental Details

General Information

Starting materials and reagents were obtained from commercial sources and used without further purification unless otherwise noted. NMR spectra were obtained on Varian 300 MHz, 500 MHz, and 600 MHz spectrometers as noted; chemical shifts are reported in parts per million (ppm) downfield from tetramethylsilane and referenced to residual solvent as an internal standard. X-ray diffraction data were collected at 173 K on a Bruker Apex diffractometer using MOKα-radiation (λ=0.71073 Å). Mass spectra were recorded using an Agilent 1100 Series LC/MSD. Absorption corrections were applied by SADABS. All structures were determined by direct methods and refined on F^2 by a full-matrix least-squares procedure. All non-H atoms were refined with anisotropic thermal parameters. H atoms were refined in calculated positions in a model of a rigid group. All calculations were performed by the Bruker SHELXTL 6.10 package (SHELXTL, version 6.10, Bruker AXS, Inc., Madison, WI, 2000).

Synthesis of 2-Mercaptoacetamides and Derivatives

2-Mercaptoacetanilide (1): Aniline (6.6 mL, 72 mmol) and thioglycolic acid (5 mL, 72 mmol) were combined in a 2-neck round bottom flask. Carbon dioxide dried over $CaCl_2$ was bubbled through the mixture while stirring. This was then heated to 110° C for three hours. Upon cooling, the reaction mixture solidified to form a white solid.

The solid was crumbled to a powder and washed with 10% HCl and water to remove any starting materials, then filtered and air-dried. (9.96 g, 63%) ^{1}H NMR ($CDCl_3$, 300 MHz): δ 8.55, 1H, s; 7.57, 2H, d, J = 9.0 Hz; 7.37, 2H, t; 7.16, 1H, t; 3.42, 2H, d; 2.05, 1H, t. ^{13}C NMR ($CDCl_3$, 75 MHz): δ 167.54; 129.35; 125.11; 120.14; 29.41. UV-vis λ_{max} = 257 nm.

Bis(2-mercaptoacetanilide) (2): Thioglycolic acid (14 mL, 201 mmol) and 1,4-phenylenediamine (9.46 g, 87 mmol) were combined in 40 mL of anhydrous methanol. Carbon dioxide dried over $CaCl_2$ was bubbled through the solution, which was heated to reflux overnight. Upon cooling, a white solid formed which was filtered off and washed with 10% HCl and water. (9.92 g, 42%) ^{1}H NMR (DMSO-d_6, 300 MHz): δ 10.05, 2H, s; 7.51, 4H, s; 3.27; 4H, s; 2.91, 2H, bs. ^{13}C NMR (DMSO-d_6, 75 MHz): δ 165.87; 127.65; 123.29; 28.17. ESI-MS calcd for $C_{10}H_{12}N_2O_2S_2$ m/z 256.03, found 257.0.

Bis(2-chloroacetamido)-2,3,5,6-tetramethylbenzene: 2,3,5,6-tetramethyl-1,4-phenylenediamine (0.429 g, 2.61 mmol) and triethylamine (0.75 mL, 5.4 mmol) were combined in 50 mL CH_2Cl_2 and chilled in an ice-water bath. Chloroacetyl chloride (0.4 mL, 5.03 mmol) was dissolved in 5 mL CH_2Cl_2 and slowly added to the amine solution. This was then stirred for 30 minutes. The solid precipitate was filtered and washed with water and 10% aqueous HCl to yield 0.742 g of the desired

product (91%). ^{1}H NMR (DMSO-d_6, 300 MHz): δ 9.70, 1H, s; 4.29, 2H, s, 2.04, 6H, s. ^{13}C NMR (DMSO-d6, 75 MHz): δ 161.53; 132.16; 100.23; 43.48; 15.66.

Bis(2-acetylmercaptoacetamido)-2,3,5,6-tetramethylbenzene: Bis(2-chloroacetamido)-2,3,5,6-tetramethylbenzene (742 mg, 2.4 mmol) was dissolved in 50 mL DMF, then slowly added to a stirring suspension of potassium thioacetate (681 mg, 6.0 mmol) in 50 mL DMF. The mixture was stirred overnight at room temperature, followed by evaporation of the solvent. The tan solid material was resuspended in DI water and stirred for 20 minutes. This was then filtered and washed twice more with DI water, yielding the desired product as a tan solid. (942 mg, 78%) ^{1}H NMR (300 MHz, DMSO-d_6): δ 9.57, 1H, s; 3.84, 2H, s; 2.39, 3H, s; 2.01, 6H, s. ^{13}C NMR (DMSO-d_6, 125 MHz): δ 195.34; 166.49; 133.94; 132.10; 33.45; 30.87; 15.69.

Bis(2-mercaptoacetamido)-2,3,5,6-tetramethylbenzene (3): Bis(2-acetylmercaptoacetamido)-2,3,5,6-tetramethylbenzene (338 mg, 0.85 mmol) was suspended in 15 mL dry MeOH. Potassium carbonate (1.361 g, 9.8 mmol) was dissolved in 15 mL DI water. The two solutions were combined and sparged with nitrogen gas for 30 minutes, then heated to 95 °C for 30 minutes. The reaction mixture was cooled to room temperature and acidified with 10% HCl until a white solid precipitated from solution. This solid was filtered and air-dried to yield the desired product. (80%) ^{1}H NMR (DMSO-d_6, 500 MHz): δ 9.47, 1H, s; 3.23, 2H, d, J = 8

Hz; 2.93, 1H, t, J = 8 Hz; 2.05, 6H, s. ^{13}C NMR (DMSO-d_6, 125 MHz): δ 169.41; 133.87; 132.14; 27.89; 15.73.

Bis(2-chloroacetamido-N-benzyl)-para-phenylenediamine: N,N'-dibenzyl-para-phenylenediamine (283 mg, 0.98 mmol) and triethylamine (0.28 mL, 2.01 mmol) were combined in 20 mL dry CH_2Cl_2 and chilled in an ice-water bath. Chloroacetyl chloride (0.16 mL, 2.01 mmol) was dissolved in 5 mL dry CH_2Cl_2 and added dropwise to the amine solution over 10 minutes; the mixture was allowed to stir in the ice bath for 45 minutes. The organic layer was washed twice with 10% HCl, then dried and rotovapped to yield 411 mg of the desired product (94.9%). ^{1}H NMR ($CDCl_3$, 500 MHz): δ 7.27-7.11, 5H, m; 7.00, 2H, s; 4.88, 2H, s; 3.81, 2H, s. ^{13}C NMR ($CDCl_3$, 125 MHz): δ 166.22; 136.20; 130.06; 129.20; 128.87; 128.23; 53.88; 41.92.

Bis(2-acetylmercaptoacetamido-*N*-benzyl)-*p*-phenylenediamine: Bis(2-chloroacetamido-*N*-benzyl)-*p*-phenylenediamine (411 mg, 0.93 mmol) was dissolved in DMF; potassium thioacetate (256 mg, 2.2 mmol) was suspended in DMF. The chloride solution was slowly added to the thioacetate suspension and allowed to stir at room temperature overnight. The DMF was rotovapped off to yield a brown oil, which was suspended in DI water, then extracted three times with methylene chloride, dried, filtered and rotovapped to yield the desired product. (485 mg, 77.3%) ^{1}H NMR ($CDCl_3$, 300 MHz): δ 7.16, 3H, m; 7.05, 2H, m; 6.96, 2H, s;

4.78, 2H, s; 3.42, 2H, s; 2.23, 3H, s. ^{13}C NMR ($CDCl_3$, 75 MHz): δ 195.4; 167.34; 141.57; 136.64; 130.12; 129.08; 128.68; 127.88; 53.72; 33.07; 30.17.

Bis(2-mercaptoacetamido-*N*-benzyl)-*p*-phenylenediamine (4): Bis(2-acetylmercaptoacetamido-*N*-benzyl)-*p*-phenylenediamine (375 mg, 0.72 mmol) was dissolved in 50 mL methanol; 10 equivalents of aqueous potassium carbonate (1.09 g, 7.9 mmol) were added and the solution sparged with nitrogen for 30 minutes. The mixture was then brought to reflux for 30 minutes at 95 °C, then cooled and acidified with HCl, producing a cloudy solution. This was extracted with small portions of methylene chloride until no more yellow color appeared in the organic phase. The organics were pooled together, dried, filtered, and rotovapped to a brown oil, then placed on a high vacuum line overnight, yielding a brown oil that was confirmed by NMR to be the desired product. (249 mg, 79%) ^1H NMR ($CDCl_3$, 300 MHz): δ 7.28-7.15, 5H, m; 7.02, 2H, s; 4.90, 2H, s; 3.06, 2H, d, J = 7.2 Hz; 2.13, 1H, t, J = 7.2 Hz.

Synthesis of Thiophenolate Complexes of Pb(II)

$Pb(SPh)_3$•NBu_4: Under N_2 atmosphere, sodium metal (0.553 g, 24 mmol) was added to 50 mL degassed methanol at a rate which controlled the evolution of hydrogen gas. The solution was stirred until the metal was completely dissolved. Thiophenol (2.47 mL, 24 mmol) was then added to the methanol solution. Lead(II) oxide (1.4 g, 6 mmol) was added to the sodium thiophenoxide solution and the

reaction mixture heated to 40° C for 24 hours. An additional 50 mL degassed methanol was added to the flask and heating was continued for an additional 16 hours, at which time all the lead oxide was in solution. Tetrabutylammonium bromide (3.88 g, 12 mmol) was dissolved in 50 mL ethanol and added slowly to the warm reacton mixture. The resulting solution was cooled to room temperature, then concentrated *in vacuo* until solid began to form. Ethanol was added to a total solution volume of 90 mL, at which time copious yellow crystalline solid precipitated from solution. This was filtered and air dried to yield $Pb(SPh)_3 \bullet NBu_4$. The microcrystalline solid was redissolved in 23 mL acetonitrile at 50° C, and 23 mL ethanol was added. Upon storage at 0° C overnight, yellow crystals suitable for characterization by X-ray crystallography formed.

$Pb(SPh)_2$: Lead(II) acetate (0.069 g, 0.18 mmol) was dissolved in 75 mL DI water; thiophenol (37 µL, 0.36 mmol) was dissolved in 75 mL CH_2Cl_2. The aqueous solution was slowly layered onto the organic solution and allowed to stand at room temperature. The aqueous layer gradually became cloudy and the organic layer slowly became light yellow in color. After 2 days, copious yellow needles formed which were identified as $Pb(SPh)_2$ by X-ray crystallography.

Synthesis of Bifunctional Thiophenol Derivatives

4,4'-dichlorosulfonyldiphenylmethane. Chlorosulfonic acid (10 mL) was cooled in an ice-water bath. Diphenylmethane (2 mL, 1.2 mmol) was added dropwise and

the solution slowly warmed to room temperature, then stirred overnight. The reaction mixture was carefully poured onto 100 mL of ice. After the ice was completely melted, the white precipitate (4,4'-dichlorosulfonyldiphenylmethane) was collected by vacuum filtration and air-dried. The sticky solid was redissolved in chloroform, washed with H_2O, dried with Na_2SO_4, then filtered and the solvent removed *in vacuo*. The resulting solid material was recrystallized from hexanes to yield the desired product (0.115 g, 26%) ^{1}H NMR ($CDCl_3$, 300 MHz): δ 7.85, 4H, d, J = 9 Hz; 7.15, 4H, d, J = 9 Hz.

4,4'-methylenedibenzenethiol: $SnCl_2$ (12.47 g, 65.8 mmol) was added to a solution of ethanol (15 mL) and concentrated HCl (15 mL). 4,4'-dichlorosulfoyldiphenylmethane (1.09 g, 2.98 mmol) was added to this solution and the mixture brought to reflux overnight. Upon cooling to room temperature and dilution with 50 mL H_2O, a yellow-white precipitate formed, which was collected by vacuum filtration. (0.111 g, 16%) ^{1}H NMR ($CDCl_3$, 300 MHz): δ 7.92, 4H, d, J = 9 Hz; 7.35, 4H, d, J = 9 Hz.

4,4'-dichlorosulfonyldiphenyl ether: Chlorosulfonic acid (20 mL) was chilled in an ice-water bath. Diphenyl ether (4 mL, 2.5 mmol) was added dropwise over one hour; when addition was complete, the solution was allowed to warm slowly to room temperature and stirred overnight. The reaction was quenched by addition to 300 mL ice, then extracted with toluene. The solvent was removed *in vacuo* to yield

the product (0.783 g, 85%). ^{1}H NMR ($CDCl_3$, 300 MHz): δ 8.11, 4H, d, J = 9 Hz; 7.21, 4H, d, J = 9 Hz.

4,4'-oxydibenzenethiol : 4,4'dichlorosulfonyldiphenyl ether (1.159 g, 3.15 mmol) was combined with zinc (2.012 g,), ethanol (8 mL), and water (20 mL). Concentrated H_2SO_4 (4 mL) was slowly added and the reaction mixture heated to reflux. After 5 hours, the mixture was cooled to room temperature and diluted with 20 mL H_2O. The resulting solid was filtered, extracted three times with chloroform, and the solvent removed to yield 0.346 g product (47%) ^{1}H NMR ($CDCl_3$, 300 MHz): δ 8.23, 4H, d, J = 9 Hz; 7.35, 4H, d, J = 9 Hz.

Bis(4-mercaptophenyl)methanone: Sodium hydrogen sulfide (0.841 g, 15 mmol) was suspended in dry DMF (20 mL), and then heated until the solid was completely dissolved and a bright blue solution formed. 4,4'-difluorobenzophenone (1.09 g, 5 mmol) was quickly added, and the reaction flask was fitted with a reflux condenser and a gas outlet such that evolved gasses were passed first through a solution of concentrated NaOH, then a solution of bleach. This was heated to 130° C for 2 hours, then cooled to room temperature and diluted with water to form a yellow-white precipitate. The precipitate was filtered and air-dried, then redissolved in 2 N NaOH, filtered, acidified with concentrated HCl, then filtered again. This process was repeated twice more, and the final product air-dried to yield a white solid

material. (.995 g, 81%) ^{1}H NMR ($CDCl_3$, 300 MHz): δ 7.65, 4H, d; 7.33, 4H, d; 3.64, 2H, s.

Crystallographic Details

$Pb(SPh)_2$: Crystal data: $C_{12}H_{10}PbS_2$, M_r = 425.51, 0.12 x 0.07 x 0.01 mm^3, orthorhombic, $Pca2_1$, a = 7.2143(12) Å, b = 5.9685(10) Å, c = 27.080(5) Å, α = 90°, β = 90°, γ = 90°, V = 1166.0(3) $Å^3$, Z = 4, ρ_{calcd} = 2.424 g cm^{-3}, μ = 14.788 mm^{-1}, $2\theta_{max}$ = , T = 173(2) K, 6659 measured reflections, 2523 independent reflections [R(int) = 0.0535], $R1$ = 0.0376, w$R2$ = 0.0696, max/min residual electron density 1.459 and -1.861 e $Å^{-3}$

CHAPTER III

MULTIPLE WEAK SUPRAMOLECULAR INTERACTIONS STABILIZE SUPRISINGLY TWISTED $AS_2\mathbf{L}_3$ ASSEMBLIES: SOLID STATE DISTORTIONS AND TEMPERATURE SENSITIVE CONFORMATIONAL CHANGES IN SOLUTION

A substantial portion of the work in this chapter has been published in *Chemical Communications*.[73] Design and synthesis of ligands and assemblies, low-level molecular modeling, NMR studies, and the preparation of the manuscript were carried out by myself; DFT calculations were performed at the University of Kansas by Dr. Kumar Vanka in conjunction with Drs. Ward H. Thompson and Brian B. Laird. Dr. Lev N. Zakharov performed crystallography at the University of Oregon. Editorial assistance was provided by Prof. Darren W. Johnson.

Introduction

Supramolecular chemistry based on metal-ligand coordination is a rapidly advancing field that has provided access to a wide variety of structures through information programmed into the coordination preferences of metal ions.[57,2] These coordination assemblies frequently display emergent properties such as guest encapsulation[74] with some metal-ligand assemblies exhibiting changes in size through a non-dissociative mechanism that has been described as "breathing".[75,76]

Interest in main-group supramolecular chemistry has flourished in recent years, as the main group elements provide access to unique coordination geometries otherwise unavailable to researchers preparing novel structures with new properties.[1] In this communication we report a novel arsenic-based supramolecular assembly whose structure is determined by a combination of As-π69,70 and edge-to-face aromatic interactions. The NMR spectra of this assembly are highly temperature dependent, suggesting that the ligand scaffold expands and contracts in response to temperature changes, in effect "breathing."

Previous work in this laboratory has focused on the preparation of dinuclear arsenic assemblies bridged by rigid ligands, such as 1,4-bis(mercaptomethyl)benzene (H_2**L**[1]), which accommodates the preference of trivalent arsenic for trigonal pyramidal coordination.33, 34, 72 This assembly was found to be thermodynamically and kinetically stable under a variety of harsh conditions and in the presence of competing metal ions and ligands, presumably due to the strength of As-S bonds (~81 kcal/mol).[77] Furthermore, the endohedrally directed lone pairs and short As-π contacts suggested the potential for unique host-guest interactions.74, 75 To date, however, no guest encapsulation has been observed with either capsule or macrocycles prepared from 1,4-bis(mercaptomethyl)benzene. Calculations to determine the interior volume of these assemblies indicated that there is insufficient space to accommodate a guest

molecule, even small metal cations. *Syn*-macrocycles prepared from a methoxy derivative of this ligand have been shown to dimerize around aromatic solvent molecules, forming clathrates in the solid state.[78] There is to date no evidence that these structures persist in solution.

Diphenylmethane in Supramolecular Chemistry

Given the apparent lack of interior space in the phenylene-derived $As_2\mathbf{L}_3$ capsule structure, we sought to prepare an analogous assembly based on a larger scaffold that would provide sufficient void space for potential guests. Many of the classic supramolecular hosts have incorporated diphenylmethane into their structures for two key reasons: it provides an expanded cavity to host structures and its moderate degree of flexibility allows for some amount of structural rearrangement while retaining a reasonably predictable structure.[58] These structures are frequently capable of reversibly binding a variety of small organic guests in both aqueous and organic media. This particular scaffold provides a well-defined, π electron rich interior surface in many macrocyclic and macrobicyclic hosts, in which guests can interact with the host walls via either cation•••π or aromatic CH•••π contacts. Diphenylmethane's conformational flexibility provides the ability for hosts to reorganize to accommodate guest molecules, but there is an energetic price associated with the loss of entropy when the host becomes more organized.[79] Several examples of diphenylmethane's versatility in supramolecular

host design are shown in Figure 3.1 – (*a*) and (*b*) are both examples of organic cyclophane-type macrocycles in which the diphenylmethane moiety is stabilized in gable conformation by back substitution of the methylene group with piperidine groups. This conformation enforces a preorganized cavity for binding aromatic guests. Figure 3.1(*c*) shows a *tren*-bridged cryptand that encapsulates terephthalate anion through multiple hydrogen bonding interactions. With the appropriate choice of "cap" for a threefold symmetric assembly, the diphenylmethane scaffold can accommodate relatively large guests, making it a desirable component for new self-assembled complexes. Indeed, inorganic triple helicates based on diphenylmethane linked bis(catecholate) ligands chelated to Ti(IV) exhibit dynamic stereochemistry in solution. These structures are anionic and bear additional Li(I) counterions in secondary coordination to the catecholate donors, further stabilizing the structure.

In the catecholate-based triple helicates, the ligand donor groups were located on the diphenylmethane scaffold itself. A large series of double and triple helicates have been prepared which place the donor groups *para* to the diphenylmethane linkage in the form of an aromatic amine/pyridine chelate group, such as that shown in Figure 3.1(*e*). These helicates have been formed with a wide variety of metal centers, as well as a diverse series of side chains on the amine.[80]

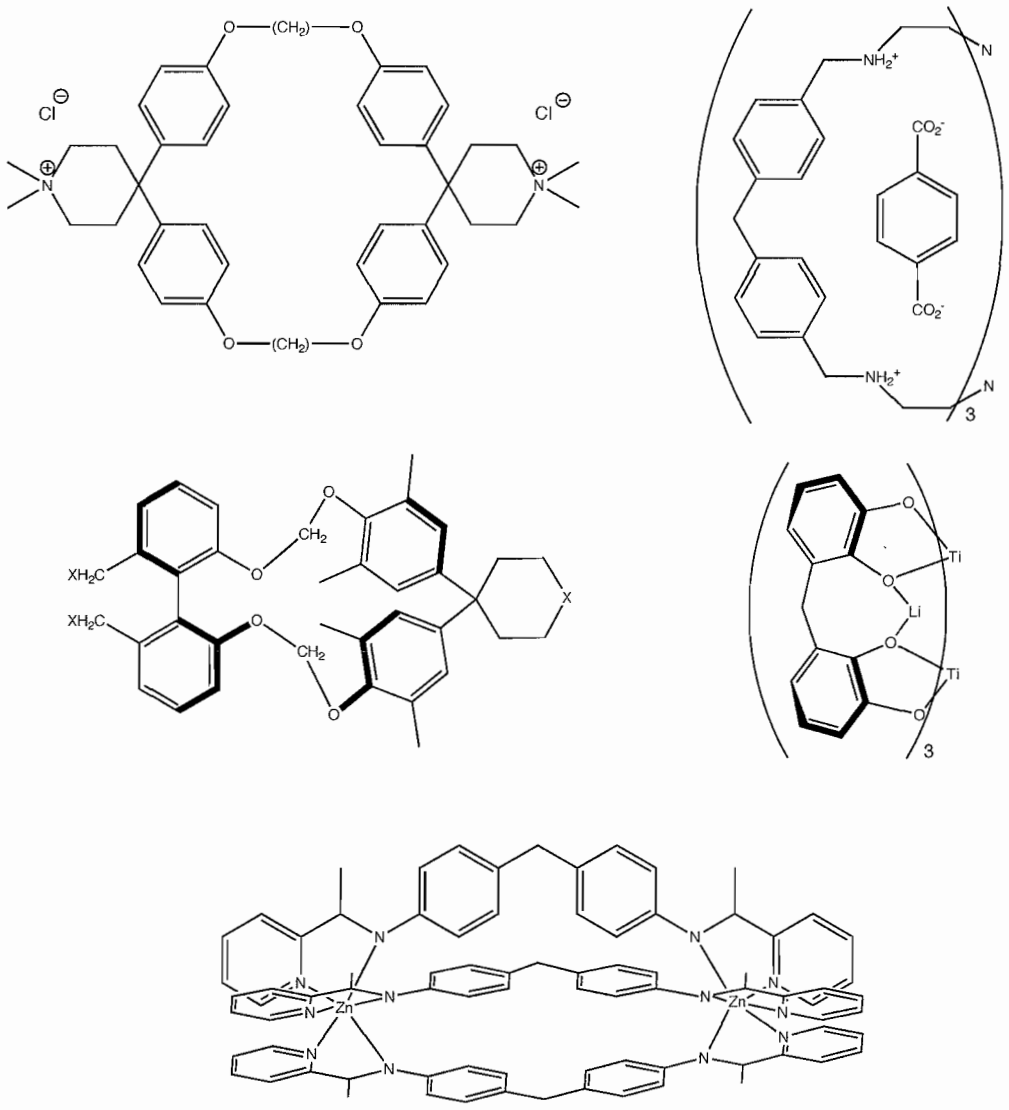

Figure 3.1. Examples of supramolecular hosts containing diphenylmethane. (*a*) and (*b*) are organic cyclophane macrocycles that bind small aromatic molecules – this binding is enhanced by the enforced gable conformation given by back-substitution with piperidine. (*c*) is a crytophane host that is sufficiently capacious to accommodate terephthalate anion through multiple hydrogen bonding contacts. (*d*) is a metallosupramolecular assembly that takes on secondary coordination from Li(I) counterions. (*e*) is a triple stranded helicate with the donor groups located away from the diphenylmethane linked unit.

Synthesis of an As_2L_3 Assembly Bridged by Diphenylmethane

The diphenylmethane scaffold was incorporated into the bisfunctional ligand (4,4'-bis(mercaptomethyl)diphenylmethane) $H_2\mathbf{L}^2$ through modifications of literature methods.[81,82] Diphenylmethane was treated with paraformaldehyde and hydrobromic acid, affording the 4,4'-bis(bromomethyl)diphenylmethane in high yield. This intermediate was then subjected to mercaptodehalogenating conditions, followed by reduction of the thiouronium salt with aqueous base. The corresponding assembly $As_2\mathbf{L}^2_3$ was then prepared (Scheme 3.1) by slow addition of $AsCl_3$ in benzene or THF to a solution of the ligand and potassium hydroxide in methanol.

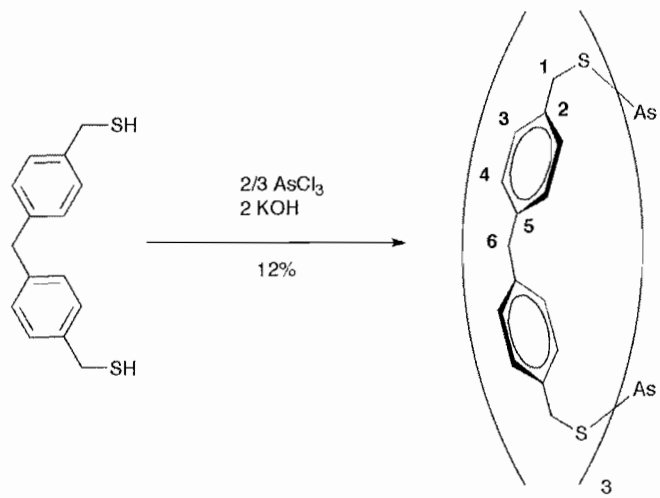

Scheme 3.1. Synthesis of $As_2L^2_3$. The supplied numbering scheme will be used to discuss the dynamic solution behavior of this assembly.

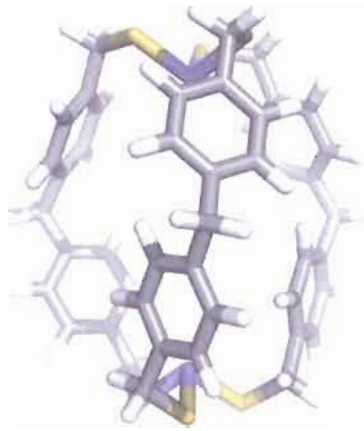

Figure 3.2. Predicted three-dimensional structure of $As_2L^2_3$ based on molecular mechanics (MM3) calculations. These calculations predict a helical assembly of idealized D_{3d} symmetry with a moderately capacious interior.

Slow evaporation of either chloroform or dichloromethane solutions of $As_2\mathbf{L}^2_3$ yielded clear, colorless blocks whose identity was confirmed through X- ray crystallography. The crystal structure of $As_2\mathbf{L}^2_3$ shown in Figure 3.3(*a*) features four close contacts of varying distance between As(III) and the nearest carbon on the phenyl rings of ligand strands $\mathbf{L}^{2a}$ and $\mathbf{L}^{2b}$. This observation is in agreement with calculations showing that the geometry of the As•••π interaction is strong (at least 7.4 kcal/mol) yet has variable directionality.[33] The solid-state structure of this complex is surprisingly distorted in comparison to the geometry predicted by MM3 calculations (Figure 3.2) and the majority of self-assembled metal-ligand complexes that exhibit a high degree of symmetry in both solution and the solid state,[57] including those containing the diphenylmethane spacer.[83] Instead, the three ligands

are unevenly distributed about the metal centers, an arrangement best described as a distorted mesocate, as the -CH_2S- groups maintain opposite twists about the two metal centers. For the purposes of this study, the counterclockwise twisted As(III) center will be described as Λ, while the clockwise As(III) center will be described as Δ. We will therefore refer to the $As_2\mathbf{L}^2{}_3$ assembly as a Δ,Λ mesocate; since the space group $P2_1/n$ is centrosymmetric, an equal amount of the structure shown in Figure 3.3(a) and its mirror image is present. In the view along the As•••As axis in Figure 3.3(b) the Δ twist faces the reader. The angles betweeen the mean planes of the phenyl rings about the Δ metal center are 48.5(1), 49.8(1), and 85.2(1) degrees, while those about the Λ center are 35.1(1), 46.7(1), and 80.9(1) degrees. The rings are twisted so as to direct the edges toward the interior of the complex, effectively filling any empty space inside.

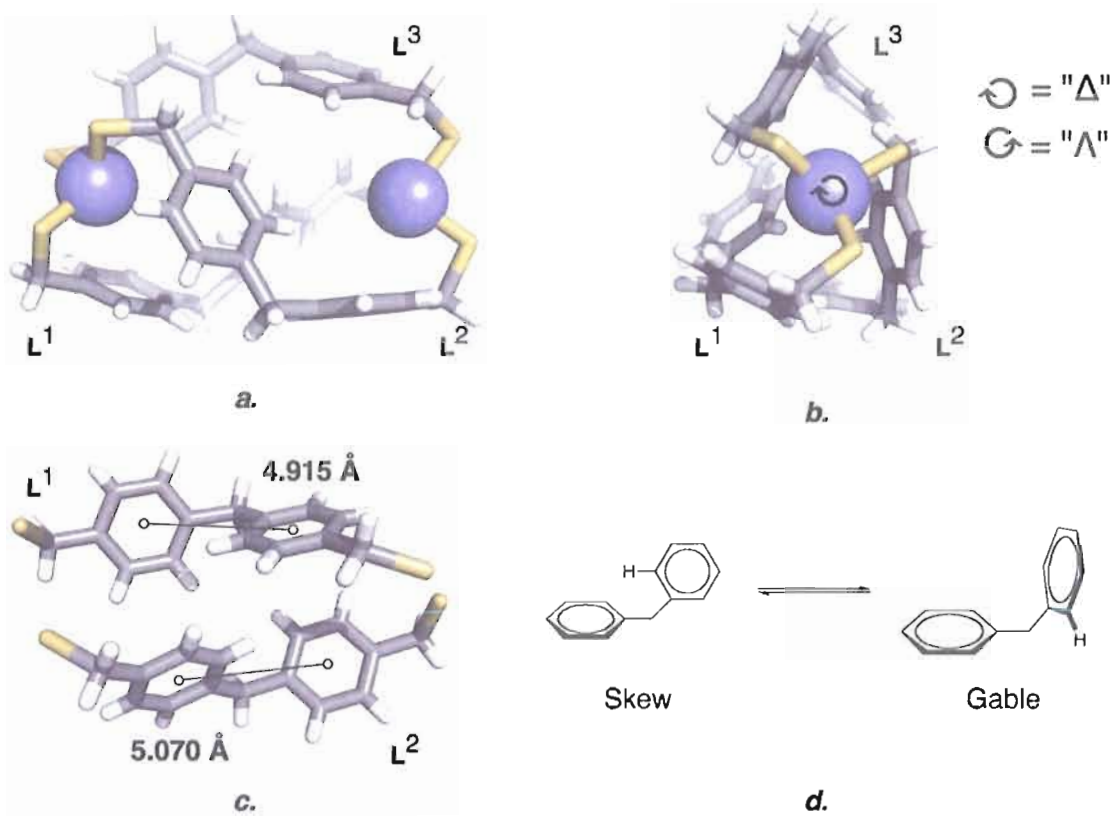

Figure 3.3. Three-dimensional structure of $As_2L^2_3$. (*a*) Crystal structure shown as wireframe; spheres represent arsenic atoms. (*b*) Crystal structure, looking down As•••As axis. Note the Δ axial chirality (clockwise twist) of As(III) facing the viewer. (*c*) Cutaway view of two lower strands showing centroid-centroid distances. (*d*) Schematic of equilibrium between skew (crowded) and gable (remote) geometries in diphenylmethane.

Calculations and long-range NMR couplings have shown that there are two predominant solution conformations of diphenylmethane, defined by the pair of dihedral angles relating the bridging methylene protons and the *ortho* aromatic protons. These conformations have been described as "skew" and "gable"[84,85] (Figure 3.3(*d*)) and are thought to exist in dynamic equilibrium in solution.

Crystalline diphenylmethane, however, is exclusively "skew" – this conformation suggests an attractive intramolecular edge-to-face aromatic interaction. Two ligand strands ($\mathbf{L}^{2a}$ and $\mathbf{L}^{2b}$) exhibit this type of interaction in which the centroids of the rings are near the ideal offset of 5.025 Å, [86] (Figure 3.3(*c*)) in nearly perpendicular skew conformations. The third ligand strand ($\mathbf{L}^{2c}$) is also skew, but not to the same degree as the other two strands. This is a relatively rare example of an "imploded" supramolecular structure similar to the imploded cryptophane observed by Holman *et al.*,[87] which contracts in the absence of an appropriate guest.

DFT Calculations Support Distorted Structure

DFT optimization of $As_2\mathbf{L}^2{}_3$ (with a 6-31+G* basis set for all atoms and the B3LYP functional[88]) produces two remarkably similar minima which differ in energy by only 4.1 kcal/mol (Figure 3.4(*a*) and (*b*)). Neither structure maintains the high degree of symmetry predicted by MM3 calculations. Instead, the phenyl rings are twisted such that the edges point toward the interior of the complex, effectively filling any empty interior space. These calculations predict the "*meso*" $As_2\mathbf{L}_3$ crystal structure with a surprising degree of accuracy: the As•••As distance is underestimated by only 0.11 Å, while the average As•••π distance is overestimated by 0.19 Å (Figure 3.4(*a*)). The calculated structure places $\mathbf{L}^{2a}$ and $\mathbf{L}^{2b}$ in nearly perpendicular skew arrangements with centroid offsets of 4.96 and 5.01 Å, in almost perfect agreement with the observed distances. The strong agreement between the

calculated structure and the crystal structure is a powerful indicator that the distorted structure is not merely an artifact of crystal packing forces, but is instead the result of a combination of supramolecular interactions.

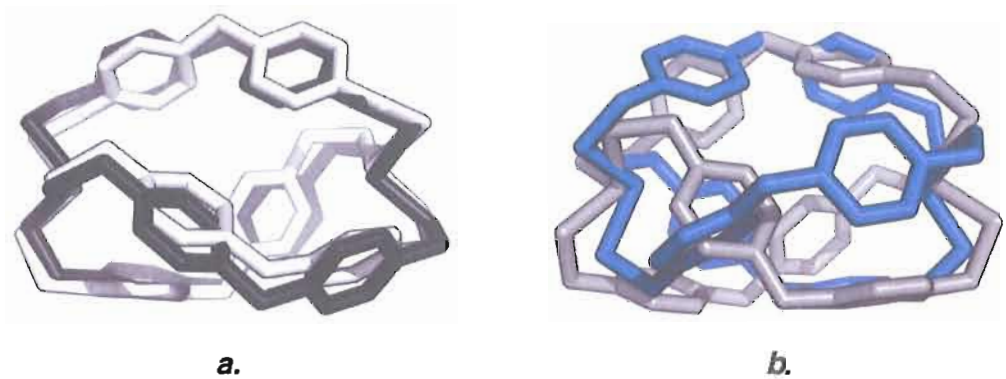

Figure 3.4. Overlays of DFT optimized geometry for $As_2L^2_3$ mesocate with crystal structure and optimized helicate geometries. (*a*) DFT geometry of mesocate (black) is overlaid with the crystal structure of $As_2L^2_3$ (gray). (*b*) DFT geometry of helicate form of $As_2L^2_3$ (blue) and crystal structure (gray). The starting geometry for (*a*) was obtained from the crystal structure, while the starting geometry for (*b*) was obtained from the MM3 minimized structure in Scheme 3.1.

$As_2L^2_3$ and Solution Stability

$As_2L^2_3$ is remarkably stable in solution: no ligand exchange is observed with free ligand and the intact assembly can be ionized from solution with APCI-MS. The ^{1}H NMR spectrum is surprisingly uncomplicated at room temperature – singlets are observed for both H1 and H6 (Figure 3.5; see Scheme 3.1 for numbering). In addition, there is accidental chemical shift degeneracy for H3 and H4 as evidenced by the presence of a singlet resonance in the aromatic region instead of the expected

set of two doublets. The ^{13}C NMR spectrum showed a similar degeneracy for C3 and C4.

These uncomplicated spectra indicate dynamic solution behavior on the NMR timescale. The simple aromatic region indicates that the phenyl rings rotate rapidly, and the singlet observed for H6 shows that the solution structure cannot be a static Δ,Λ mesocate at the As(III) centers. There must therefore be fast interconversion between Δ_1,Λ_2 and Λ_1,Δ_2 isomers on the NMR timescale, either by simultaneous interconversion or through a Δ_1,Δ_2 or Λ_1,Λ_2 intermediate with a lifetime too short to observe.

Conformational Equilibrium Based on Intramolecular CH•••π Interactions

In order to resolve the discrepancy between the solid and solution phase data, variable temperature NMR experiments were carried out. No resolution of either set of methylene protons was observed even at -80 °C (in contrast to other diphenylmethane bridged supramolecular systems[83]), but a strong upfield shift was observed for one aromatic proton, lifting the accidental degeneracy of H3 and H4. H1 also displayed a noticeable upfield shift as the temperature was decreased, consistent with a weak contact with a neighboring aromatic ring observed in the crystal structure. The accidental degeneracy in carbon signals C3 and C4 was also lifted as the temperature decreased. Returning the sample to room temperature reversed the chemical shift change and returned the aromatic protons to their

coincidentally degenerate state. In contrast, VT-NMR experiments with the original phenylene spaced assembly[33] ($As_2\mathbf{L}^1_3$, Figure 3.5) showed no appreciable changes at lowered temperature. This is a strong indication that the changes in the NMR spectra are related to changes in conformation along the diphenylmethane spacer rather than activity about the As(III) centers.

The identity of the upfield shifted aromatic proton was confirmed as H3 by low-temperature HMBC and HMQC spectra (see experimental details). Similar flexible molecules capable of intramolecular edge-to-face aromatic interactions are known to interconvert rapidly between "crowded" and "remote" limiting geometries on the NMR time scale at experimentally accessible temperatures. In that analysis, lower temperatures favor a more crowded geometry, enhancing edge-to-face aromatic interactions and a contracted structure. At higher temperatures, entropy apparently disfavors the edge-to-face interaction, promoting a more remote geometry and an expanded structure; intermediate conformations would be expected over the observed temperature range. In either case, the conformations exist in a fast equilibrium; the observed NMR shift is a weighted average of the populations of all conformers present.[89] For $As_2\mathbf{L}^2_3$, the remote geometry corresponds to a gable-like conformation of the diphenylmethane spacer at room temperature, while the crowded geometry observed at lowered temperatures corresponds to a more skew-like conformation.

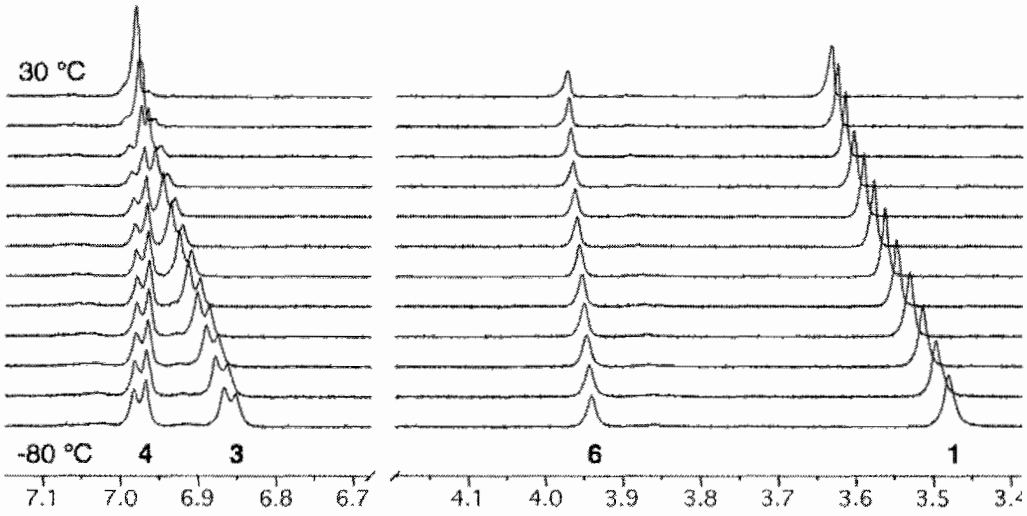

Figure 3.5. VT-NMR of $As_2L^2_3$ in CD_2Cl_2. Spectra are referenced to residual solvent signal and are taken at 10 °C intervals. The presence of singlets for both pairs of diastereotopic protons indicates that conformational interconversion is fast on the NMR time scale.

Edge-to-Face Aromatic Interactions

While interactions between arene rings are generally relatively weak in energetic terms, they frequently play a supporting role in determining the overall structure of larger macromolecular assemblies. The crystal structure of benzene is the classic example of the edge-to-face interaction; individual benzene units stack in a "herringbone" fashion, where the edge of one benzene ring interacts with the face of a neighboring ring.

The overall structures of many small, flexible organic molecules are stabilized by the presence of these weak edge-to-face aromatic interactions. This stabilization has been demonstrated for both acyclic and macrocyclic organic

compounds, and in some cases can be quantified in solution. The first example of this was shown by Jennings *et al.*,[90] in which an aromatic proton displayed a rather unexpected upfield NMR shift; the X-ray structure of this compound revealed that this proton was located in close proximity to a second arene ring. The location of this proton was exquisitely sensitive to temperature – rotation of the benzyl group away from the naphthyl group at elevated temperatures shifted the proton downfield, away from the shielding zone. Linkages containing imines, alkenes, and nitrones were all found to exhibit this behavior in solution. Other common examples of temperature sensitive edge-to-face aromatic interactions are found in cyclophanes and macrocyclic crown ethers,[91] as well as Wilcox's molecular "torsion balance" (Figure 3.6(*a*))[92] Several examples of these structures are shown in Figure 3.6(*b*) and (*c*).

Alkyl CH•••π contacts have also been observed, though not in the same frequency as aryl contacts. [86] As an upfield shift for H1 of $As_2\mathbf{L}^2_3$ is also observed, and a close contact is observed in the crystal structure, it seems likely that the structure of this complex at lower temperature also features an interaction between the benzylic protons and neighboring arene rings.

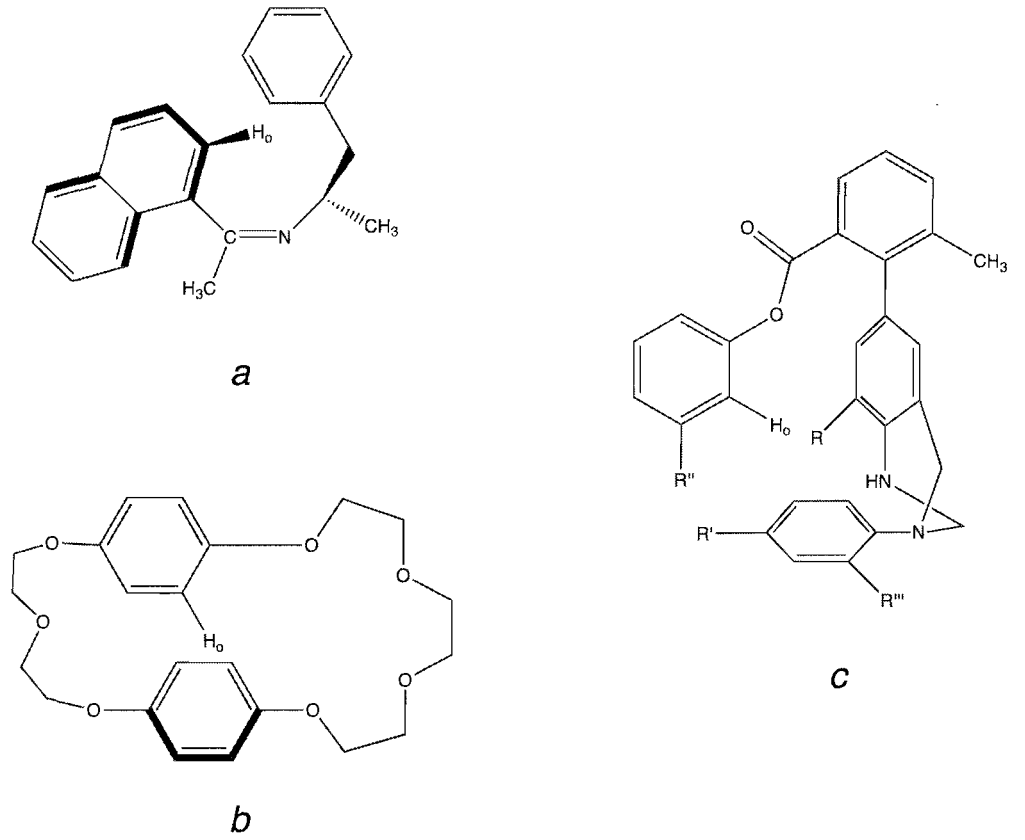

Figure 3.6. Examples of edge-to-face aromatic interactions. The proton involved in the intramolecular edge-to-face interaction is designated as Ho. (*a*) Acyclic imine. Analogous structures bearing alkene and nitrone linkages are also known. (*b*) Example of macrocyclic crown ether structure. (*c*) Wilcox's molecular torsion balance. (**R–R'''** are alkyl and alkoxy substituents.)

The chemical shifts of protons involved in edge-to-face aromatic interactions are frequently temperature dependent, due to fast equilibrium between "crowded" structures containing the interaction and "remote" structures without the interaction. The observation of this effect in $As_2\mathbf{L}^2_3$ again is strong evidence that the edge-to-face interactions observed in the crystal structure persist in solution.

Open-Closed Equilbrium Based on Edge-to-Face Interactions

The conformational interconversion observed for $As_2\mathbf{L}^2_3$ can be expressed in terms of the equilibrium between "open" and "closed" conformations, in which the "closed" conformation contains the edge-to-face interactions and the "open" conformation does not:

$$As_2\mathbf{L}^2_{3,closed} \rightleftharpoons As_2\mathbf{L}^2_{3,open}$$

A nonlinear curve-fitting procedure (Appendix A) was employed to extract thermodynamic parameters from the variable temperature NMR data. As these subtle edge-to-face interactions are frequently quite sensitive to nature of the solvent in which they are studied, the thermodynamic parameters in for the interconversion between the open and closed conformations of $As_2\mathbf{L}^2_3$ were determined in other chlorinated solvents are varying size. These results are summarized in Table 3.x and are based on the upfield shift of H3 in each solvent. Since the complex has effective threefold symmetry about the As•••As axis and time-averaged symmetry across the Ar-CH_2-Ar mirror plane, each CH•••π interaction is contributes 1/6 toward the total stabilization energy. The general trend is that as solvent size increases, the equilibrium moves toward the "open" conformation.

$\Delta H°$ and $\Delta S°$ increase steadily as the solvent size is increased – there is a small change in both parameters when moving from CD_2Cl_2 to $CDCl_3$. When the

solvent size is nearly doubled between CD_2Cl_2 and $CDCl_2CDCl_2$, there is a larger increase in both the enthalpy and entropy contributions. The slight drop in $\Delta G°$ between CD_2Cl_2 and $CDCl_3$ despite the increase in the magnitude of $\Delta H°$ and $\Delta S°$ is the result of the unfavorable enthalpy for the equilibrium increasing faster than the favorable entropy term. This enthalpy/entropy compensation is probably of the "strong" variety, as it is observed in response to varying some external variable (here, the size of the solvent molecule). Despite the relatively subtle effects of this enthalpy/entropy compensation there does appear to be a correlation between the size of the solvent and the ability of the $As_2\mathbf{L}^2_3$ assembly to breathe in solution. At room temperature in the two smaller solvents, the assembly is estimated to be approximately 45-47% in the closed conformation. In $CDCl_2CDCl_2$, however, the assembly is calculated to be only 25% in the closed conformation. This can alternately be viewed as the complex being 75% open in the larger solvent, pointing to the more likely possibility of guest encapsulation when the solvent encourages the complex to adopt a conformation with an expanded interior. One possible explanation for the preference toward the open conformation in the larger solvent is that when the complex is "closed" due to the presence of edge-to-face aromatic interactions, the smaller CD_2Cl_2 and $CDCl_3$ are able to better solvate the exposed exterior edges of the arene rings. Given the larger size of $CDCl_2CDCl_2$, the exposed edges are likely to be more poorly solvated, encouraging the assembly to rotate the

Table 3.1. Thermodynamic parameters for closed-open equilibrium of $As_2L^2_3$ in CD_2Cl_2, $CDCl_3$, and $CDCl_2CDCl_2$ based on the chemical shift changes associated with H3. Due to the time-averaged D3h symmetry of $As_2L^2_3$ at experimentally accessible temperatures, six CH•••π contacts contribute to the overall free energy change.

Solvent	*ΔH° (kcal/mol)*	*ΔS° (cal/mol K)*	*ΔG° (kcal/mol, 298 K)*	*K (298 K)*
CD_2Cl_2	2.1	7.5	-0.11	1.2
$CDCl_3$	2.8	9.5	-0.07	1.0
$CDCl_2CDCl_2$	3.5	13.7	-0.64	2.97

rings out slightly to "smooth" the surface of the complex and minimize the exposed surface area.

These NMR experiments show that the CH•••π interaction is conserved in solution, and that while it is a relatively low-energy interaction, it does play a role in determining the solution structure of $As_2\mathbf{L}^2_3$. The high symmetry of the complex even at the lowest accessible temperatures indicates that this process is dynamic and fast on the NMR time scale, as only two resonances are ever observed in the aromatic region and one for each of the methylene groups.

Summary and Conclusions

In summary, weak forces such as edge-to-face aromatic and arsenic•••π interactions play an important role in determining the solution and solid-state structures of supramolecular complexes. In particular, the arsenic•••π interaction appears to persist in the presence of flexible ligand scaffolds, showing that it is an

important component of arsenic ligand design and can itself be considered an emerging supramolecular interaction. The varying strength and geometry in the crystal structure and the temperature dependence of these weak aromatic interactions in solution have been shown to dramatically affect the structure of a new $As_2\mathbf{L}_3$ assembly with a flexible ligand scaffold. In particular, we have observed expansion and contraction or "breathing" of $As_2\mathbf{L}^2{}_3$ in solution over a range of temperatures and solvents. This may have significant implications in the design of expanded arsenic-containing host structures – the addition of conformationally mobile spacer units may play a role in determining the size, shape, and exchange mechanism of guests. The use of larger solvents such as $CDCl_2CDCl_2$ to study assemblies such as $As_2\mathbf{L}^2{}_3$ in solution may have two important benefits: the larger solvent appears to stabilize the assembly in the open conformation, and the significant size of the solvent should preclude any complications arising from solvent competition with potential guests.

Experimental Details

General Information

Starting materials and reagents were obtained from commercial sources and used without further purification unless otherwise noted. NMR spectra were obtained on Varian 300 MHz, 500 MHz, and 600 MHz spectrometers as noted; chemical shifts are reported in parts per million (ppm) downfield from tetramethylsilane and referenced to residual solvent as an internal standard. X-ray diffraction data were collected at 173 K on a Bruker Apex diffractometer using MOKα-radiation (λ=0.71073 Å). Mass spectra were recorded using an Agilent 1100 Series LC/MSD. Absorption corrections were applied by SADABS. All structures were determined by direct methods and refined on F^2 by a full-matrix least-squares procedure. All non-H atoms were refined with anisotropic thermal parameters. H atoms were refined in calculated positions in a model of a rigid group. All calculations were performed by the Bruker SHELXTL 6.10 package (SHELXTL, version 6.10, Bruker AXS, Inc., Madison, WI, 2000).

Ligand Syntheses

4,4'-Bis(bromomethyl)diphenylmethane: Diphenylmethane (3.03 g, 18 mmol) and paraformaldehyde (1.08 g) were combined with 30 mL HBr (33% in HOAc) at room temperature. $ZnBr_2$ (6 g, 27 mmol) was slowly added and the mixture heated to 95° C overnight. After cooling to room temperature, the off-white solid material

was filtered and washed with water. Recrystallization from benzene yielded the intended product as a white, microcrystalline solid (3.97 g, 62%). ^{1}H NMR (300 MHz; $CDCl_3$) 7.22 (4H, d, J = 8.1 Hz), 7.11 (4H, d, J = 8.1 Hz), 3.92 (2H, s), 3.70 (4H, s).

4,4'-Bis(mercaptomethyl)diphenylmethane (H_2L^2): 4,4'-bis(bromomethyl)-diphenylmethane (0.616 g, 1.74 mmol) was slurried in 15 mL EtOH and thiourea (0.288 g, 3.78 mmol) was added. The mixture was heated to 70 °C for 16 hours, then cooled to room temperature and concentrated to half the original volume. Diethyl ether was added to precipitate a white solid, which was filtered and washed with additional ether, then air-dried to yield the dithiouronium bromide salt (2, 0.679 g, 75%). Under nitrogen atmosphere, 2 (0.177 g, 0.35 mmol) was treated with aqueous NaOH (2N, 10 mL) and heated to 100 °C for 2 hours. After cooling to room temperature, the reaction mixture was washed with degassed diethyl ether, then acidified with concentrated HCl. The aqueous mixture was then extracted three times with ether, then concentrated in vacuo to yield $H_2\mathbf{L}^2$ as white solid (88 mg, 96%) ^{1}H NMR: ($CDCl_3$, 300 MHz) 7.22 (4H, d, J = 8.1 Hz), 7.11 (4H, d, J = 8.1 Hz), 3.92 (2H, s), 3.70 (4H, d, J = 7.5 Hz), 1.72 (2H, t, J = 7.5 Hz).

4,4'-Bis(bromomethyl)benzophenone: 4,4'-dimethylbenzophenone (0.292 g, 1.39 mmol) was combined with *N*-bromosuccinimide (0.742 g, 4.17 mmol) and benzoyl peroxide (36 mg) and placed under N_2 atmosphere. 12 mL dry, degassed chloroform was added to this mixture and heated to reflux for 5 hours, then cooled

to room temperature and placed in an ice bath to cool further. The small amount of pale yellow precipitate was filtered and washed with 2 N HCl, then 2 N NaOH. The orange organic layer was then separated and washed twice with 2 N HCl, then twice with 2 N NaOH, dried with Na_2SO_4, and the solvent removed to obtain the white solid product (0.437 g, YIELD). ^{1}H NMR ($CDCl_3$, 300 MHz): 7.78, 4H, d, J = 8.1 Hz; 7.51, 4H, d, J = 8.1 Hz; 4.54, 4H, s.

4,4'-Bis(mercaptomethyl)benzophenone: 4,4'-Bis(bromomethyl)benzophenone (amount) was dissolved in ethanol (10 mL) and thiourea (250 mg) was added. The mixture was heated to 70° C overnight, then cooled to room temperature and concentrated until ca. 0.5 mL solution remained. This was triturated with diethyl ether to obtain a sticky, light yellow solid material. The solid was placed under nitrogen atmosphere, then dissolved in 15 mL degassed 2 N NaOH and brought to reflux for 2.5 hours. The reaction mixture was cooled to room temperature, then acidified with concentrated HCl, extracted three times with dichloromethane, dried with Na_2SO_4, filtered, and the solvent removed in vacuo to yield a yellow solid material. ^{1}H NMR ($CDCl_3$, 300 MHz): 7.76, 4H, d, J = 8.4 Hz; 7.44, 4H, d, J = 8.4 Hz; 3.81, 4H, d, J = 7.8 Hz; 1.83, 2H, t, J = 7.8 Hz.

Synthesis of As_2L_3 Assemblies

$As_2L^2_3$ (Method 1): Degassed KOH (0.1023 N in MeOH) was added to H_2L^2 under N_2. The solution was heated to 50 °C and a solution of $AsCl_3$ in benzene was added

dropwise. Heating was continued for 3 hours, then filtered to remove the white precipitate that formed. The solvent was removed *in vacuo* to yield 12% of the desired product. ^{1}H NMR (500 MHz; CD_2Cl_2; -20 °C): δ 7.03 (d, J = 7.5 Hz, 12H), 6.98 (d, J = 7.5 Hz, 12H), 4.01 (s, 6H), 3.62 (s, 12H). ^{13}C NMR (125 MHz; CD_2Cl_2; -20 °C): δ 140.45, 138.00, 129.71, 129.56, 41.28, 35.94; APCI-MS found m/z 924.8, calc. 924.00.

$As_2L^2_3$ (Method 2): H_2L^2 was dissolved in THF and treated with 2/3 equivalent $AsCl_3$ and allowed to stir at room temperature for 2 hours. Saturated aqueous Na_2CO_3 was then added and the solution stirred vigorously for 15 minutes, then extracted three times with CH_2Cl_2, dried with Na_2SO_4, and concentrated *in vacuo* to yield $As_2L^2_3$.

$As_2L^2_3$ (Method 3): H_2L^2 was dissolved in dry THF and treated with 2/3 equivalent $AsCl_3$, then stirred at room temperature for two hours. To this mixture was then added 2/3 equivalent diisopropylethylamine (DIPEA) and stirred for 2 more hours. The solution was diluted with water, then extracted three times with CH_2Cl_2, dried, and concentrated *in vacuo* to yield $As_2L^2_3$.

Crystallographic Data

Crystal data for $As_2L^2_3$: $C_{45}H_{42}As_2S_6$, M_r = 942.99, 0.18 x 0.14 x 0.08 mm, monoclinic, P21/n, a = 14.5184(16) Å, b = 12.9661(14) Å, c = 23.094(3) Å, β = 106.773(2)°, V = 4162.3(8) Å^3, Z = 4, ρ_{calcd} = 1.476 g cm^{-1}, μ = 1.939 mm^{-1}, $2\theta_{max}$ = 54.00°, T = 173(2)

K, 37996 measured reflections, 9082 independent reflections [R_{int} = 0.0644], 478 parameters, *R*1 and *wR*2 = 0.0414 and 0.0835($I > 2\sigma(I)$); 0.0678 and 0.0954 (all), GOF = 1.013 for all 9082 reflections, max/min residual electron density +0.483/-0.340 e Å^{-3}. CCDC 685997.

2-Dimensional NMR Spectra

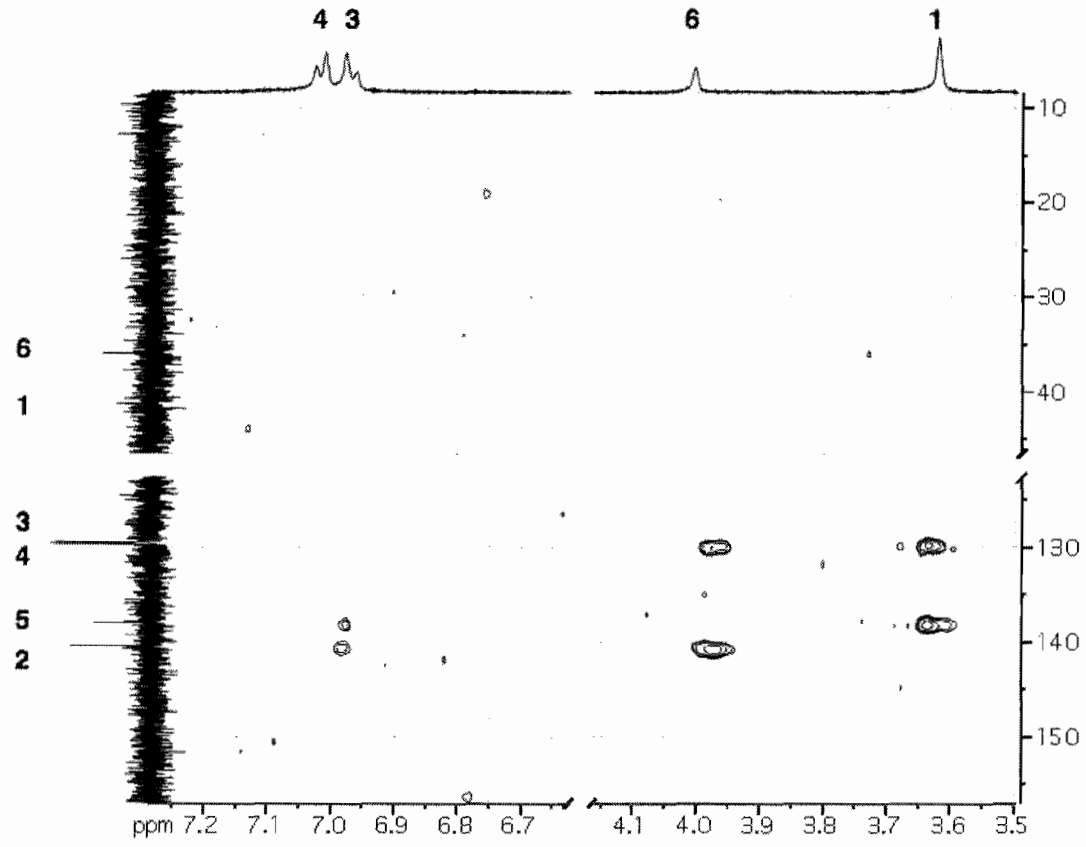

Figure 3.7. gHMBC of $As_2L^2_3$ (CD_2Cl_2, 500 MHz, -20 °C). Correlations H3-C5 and H4-C2 establish connectivity on the aromatic scaffold.

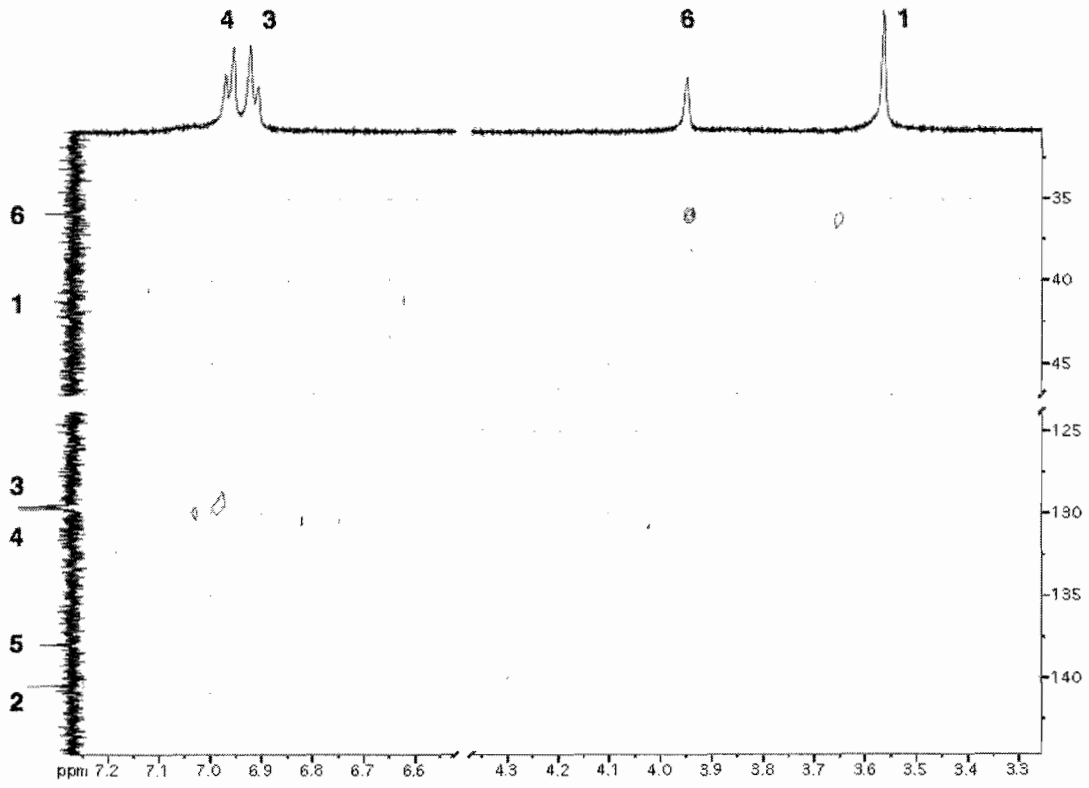

Figure 3.8. gHMQC of $As_2L^2_3$ (CD_2Cl_2, 500 MHz, -20 °C). H3-C3 and H4-C4 correlations establish connectivity on aromatic scaffold.

Variable Temperature NMR Spectra

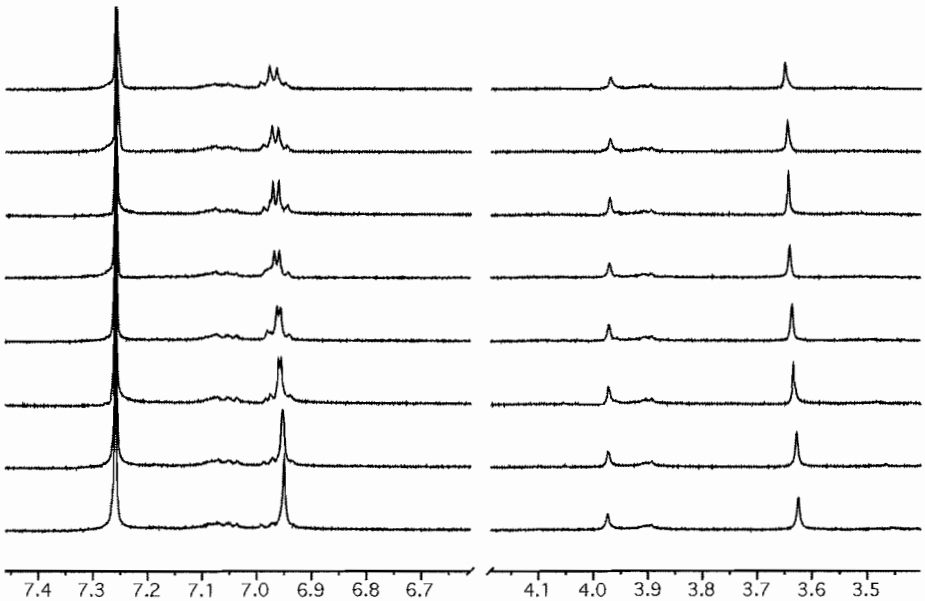

Figure 3.9. Variable temperature ^{1}H NMR of $As_2L^2_3$ in $CDCl_3$.

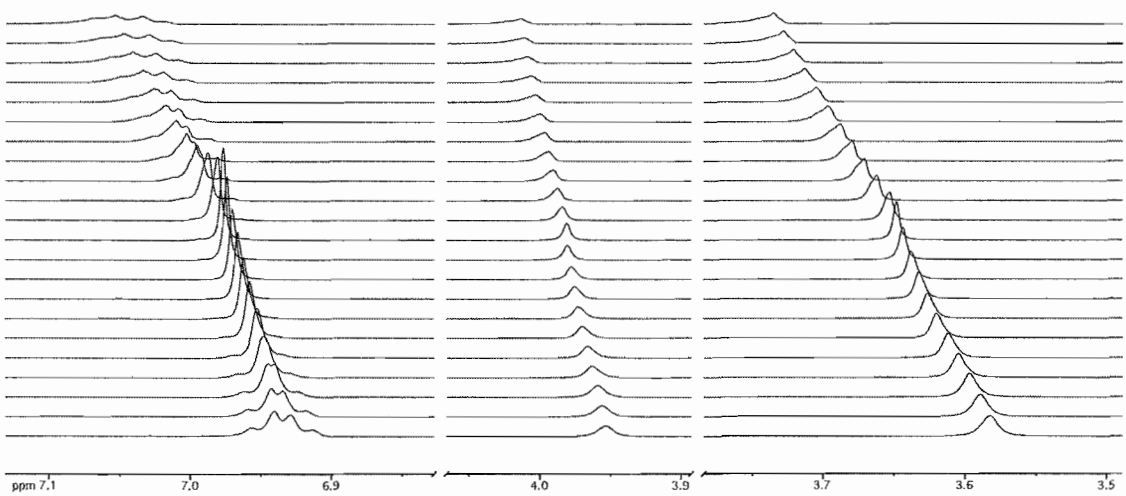

Figure 3.10. Variable temperature ^{1}H NMR of $As_2L^2_3$ in $CDCl_2CDCl_2$.

Thermodynamic Parameters

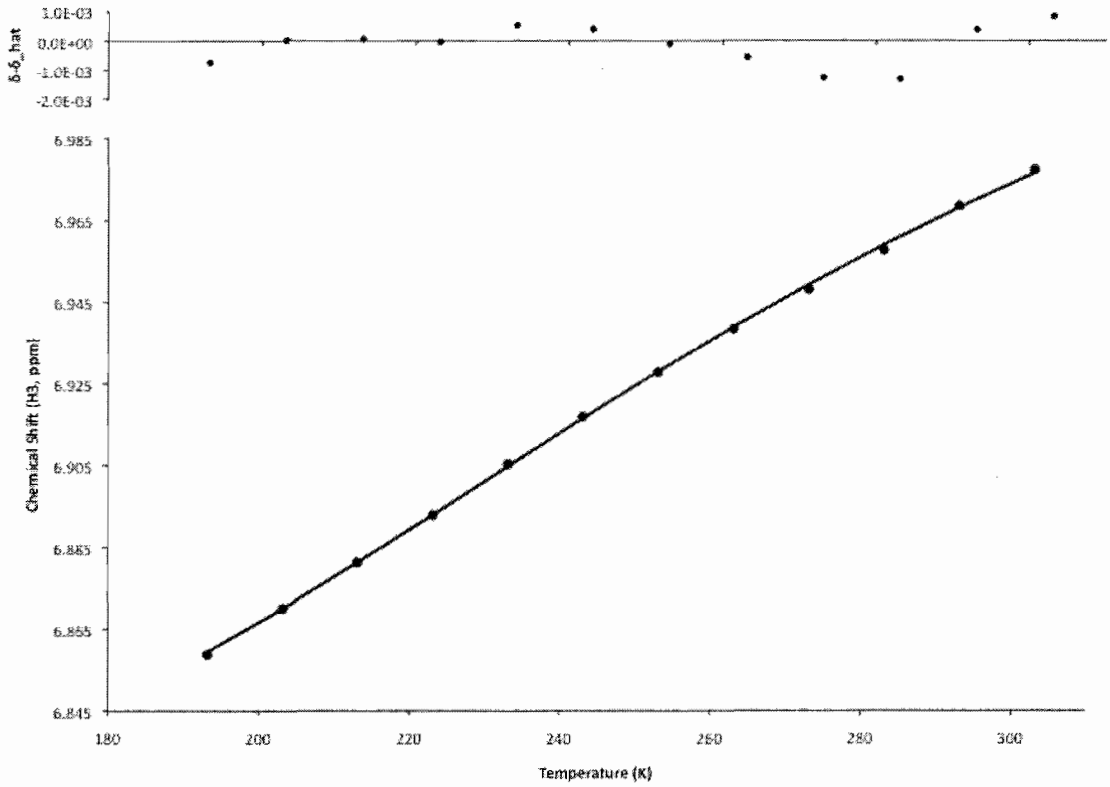

Figure 3.11. Chemical shift of H3 in $As_2L^2_3$ as a function of temperature in CD_2Cl_2. Marked data points represent experimental data, while the solid line represents calculated chemical shifts. Residuals (δ-δ_hat) are plotted above.

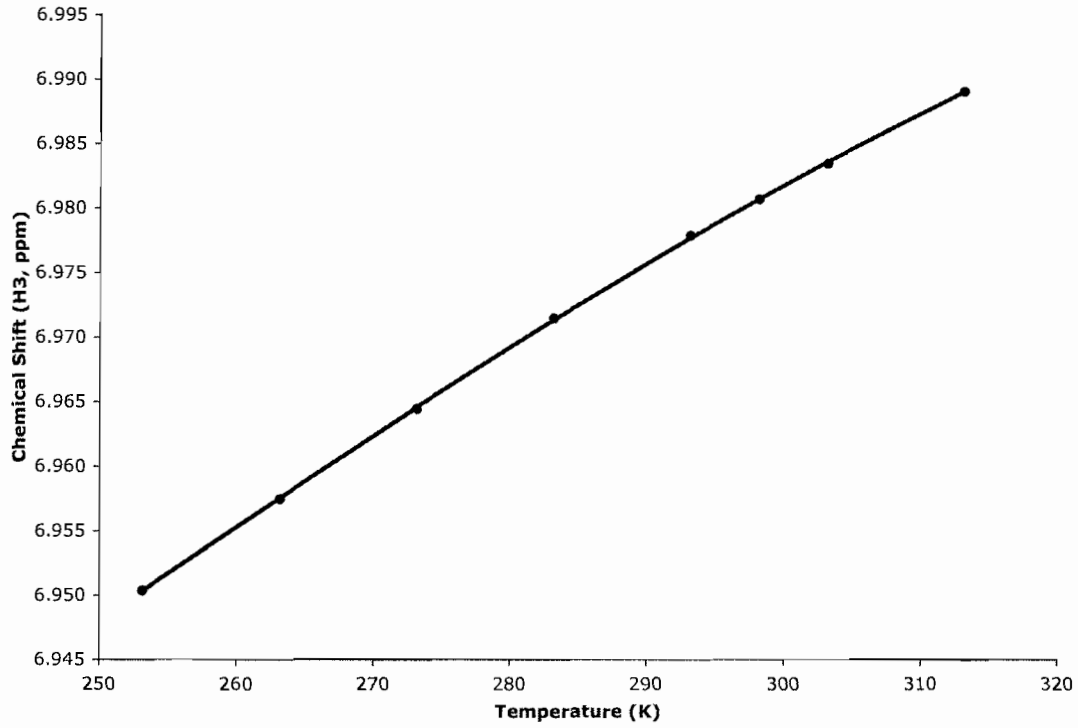

Figure 3.12. Observed and calculated chemical shifts for H3 of $As_2L^2_3$ in $CDCl_3$. Experimental values are shown as solid circles and the calculated values are shown as the solid line. Residuals are plotted above.

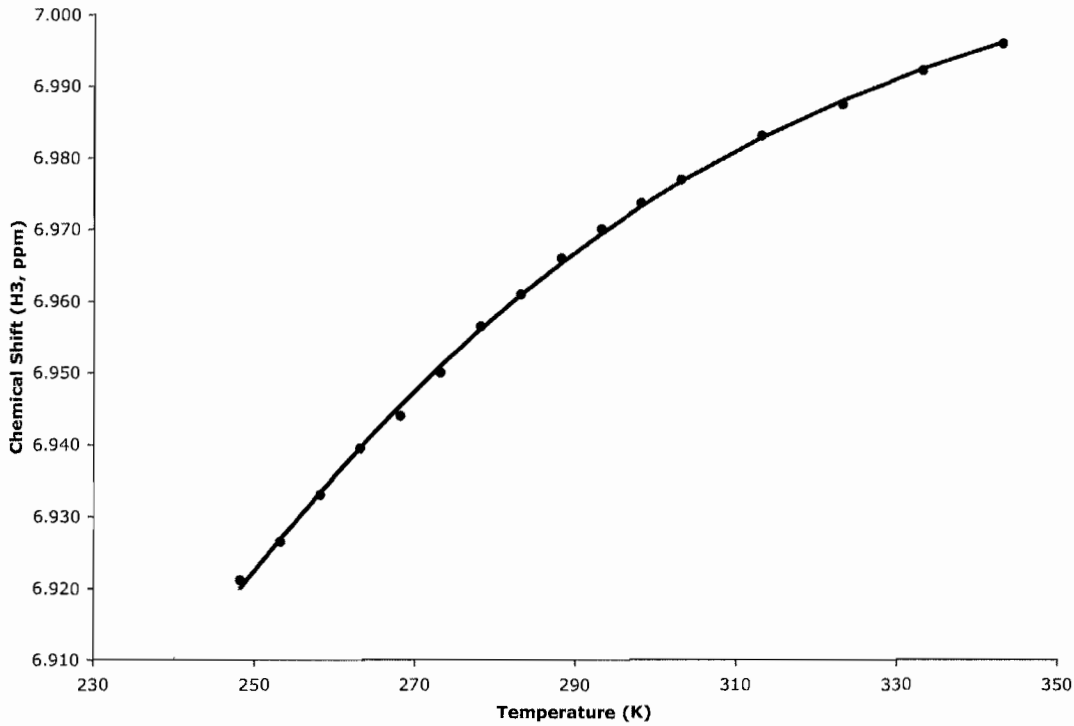

Figure 3.13. Observed and calculated chemical shifts for H3 of $As_2L^2{}_3$ in $CDCl_2CDCl_2$. Experimental values are shown as solid circles and the calculated values are shown as the solid line. Residuals are plotted above.

Table 3.2. Observed chemical shift of H3 and derived values for P_c, $\hat{\delta}$, and K for $As_2L^2{}_3$ in CD_2Cl_2.

Temperature (K)	$\delta_{observed}$	P_c	$\hat{\delta}$	K
193	6.859	0.854	6.859	0.17
203	6.870	0.817	6.870	0.22
213	6.881	0.777	6.881	0.29
223	6.893	0.736	6.893	0.36
233	6.905	0.694	6.905	0.44
243	6.917	0.653	6.917	0.53
253	6.928	0.612	6.928	0.63
263	6.938	0.574	6.939	0.74
273	6.948	0.537	6.949	0.86
283	6.958	0.502	6.959	0.99
293	6.969	0.470	6.968	1.13
303	6.977	0.440	6.977	1.27

Table 3.3. Observed chemical shift of H3 and derived values for P_c, $\hat{\delta}$, and K for $As_2L^2{}_3$ in $CDCl_3$.

Temperature (K)	$\delta_{observed}$	P_c	$\hat{\delta}$	K
253	6.950	0.670	6.950	0.49
263	6.958	0.623	6.958	0.61
273	6.965	0.577	6.965	0.73
283	6.972	0.533	6.971	0.88
293	6.978	0.491	6.978	1.04
298	6.981	0.471	6.981	1.12
303	6.984	0.452	6.984	1.21
313	6.989	0.416	6.989	1.40

Table 3.4. Observed chemical shift of H3 and derived values for P_c, $\hat{\delta}$, and K for $As_2L^2{}_3$ in $CDCl_2CDCl_2$.

Temperature (K)	$\delta_{observed}$	P_c	$\hat{\delta}$	K
248	6.921	0.520	6.920	0.92
253	6.927	0.486	6.927	1.06
258	6.933	0.453	6.933	1.21
263	6.940	0.421	6.940	1.37
268	6.944	0.392	6.945	1.55
273	6.950	0.364	6.951	1.75
278	6.957	0.338	6.956	1.96
283	6.961	0.314	6.961	2.19
288	6.966	0.291	6.965	2.44
293	6.970	0.270	6.969	2.70
298	6.974	0.251	6.973	2.98
303	6.977	0.234	6.977	3.28
313	6.983	0.202	6.983	3.94
323	6.988	0.176	6.988	4.68
333	6.992	0.154	6.992	5.50
343	6.996	0.135	6.996	6.40

DFT Calculations

DFT calculations were performed with the Gaussian 2003 package using the 6-31+G* basis set for all atoms and the B3LYP functional.

Table 3.5. Atomic Coordinates for (Δ,Δ)-$As_2L^2_3$ DFT Geometry.

Atom	X	Y	Z	Atom	X	Y	Z
C	3.021	2.053	-2.682	H	0.003	-4.8	-3.017
C	1.714	1.731	-3.076	S	5.459	0.858	-1.745
C	0.649	2.586	-2.797	S	5.592	-1.442	0.836
C	0.846	3.776	-2.082	S	4.943	1.841	1.376
C	2.152	4.098	-1.697	C	-1.366	4.008	-0.813
C	3.227	3.256	-1.995	C	-0.933	-2.974	-2.401
H	1.525	0.802	-3.611	C	-1.638	-0.996	3.736
H	-0.354	2.311	-3.117	C	-2.996	-1.221	4.021
H	2.337	5.016	-1.141	C	-3.822	-1.9	3.127
H	4.227	3.524	-1.667	C	-3.315	-2.382	1.909
C	4.147	1.104	-3.032	C	-1.966	-2.147	1.62
H	3.737	0.129	-3.309	C	-1.141	-1.458	2.513
H	4.717	1.472	-3.895	H	-3.409	-0.868	4.965
C	-0.33	4.663	-1.721	H	-4.871	-2.049	3.372
H	-0.835	4.997	-2.638	C	-4.184	-3.106	0.915
H	0.046	5.575	-1.238	H	-1.554	-2.49	0.674
C	0.628	0.09	4.309	H	-0.101	-1.289	2.254
C	1.685	-0.826	4.38	C	-2.721	4.366	-0.908
C	2.969	-0.479	3.953	C	-3.678	3.81	-0.06
C	3.237	0.801	3.45	C	-3.312	2.88	0.925
C	2.176	1.714	3.361	C	-1.962	2.513	1.011
C	0.896	1.366	3.791	C	-1.004	3.067	0.158
H	1.506	-1.822	4.781	H	-3.033	5.088	-1.661
H	3.774	-1.205	4.029	H	-4.723	4.091	-0.172
H	2.358	2.711	2.965	C	-4.325	2.273	1.863
H	0.095	2.099	3.73	H	-1.654	1.777	1.75
C	-0.763	-0.29	4.77	H	0.033	2.758	0.252
H	-0.682	-0.944	5.65	C	-2.136	-3.159	-3.106
H	-1.287	0.61	5.118	C	-2.988	-2.089	-3.374
C	4.65	1.188	3.088	C	-2.662	-0.789	-2.957
H	5.333	0.353	3.262	C	-1.468	-0.606	-2.25
H	4.992	2.021	3.715	C	-0.618	-1.681	-1.971
C	4.002	-3.1	-0.88	H	-2.404	-4.154	-3.454
C	3.611	-3.022	-2.225	H	-3.919	-2.265	-3.909
C	2.323	-3.385	-2.622	C	-3.562	0.386	-3.239
C	1.379	-3.83	-1.687	H	-1.197	0.386	-1.899
C	1.772	-3.907	-0.343	H	0.303	-1.498	-1.428

Table 3.5 (continued)

Atom	X	Y	Z	Atom	X	Y	Z
C	3.06	-3.548	0.056	H	-3.824	1.678	2.632
H	4.328	-2.687	-2.972	H	-4.909	3.05	2.37
H	2.046	-3.316	-3.672	S	-5.636	1.208	1.074
H	1.058	-4.252	0.403	H	-3.567	-3.583	0.15
H	3.335	-3.607	1.107	H	-4.784	-3.882	1.403
C	5.413	-2.733	-0.486	S	-5.457	-2.055	0.036
H	5.944	-3.597	-0.068	H	-3.021	1.324	-3.093
H	5.974	-2.391	-1.36	H	-3.929	0.363	-4.271
C	-0.032	-4.174	-2.116	S	-5.13	0.473	-2.225
H	-0.5	-4.797	-1.34	As	-4.277	-0.116	-0.194
				As	4.178	0.167	0.017

Table 3.6. Atomic Coordinates for (Δ,Λ)-$As_2L^2{}_3$ DFT Geometry

Atom	X	Y	Z	Atom	X	Y	Z
C	-0.49	2.751	-1.501	C	1.197	-1.544	-1.855
C	-0.801	4.081	-1.201	C	2.204	-1.937	-2.747
C	-2.123	4.509	-1.414	C	2.094	-3.198	-3.35
C	-3.095	3.641	-1.901	C	1.025	-4.043	-3.052
C	-2.778	2.309	-2.217	C	3.368	-1.035	-3.059
C	-1.463	1.881	-2.004	S	4.93	-1.416	-2.105
C	0.226	5.074	-0.661	H	-1.247	-5.305	-2.648
C	1.61	4.514	-0.411	H	3.108	0.017	-2.908
C	2.56	4.467	-1.444	H	-6.662	-1.665	-1.328
C	3.827	3.929	-1.231	H	-0.778	-5.259	-0.961
C	4.196	3.432	0.029	H	-6.936	-2.85	-0.042
C	3.248	3.474	1.059	H	3.675	-1.141	-4.104
C	1.975	4.011	0.843	H	-3.483	3.356	2.955
C	5.582	2.89	0.278	H	0.213	-1.598	5.316
S	6.115	1.525	-0.867	H	5.028	-3.301	0.676
As	4.63	-0.105	-0.272	H	-0.561	-2.701	4.197
S	6.137	-1.17	1.061	H	-2.774	3.114	1.354
C	5.171	-2.675	1.561	H	5.864	-3.203	2.228
C	3.852	-2.416	2.25	H	5.695	2.56	1.315
C	3.766	-1.622	3.404	H	6.341	3.663	0.105
C	2.545	-1.429	4.048	H	-4.17	1.703	-3.756
C	1.368	-2.019	3.563	H	-3.377	0.365	-2.922
C	1.455	-2.807	2.409	H	-4.115	3.995	-2.033
C	2.677	-2.999	1.759	H	-2.395	5.539	-1.186
C	0.04	-1.782	4.247	H	0.522	2.388	-1.351
C	-0.795	-0.631	3.689	H	-1.189	0.853	-2.232
C	-0.388	0.147	2.602	H	0.299	5.912	-1.369
C	-1.189	1.19	2.127	H	-0.163	5.506	0.271
C	-2.421	1.486	2.72	H	2.3	4.855	-2.427
C	-2.832	0.703	3.812	H	4.542	3.897	-2.05
C	-2.029	-0.327	4.292	H	3.507	3.093	2.044
C	-3.276	2.606	2.182	H	1.259	4.034	1.662
S	-4.982	2.107	1.626	H	-0.852	1.772	1.273
As	-4.422	0.447	0.17	H	0.561	-0.057	2.116
S	-5.371	1.198	-1.776	H	-2.368	-0.915	5.143
C	-3.811	1.359	-2.778	H	-3.793	0.899	4.282
S	-6.164	-0.824	0.899	H	2.503	-0.811	4.943
C	-6.222	-2.116	-0.435	H	4.664	-1.152	3.799
C	-4.9	-2.763	-0.766	H	2.714	-3.614	0.862
C	-4.37	-2.658	-2.062	H	0.557	-3.273	2.009
C	-3.155	-3.258	-2.393	H	-4.923	-2.106	-2.819
C	-2.423	-3.976	-1.438	H	-2.768	-3.164	-3.406
C	-2.951	-4.077	-0.143	H	-2.404	-4.635	0.615
C	-4.166	-3.476	0.191	H	-4.546	-3.562	1.207
C	-1.101	-4.624	-1.799	H	0.963	-5.016	-3.537
C	0.026	-3.658	-2.147	H	2.856	-3.525	-4.055

Table 3.6 (continued)

Atom	X	Y	Z	Atom	X	Y	Z
C	0.127	-2.39	-1.557	H	1.253	-0.566	-1.38
				H	-0.636	-2.059	-0.857

CHAPTER IV

ARSENIC-π INTERACTIONS INFLUENCE MECHANICAL COUPLING IN A SERIES OF SUPRAMOLECULAR ASSEMBLIES

The material in this chapter was prepared in collaboration with Sean A. Fontenot, Aaron C. Sather, Lev N. Zakharov, and Darren W. Johnson for submission to *Angewandte Chemie, International Edition in English.* $As_2\mathbf{L}^4{}_3$ was prepared by S.A.F.. $As_2\mathbf{L}^5{}_3$ was prepared by A.C.S. Crystallography was performed by L.N.Z., and editorial assistance with manuscript preparation was provided by D.W.J.

Introduction: Mechanical Coupling in Supramolecular Chemistry

Fabrication of complex structures from simple components has been a research topic of great interest in recent years.[22,2,93-95] Supramolecular self-assembly processes and dynamic covalent chemistry[96,97] present a powerful set of tools for the bottom-up synthesis of complex structures with new properties and emergent functionality.[98] A defining feature of these synthetic strategies is that information contained within relatively simple components determines the formation of much more complex structures when combined under appropriate conditions. While the self-assembly of metal-ligand complexes incorporating transition metals is well established, with an enormous library of components, main

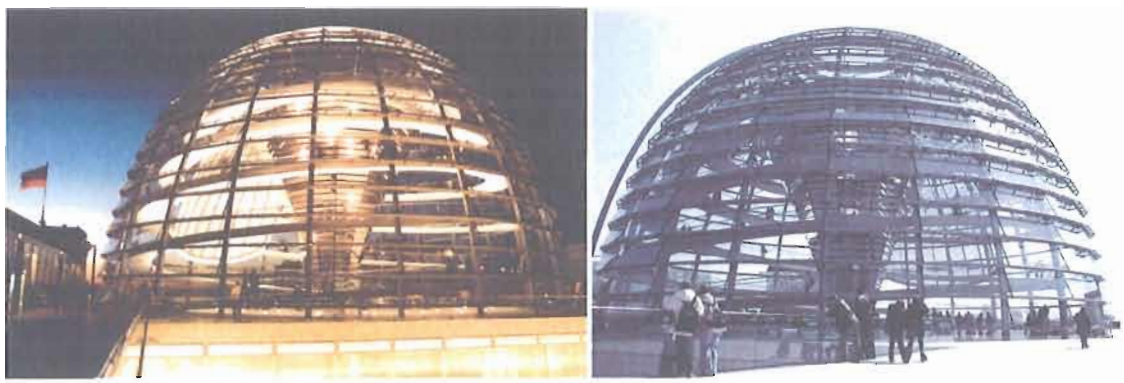

Figure 4.1. The new dome of the German Reichstag building in Berlin displays a prominent pair of right-handed helices: the helical twist created by the spiraling walkway echoes that of the corresponding negative space.

group supramolecular chemistry is still developing the tools for the predictable formation of well-defined structures.[1] These structures are simultaneously chemically elegant and aesthetically pleasing, often echoing the structural and geometric features common found in art and architecture (Figure 4.1). The main group elements possess properties that diverge from those of the transition metals, presenting an attractive target for the supramolecular chemist seeking novel properties and alternative functionalities. As helicates have been described as "the drosophila of supramolecular chemistry,"[99] probing the contributions of secondary bonding interactions to the overall structure of main group helicates will provide vital insights toward the construction of larger assemblies.

In this communication, we present three new structures based on a self-assembly framework driven by arsenic-π interactions. Mechanical coupling across

the ligand scaffold influences the local stereochemistry at the metal centers, revealing that weak secondary bonding interactions may communicate stereochemical information in the same manner as more traditional systems bearing chelate rings. The secondary bonding nature of this interaction, however, introduces additional freedom in the geometric possibilities for complex structures: the helical twist in the ligand spacer is decoupled from the stereochemistry at the metal centers. The vast majority of metallosupramolecular helicates rely on rigid chelating groups; for example, 2,2'-bipyridine, catecholate, β-diketonate, or 8-hydroxyquinolinate.[83] The use of secondary bonding interactions to complete a chelate ring suggests future possibilities combining symmetry based self-assembly with the weak-link approach.[100,101]

Lewis acid/base adducts formed by interactions between pnictogens and arene rings have been described extensively by Schmidbaur and co-workers,[102-108] but only recently have they been used in a supramolecular context as a structural motif in the design of larger, higher order assemblies.[33-35,109,73] We have previously reported the synthesis and crystal structures of two $As_2\mathbf{L}_3$ mesocates based on trigonal pyramidal coordination of bis(mercaptomethyl)arene ligands to As(III). Primary As-S bonds are providede by the mercaptomethyl groups, while a five-membered chelate-type ring is completed by the secondary intramolecular As-π interactions. In this context, arsenic-π interactions are defined as contacts between

the trivalent metal center and arene carbon atoms less than the sum of their respective van der Waals radii; the interaction is measured between the As(III) center and the centroid of these close contacts. η^2-coordination is typically observed, though in some cases hapticity can be as high as η^6 when sterically demanding ring substituents center the metal over the ring.[103,104,110] Preliminary DFT studies estimate that this mode contributes >7.4 kcal/mol of stabilization per interaction.[33]

Stereochemical Descriptions of As_2L_3 and Other Supramolecular Assemblies

The first reported supramolecular assembly based around As-π interactions and the bis(mercaptomethyl)arene scaffold, (Δ,Λ)-$As_2\mathbf{L}^1_3$ ($H_2\mathbf{L}^1$ = 1,4-bis(mercaptomethyl)benzene), bridged two As(III) centers with a phenylene spacer.[33] In this mesocate, the interaction between the As(III) centers and the arene rings of the ligands pulled the lone pair of the metal center toward the interior of the assembly; the twisted disposition of ligands around the C_3 axis generated a stereocenter at each metal in the crystalline state. The bidentate nature of the primary/secondary coordination spheres creates in effect a distorted octahedral coordination environment around the As(III) center which can then be described with established stereochemical conventions: the absolute configuration at each metal is defined by the direction of torsional twist observed down the As-As axis. A

clockwise twist is designated as Δ and a counter clockwise twist is designated as Λ (Scheme 4.1).

Helicity in metallosupramolecular architectures has two other origins dictated by the dictated by the ligand spacer: helical induction by (i) structural or (ii) axial chirality.[111,112] The asymmetric conformation adopted by the diphenylmethane spacer in $(\Delta,\Lambda,M/\Delta,\Lambda,P)$-$As_2\mathbf{L}^2{}_3$ ($H_2\mathbf{L}^2$ = 4,4'-

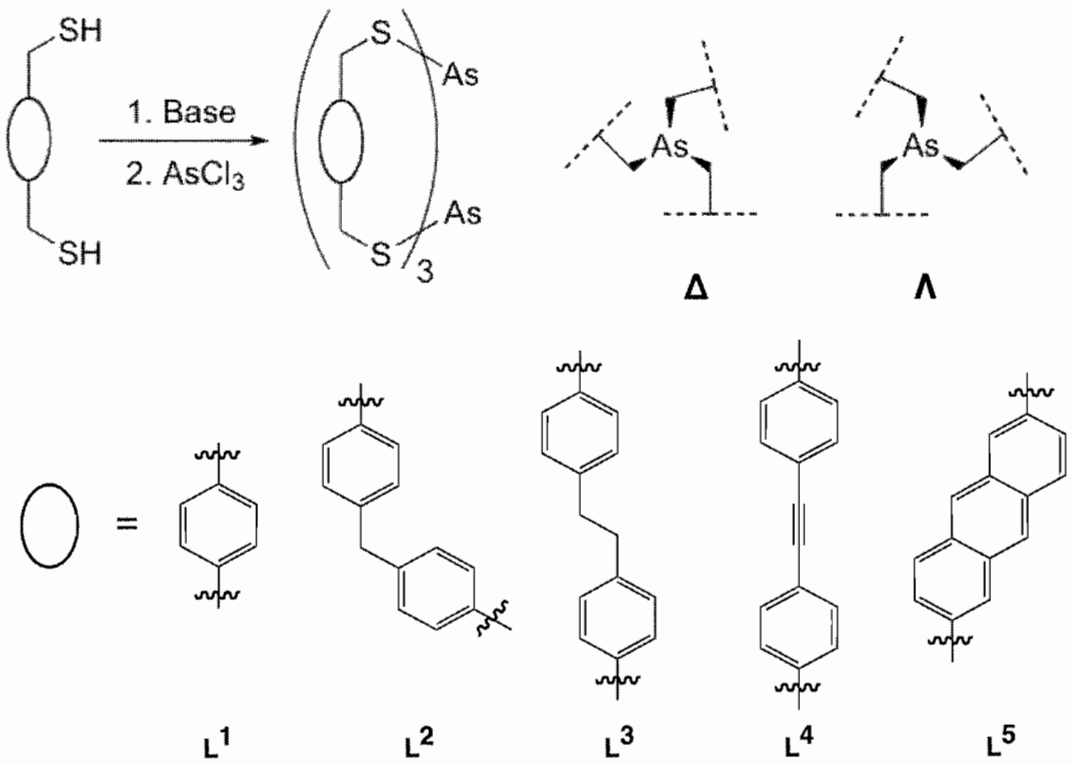

Scheme 4.1. General self-assembly reaction forming As_2L_3 helicates and mesocates from bis(mercaptomethyl)arene ligands and illustration of local stereochemistry of arsenic(III) centers. Dashed lines represent the edges of arene rings; sulfur atoms lie at the ends of wedged bonds. Ligand spacers are defined below.

bis(mercaptomethyl)diphenylmethane)[73] causes the assembly to crystallize as a racemic pair of helices. This complex is an example of a chiral structure originating from a coordination assembly lacking homoconfigurational metal centers.

Descriptions of the overall chirality of a given system can be challenging due to the variety of nomenclatures,[112] however, based on these examples, we will describe the chiral elements of $As_2\mathbf{L}_3$ assemblies first by absolute configuration of the metal centers (Δ/Λ), then by the direction of helical pitch along the ligand spacer (M/P).

The choice of ligand spacer in the design of supramolecular helicates directly affects final product, as the local stereochemistry of metal centers in supramolecular helicates and higher order structures is communicated between the metal centers by the ligands' structure.[113] This mechanical coupling is especially apparent in homoconfigurational catecholamide $M_4\mathbf{L}_6$ tetrahedra in which the overall chirality is enforced by communication along the six ligands that form the edges of the cage.[114,115]

The general method for preparation of $As_2\mathbf{L}_3$ assemblies based on this design strategy is shown in Scheme 4.1: a C_2 symmetric bis-thiolate ligand with a rigid or semi-rigid aromatic spacer is treated with a base, followed by the addition of $AsCl_3$. Slow evaporation of solvent from a solution of the assemblies yielded crystals of $As_2\mathbf{L}^3{}_3$, $As_2\mathbf{L}^4{}_3$, and $As_2\mathbf{L}^5{}_3$ suitable for analysis by X-ray crystallography (Figure 4.2).

Ligand Scaffolds and Effects on Helicity

The diphenylethane spacer in $As_2\mathbf{L}^3{}_3$ ($H_2\mathbf{L}^3$ = 4,4'-bis(mercaptomethyl)diphenylethane) generates the (Δ,Δ,*M*/Λ,Λ,*P*)-$As_2\mathbf{L}^3{}_3$ racemic pair of helicates of idealized D_3 symmetry, in contrast to (Δ,Λ)-$As_2\mathbf{L}^1{}_3$ and (Δ,Λ,*M*/Δ,Λ,*P*)-$As_2\mathbf{L}^2{}_3$ in which the spacers encourage opposing configurations at the metal centers. The conformation of the ethylene spacer generates a helical domain of its own, directing the mercaptomethyl groups at the ends of the ligand strand in opposite directions and encouraging the ligand to "wrap" around the threefold axis rather than coordinate the metal center edge-on.[113] The homoconfigurational (Δ,Δ,*M*/Λ,Λ,*P*)-$As_2\mathbf{L}^3{}_3$ is estimated to be more stable than the *meso* (Δ,Λ,*M*/Δ,Λ,*P*)-$As_2\mathbf{L}^3{}_3$ by ~1.5 kcal/mol based purely on steric factors,† indicating that the mechanical coupling between the metal centers is relatively weak, an expected result based on the conformational freedom of the spacer.‡

Likewise, the $As_2\mathbf{L}_3$ assemblies formed on diphenylacetylene and anthracene scaffolds crystallize as D_3 helices. Instead of communicating stereochemical information between metal centers through the *conformation* of the ligand spacer,

---

† Computations were performed with Fujitsu CAChe 5.0; the geometry at the metal centers was held fixed while the ligand spacer's orientation was varied in order to compare, for example, Δ,Δ,*M*/Λ,Λ,*P* configurations in a given assembly.

‡ Crystallographic data obtained between -100° C and 23° C show only slight structural changes as the temperature is increased. See experimental section for changes to cell parameters with temperature.

the information is transmitted directly across the ligand spacer. For $As_2\mathbf{L}^4{}_3$, the 4,4' substitution pattern of the mercaptomethyl groups generates a slight helical pitch around the primary C_3 axis and yields ($\Delta,\Delta,M/\Lambda,\Lambda,P$)-$As_2\mathbf{L}^4{}_3$ in the solid state. The calculated difference in energy between ($\Delta,\Delta,M/\Lambda,\Lambda,P$)-$As_2\mathbf{L}^4{}_3$ and ($\Delta,\Lambda,M/\Delta,\Lambda,P$)-$As_2\mathbf{L}^4{}_3$ is small – the chiral assembly is estimated to be more stable by only 0.8 kcal/mol.

The anthracene spacer in ($\Delta,\Delta,P/\Lambda,\Lambda,M$)-$As_2\mathbf{L}^5{}_3$ ($H_2\mathbf{L}^5$ = 2,6-bis(mercaptomethylanthracene)) has a more dramatic effect due to the offset supplied by the 2,6 substitution pattern. Surprisingly, the helical twist of the ligand domain is not the same as that of the metal centers' configurations: most $As_2\mathbf{L}_3$ assemblies prepared thus far bear ligands twisted in the same helicity as that found at the metal centers, and the As-π contact is observed to occupy the "leading edge" of the ligand arene rings. The anthracene scaffold deviates from this trend, as the contact occupies the "trailing edge" of the ligand. This is no doubt the result of the offset in the mercaptomethyl substituents located in the 2,6 positions rather than the 4,4' positions occupied in other ligands. Reversing the observed *P* helicity to *M* helicity would have the effect of destabilizing the assembly: (Δ,Δ,P)-$As_2\mathbf{L}^5{}_3$ is preferred over (Δ,Δ,M)-$As_2\mathbf{L}^5{}_3$ by ~8 kcal/mol. (Δ,Λ,M)-$As_2\mathbf{L}^5{}_3$ and (Δ,Λ,P)-$As_2\mathbf{L}^5{}_3$, while not observed in the solid state, are calculated to lie between the homochiral isomers at approximately the same energy.

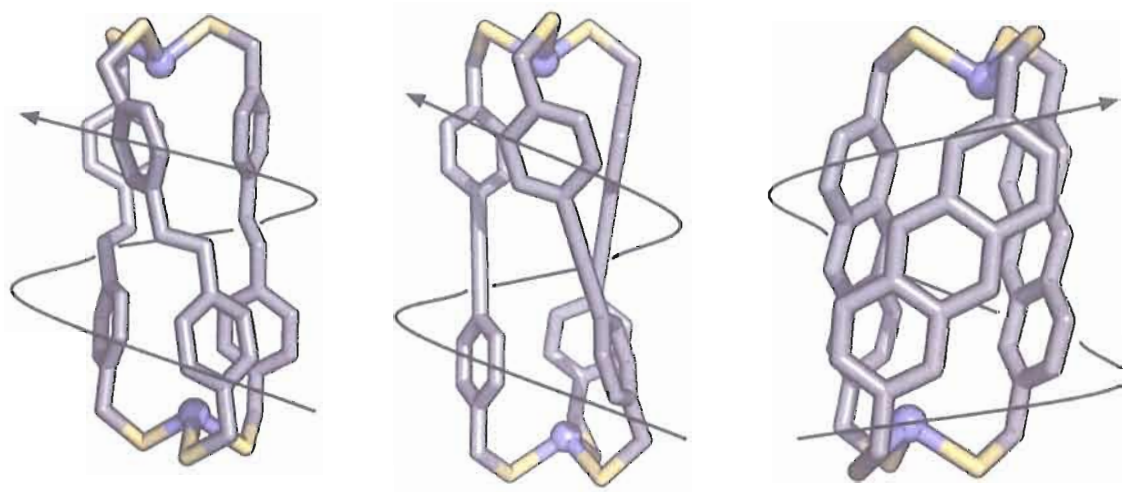

Figure 4.2. Crystal structures of new As_2L_3 assemblies shown as the ΔΔ isomer. Ligands are represented as sticks, while As(III) centers are shown as spheres. Curved arrows indicate direction of helicity in the ligand domain.

Structural Effects of Pnictogen•••Arene Interactions

The relatively consistent length (and likely strength) of the As-π interaction across the series of ligand spacers (Table 4.1) points to its importance in the overall structure of these assemblies. While the specific ligand spacer employed in designed As_2L_3 assemblies clearly impacts the chirality of the product, the overall strength of the metal-arene interaction that stabilizes the assembly has an effect on the chirality as well. The helical diastereomer is frequently more stable than the corresponding *meso* diastereomer in dinuclear helicates,[116] possibly due to the additional interior space created when a helicate "unwinds" into a mesocate with an increased metal-metal distance. External factors such as guest inclusion can influence this

Table 4.1. Stereochemical outcomes for As_2L_3 assemblies. Rigid spacers and stronger secondary bonding interactions lead to helicate formation over mesocate formation.

Complex	As/Sb-π (Å)[a]	Configuration[b]
$As_2\mathbf{L}^1{}_3$	3.30	Δ,Λ
$As_2\mathbf{L}^2{}_3$	3.48	Δ,Λ,*M*+*P*[c]
$As_2\mathbf{L}^3{}_3$	3.29	Δ,Δ,*M*
$As_2\mathbf{L}^4{}_3$	3.33	Δ,Δ,*M*
$As_2\mathbf{L}^5{}_3$	3.33	Δ,Δ,*P*
$Sb_2\mathbf{L}^1{}_3$	3.37[d]	Δ,Δ,*P*

[a] Average distance between metal center and centroid of close contacts with neighboring arene rings. [b] See Figure 2 for description of helical domain designations; for homochiral assemblies, the Δ,Δ isomer is shown. [c] (Δ,Λ,*M*)- and (Δ,Λ,*P*)-$As_2\mathbf{L}^2{}_3$ form as a racemic mixture. [d] See text for method of comparing strength of secondary bonding interactions.

phenomenon, inducing a transformation between a mesocate and the helicate when the metal-metal distance is decreased due to interactions with the guest.[117] A similar effect may be observed in supramolecular assemblies incorporating As-π or Sb-π interactions – the increased strength of the secondary bonding interaction involving Sb(III) relative to As(III) decreases the metal-metal distance.[108] Although the pnictogen-arene interaction distance increases slightly (0.07 Å) between $As_2\mathbf{L}^1{}_3$ and $Sb_2\mathbf{L}^1{}_3$ (Table 4.1), the interaction is in fact comparatively stronger: the As-S bond length is 2.24 Å, while the Sb-S bond length is 2.43 Å.[35] The ratio of pnictogen•••π interaction distance to pnictogen-sulfur bond length thus decreases from 1.47 to 1.38 between As(III) and Sb(III). Antimony therefore interacts more strongly with arenes than with arsenic;[108] the overall structural effect is that the pnictogen-arene interaction plays a similar structural role as a water guest in the induction of helicity in an otherwise *meso* supramolecular assembly. Stronger secondary bonding

interactions improve the ability of ligands to transfer stereochemical information throughout an assembly.

Conclusions: The Arene-CH_2SH Group as a Chelating Moiety

We have thus shown that bis-bidentate ligands whose chelate ring consists of a pair of a pair of strong (thiolate coordination) and weak (π-basic) donors may be used to prepare supramolecular $As_2\mathbf{L}_3$ assemblies in which the local stereochemistry of the metal centers is influenced by mechanical coupling across the ligand spacer in three new supramolecular assemblies. This coupling follows the general pattern established by more rigid chelate systems – information is transferred through both ligand structure and conformation, although the helicity of the ligand domain is decoupled from the stereochemistry of the metal centers when the donor groups are offset from one another as shown in 2,6-substituted anthracene assembly. The differing strength of pnictogen-π interactions can serve the same structural role as guest inclusion in determining the formation of helicates or mesocates with a given ligand. The fact there is nearly an order of magnitude difference in the strength of the As-S bond and the As-π interaction suggests that this structural motif could treated as a hemilabile ligand under the weak link self-assembly framework[100] – ligand spacers with the ability to transmit stereochemical information are a key component in expanding this design strategy to larger structures.

Experimental Details

General Information

Starting materials and reagents were obtained from commercial sources and used without further purification unless otherwise noted. NMR spectra were obtained on Varian 300 MHz, 500 MHz, and 600 MHz spectrometers as noted; chemical shifts are reported in parts per million (ppm) downfield from tetramethylsilane and referenced to residual solvent as an internal standard. X-ray diffraction data were collected at 173 K on a Bruker Apex diffractometer using MOKα-radiation (λ=0.71073 Å). Mass spectra were recorded using an Agilent 1100 Series LC/MSD. Absorption corrections were applied by SADABS. All structures were determined by direct methods and refined on F^2 by a full-matrix least-squares procedure. All non-H atoms were refined with anisotropic thermal parameters. H atoms were refined in calculated positions in a model of a rigid group. All calculations were performed by the Bruker SHELXTL 6.10 package (SHELXTL, version 6.10, Bruker AXS, Inc., Madison, WI, 2000).

General Method for Synthesis of As_2L_3 Assemblies

To a solution of H_2**L** in THF under N_2 atmosphere was added 2 equivalents of KOH in methanol. This solution was warmed to 50 °C and $AsCl_3$ (0.67 equivalents) was carefully added. After continued heating for 2 hours, the solution was filtered through glass wool and concentrated *in vacuo* to yield an off-white solid from which

crystals suitable for analysis by X-ray diffraction were prepared by slow evaporation.

Crystallographic Data

$As_2\mathbf{L}^3{}_3$: ^{1}H NMR (300 MHz, $CDCl^3$): δ = 6.98 (24H, m), 3.78 (12H, s), 2.80 (12H, s). ^{13}C NMR (126 MHz, $CDCl_3$, -20° C): δ = 140.14, 136.33, 128.98, 128.17, 38.31, 35.03; MS [M+H$^+$] $C_{48}H_{48}As_2S_6$ requires 966.1, found 967.0. Crystal data: $C_{48}H_{48}As_2S_6$, M_r = 967.06, 0.37 x 0.14 x 0.04 mm, monoclinic, C2/c (N 15), a = 30.468(3) Å, b = 13.6420(12) Å, c = 11.0855(10) Å, β = 106.397(1)°, V = 4420.2(7) Å^3, Z = 4, Z'=0.5, ρ_{calcd} = 1.453 g cm^{-1}, μ = 1.829 mm$_{-1}$, $2\theta_{max}$ = 54.00°, T = 173(2) K, 24133 measured reflections, 4837 independent reflections [R_{int}=0.0417], 253 independent refined parameters, $R1$ = 0.0468, w$R2$ = 0.1210 (with $I > 2\sigma(I)$), $R1$ = 0.0670, $wR2$ = 0.1416 (all data), GOF = 1.088, max/min residual electron density +1.064/-0.452 e Å^{-3}.

$As_2\mathbf{L}^4{}_3$: $C_{48}H_{36}As_2S_6$, M_r = 954.97 , 0.18 x 0.16 x 0.12 mm, monoclinic, C2/c (N 15), a = 31.093(2) Å, b = 13.5902(10) Å, c = 10.6951(8) Å, β = 107.090(1)°, V = 4319.7(5) Å^3, Z = 4, ρ_{calcd} = 1.468 g cm^{-1}, μ = 1.871 mm^{-1}, $2\theta_{max}$ = 54.00°, T = 173(2) K, 19714 measured reflections, 4719 independent reflections [R_{int}=0.0416], 253 independent refined parameters, $R1$ = 0.0420, w$R2$ = 0.0897 (with $I > 2\sigma(I)$), $R1$ = 0.0619, w$R2$ = 0.1015 (all data), GOF = 1.094, max/min residual electron density +0.607/-0.238 e Å^{-3}.

$As_2\mathbf{L}^5{}_3$: $C_{54}H_{42}As_2S_6$, M_r = 1033.08, 0.07 x 0.06 x 0.05 mm, monoclinic, C2/c (N 15), a = 26.660(7) Å, b = 10.399(3) Å, c = 20.779(6) Å, β = 125.192(7)°, V = 4708(2) Å^3, Z = 4, ρ_{calcd} = 1.458 g cm^{-1}, μ = 1.723 mm^{-1}, $2\theta_{max}$ = 54.00°, T = 173(2) K, 9193 measured reflections, 4993 independent reflections [R_{int}=0.0856], 280 independent refined parameters, $R1$ = 0.0756, w$R2$ = 0.1014 (with $I > 2\sigma(I)$), $R1$ = 0.1318, w$R2$ = 0.1626 (all data), GOF = 1.004, max/min residual electron density +0.752/-0.453 e Å^{-3}.

CHAPTER V

DESIGN CONSIDERATIONS FOR THE GROUP 15 ELEMENTS: THE PNICTOGEN•••π INTERACTION AS A COMPLEMENTARY COMPONENT IN SUPRAMOLECULAR ASSEMBLY DESIGN

We study the origins of the pnictogen•••π effect and relate this to its utility as a design element for the preparation of $M_2\mathbf{L}_3$ and $M_2\mathbf{L}_2Cl_2$ supramolecular assemblies. Crystallographic, computational, and synthetic strategies have been employed to probe the contributions of electrostatics, charge-transfer interactions, and steric factors in determining the strength and directionality of this interaction in a variety of contexts. The crystal structure database search, structure and data analysis, and writing of this chapter was done by myself with input from D. W. Johnson. Virginia M. Cangelosi and Corrine A. Allen contributed new crystal structures (solved by Dr. Lev N. Zakharov) to include in the discussion of supramolecular assemblies.

Introduction

The great success of supramolecular chemistry in the preparation of rationally designed supermolecules from simple components[118,10,2,119,120] has led to a concomitant surge of interest in study of the main group elements.[1] Main group

metals occupy an interesting position in the periodic table: the nature of their bonding is generally coordinative, while simultaneously mimicking the nonmetals in regards to their geometric preferences.[1] As the main group metals are used more in supramolecular chemistry, their coordination preferences have been incorporated into predictive design strategies that have led to the formation of rather spectacular self-assembled structures. The development of these design strategies has, however, been hampered by the unpredictable coordination preferences of these elements.[3] Secondary bonding interactions also introduce new challenges to rational design strategies. Weak interactions with arene rings,[86] secondary coordination to Lewis basic elements,[59] and steric strain all play a role in determining the overall structure of supramolecular assemblies; the main-group elements and pnictogens in particular appear to have a unique susceptibility to unusual coordination behavior.

Pnictogen•••Arene Interactions Observed in Mononuclear Complexes

Interactions between arene rings and pnictogen metal centers are of particular interest in the development of supramolecular design strategies with main-group elements. While this type of interaction has been known for quite some time,[102-106,110,107,108] only recently has it been used as a specific design element in supramolecular assemblies.[33-35,78,73] These interactions were first discovered through the observation that combinations of benzene or naphthalene with

antimony trichloride produced highly crystalline solids; the unusually high solubility of pnictogen trihalides in neutral organic solvents has also been attributed to noncovalent interactions between the metal and the solvent. This interaction appears to be quite strong, but its geometry is also variable. Examples of the closest pnictogen•••arene interactions for As(III), Sb(III) and Bi(III) found in a survey of the Cambridge Structural Database are shown in Figure 5.1. Of note is the fact that for As(III) and Bi(III), the closest interactions with arene rings are found when the space occupied by the metal's lone pair is oriented perpendicular to the face of the ring, while for Sb(III), the closest interaction places the metal in a tilted orientation with respect to the arene.

A number of computational studies on these so-called "Menshutkin complexes" describe the interaction as a ligand to metal charge transfer interaction and suggest that ligand-based donor orbitals interact with 6p acceptor orbitals on the metal center.[108] While these calculations do provide insight into the fact that there is likely some degree of charge transfer character to the interaction, there is still disagreement regarding the bonding strength and are considered unsatisfactory to completely explain the bonding observed between pnictogens and neutral arene rings. In particular, antimony complexes bear off-center interactions much more frequently than do arsenic or bismuth – these calculations provide no explanation for this phenomenon.

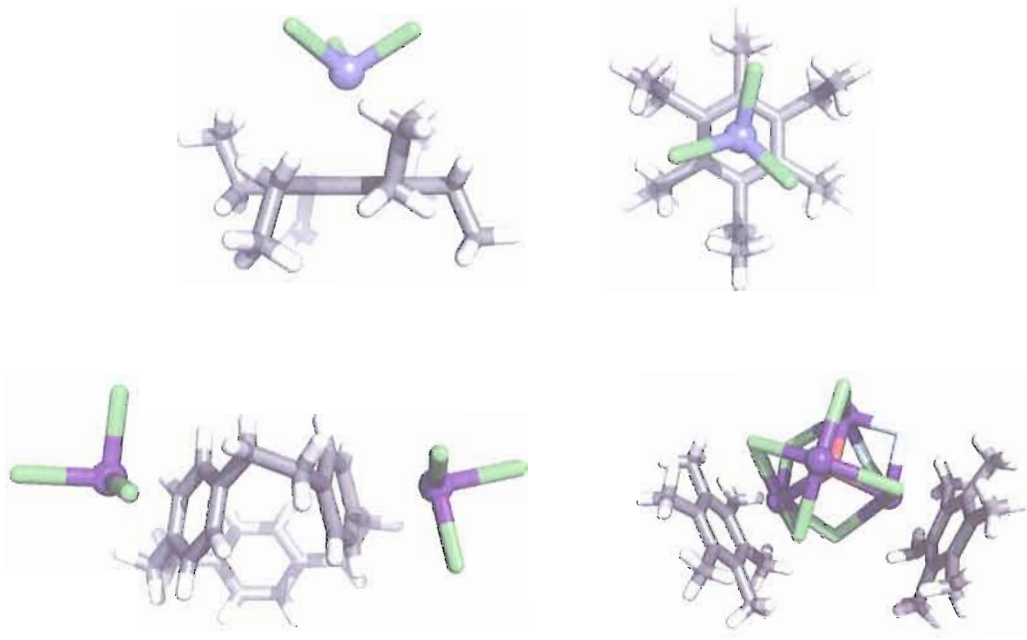

Figure 5.1. Examples of structures from the CSD with particularly short pnictogen•••arene distances. Top: Hexaethylbenzene•••$AsCl_3$ adduct with perpendicular orientation. Lower left: Cyclophane•••$SbCl_3$ adduct with tilted geometry. Lower right: Hexamethylbenzene•••Bi cluster adduct with perpendicular geometry.

Pnictogen•••Arene Interactions in a Supramolecular Context

We have recently reported the development of a supramolecular design strategy for the preparation of helicates, mesocates, and macrocycles from bis(functional) benzylic thiolates bridged by rigid and semirigid aromatic spacers coordinated to trigonal pyramidal pnictogen centers.[33] The primary thiolate coordination sphere is supplemented by intramolecular secondary bonding interactions between the pnictogen and the ligand scaffold. This stands in contrast to previous examples of pnictogen•••arene interactions, which tend to be

intermolecular adducts. Several examples of supramolecular $M_2\mathbf{L}_3$ and $M_2\mathbf{L}_2Cl_2$ structures prepared through this strategy are shown in Figure 5.2. The assembly shown in (*a*) is the first example of pnictogen•••arene interactions so intimately involved in the overall structure of a supramolecular coordination complex. This design strategy was shown to be general to ligands bearing benzylic thiolate donor groups; one example of an extended structure is shown in (*b*).[73] Several examples of macrocycles based on this design strategy have been reported as well, and some of these are capable of interacting further with aromatic solvent molecules in the solid state to form inclusion structures.[78]

Figure 5.2. Examples of supramolecular assemblies featuring pnictogen•••arene interactions. (*a*) Basic $As_2\mathbf{L}_3$ assembly based on phenylene spacer. (*b*) Expanded $As_2\mathbf{L}_3$ assembly based on an extended ligand. (*c*) $As_2\mathbf{L}_2Cl_2$ macrocycles capable of dimerizing around a solvent guest in the solid state.

Factors Contributing to Pnictogen•••Arene Interactions

The nature of the pnictogen••arene interaction clearly has some bearing on its utility in supramolecular assembly design. The possibility of covalent character (if the interaction were caused, for example, by interactions between π electrons and the As-S σ* orbital) would imply that very specific structural arrangements are required for this interaction to be used as a design element; conversely, a primarily electrostatic interaction would allow considerably more latitude in how the interaction could be incorporated into assembly design.

Charge Transfer Model for the Pnictogen•••Arene Interaction

A closer examination of assembly $As_2\mathbf{L}^1{}_3$ in Figure 5.2 provides a visual depiction of how the pnictogen•••π interaction might be caused by overlap between the As-L antibonding orbital and the arene's π electrons to form a charge transfer complex. In Figure 5.3, the "stick" representation of $As_2\mathbf{L}^1{}_3$ is shown in (*a*). The primary ligand coordination sphere about the As(III) center is shown in more detail in (*b*); in particular, the σ* orbitals associated with the As-S bonds are drawn in their approximate locations, though not to scale. Figure 5.3(*c*) is a view down the As-As axis of the supramolecular assembly, showing how the π systems of the ligand spacer arene rings might interact with these σ* orbitals to stabilize the overall assembly.

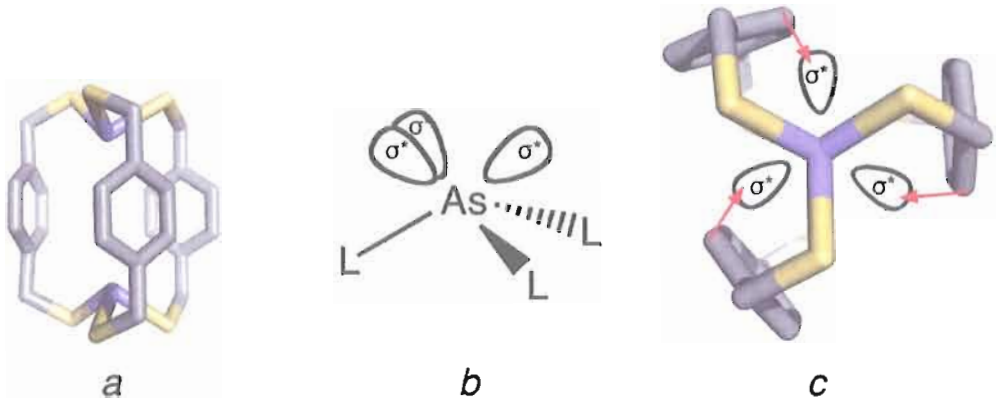

Figure 5.3. A charge transfer model for the pnictogen•••arene interaction in supramolecular assemblies. (*a*) Assembly $As_2\mathbf{L}^1_3$ shown as a stick model. (*b*) Locations of σ* orbitals in the primary coordination sphere about an As(III) center; the generic ligand **L** replaces the sulfur ligand in this view. (*c*) View down the As-As axis showing the possibility of interactions (red arrows) between the π systems of the arene spacers with the σ* orbitals.

Structural Survey

A systematic survey of the Cambridge Structural Database was undertaken in order to examine how pnictogen size and other factors contribute to the strength of geometry of their interactions with arene rings.§ Structures included in this survey are those containing As, Sb, or Bi in close proximity (*i.e.*, less than the sum of their van der Waals radii) to aromatic rings. As shown in Figure 5.4, the distance for the interaction d and the interaction angle θ were then measured, tabulated, and

§ In most cases, the pnictogen center interacts in an η^2 or η^3 fashion with neighboring arene rings. On occasion the pnictogen may have η^1, η^4, η^5, or η^6 contacts with arenes. The interaction is measured using the centroids of the close contacts.[108]

compared with the interactions observed in supramolecular pnictogen•••arene assemblies.

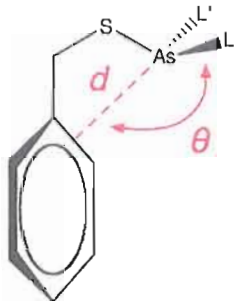

Figure 5.4. Schematic for measurement of pnictogen•••arene interaction distances and interaction angles. The interaction distance *d* refers to the distance between the centroid of observed close contacts and the pnictogen center, while the interaction angle θ refers to the angle between this centroid, the pnictogen center, and the ligand (**L**) opposite the interaction. The As•••π interaction is depicted here as an η^2 contact.

Trends Observed in Pnictogen•••Arene Interactions

Examination of the distances found in the CSD search broken down by pnictogen type shows two important facts about the pnictogen•••π interaction. The first is that the average distance decreases with increasing pnictogen size, as shown in Figure 5.5. Arsenic•••π interactions average 3.45 Å, while interactions with antimony and bismuth are 3.40 and 3.32 Å respectively. The second notable feature is that as the pnictogen size increases, the distribution of the interaction distance increases considerably. The standard deviation for arsenic•••π interactions is 0.09 Å, or 2.5%, which increases to 8.62% for bismuth. This data, while not particularly

conclusive, does suggest that increasing pnictogen size results in a wider range of possible interactions.

The angular preferences associated with this interaction provide a slightly different picture of the pnictogen•••π interaction. The mean angle associated with the pnictogen•••arene interaction (Figure 5.6) decrease only slightly as the metal size is increased, and the standard deviations associated with these values are also significant. The actual deviation of the angle, however, does not increase or decrease significantly with increasing pnictogen size.

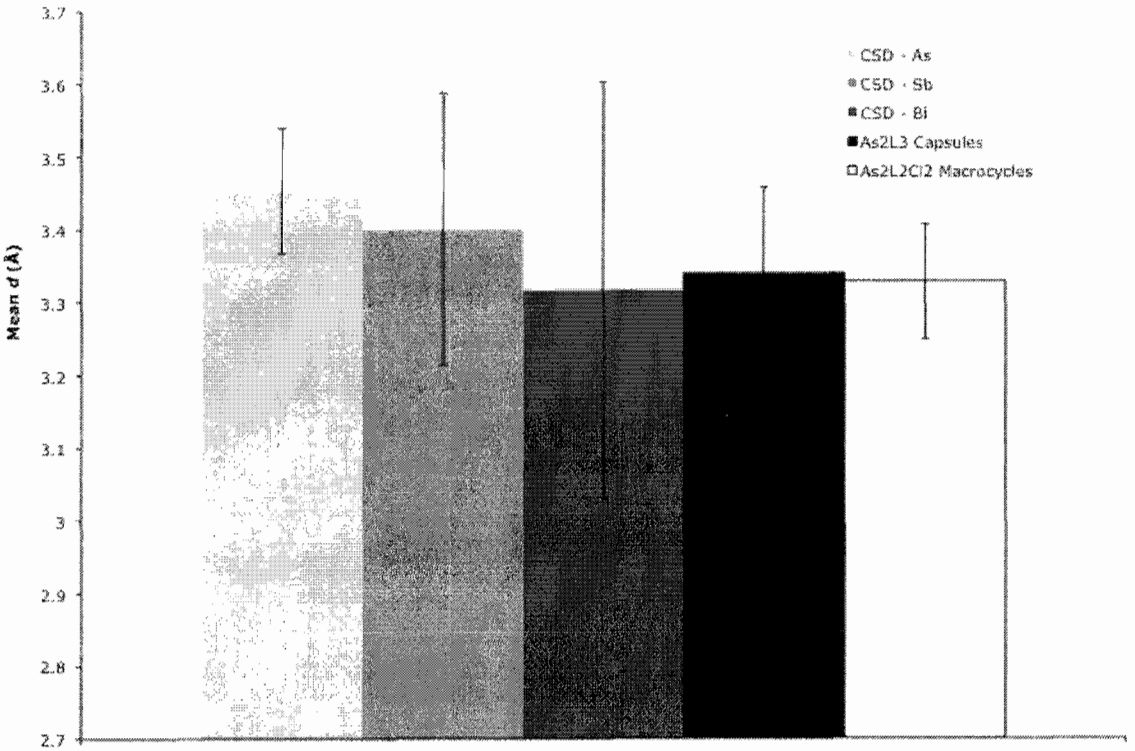

Chart 5.1. Mean pnictogen•••π distances observed in the CSD. See Table 5.1 for data values.

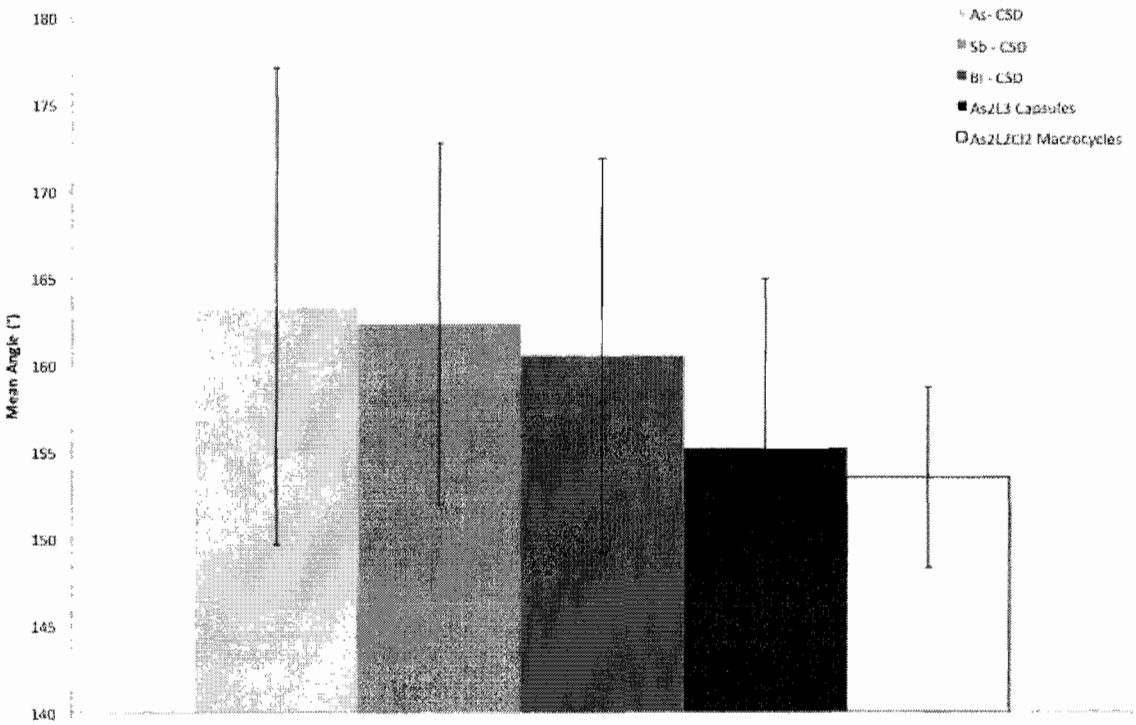

Chart 5.2. Mean angles for pnictogen•••π interactions observed in the CSD. See Table 5.1 for data values.

Table 5.1. Mean interaction distances and angles for pnictogen•••π interactions.

Pnictogen Type	Mean *d* (Å)	Deviation (Å)	Deviation (%)	Mean θ (°)	Deviation (°)	Deviation (%)
As – CSD	3.45	0.09	2.49	163.38	13.71	8.39
Sb – CSD	3.40	0.19	5.49	162.35	10.40	6.40
Bi – CSD	3.32	0.29	8.62	160.53	11.36	7.08
$As_2\mathbf{L}_3$	3.34	0.12	3.54	155.22	9.76	6.29
$As_2\mathbf{L}_2Cl_2$	3.33	0.08	2.36	153.51	5.19	3.38

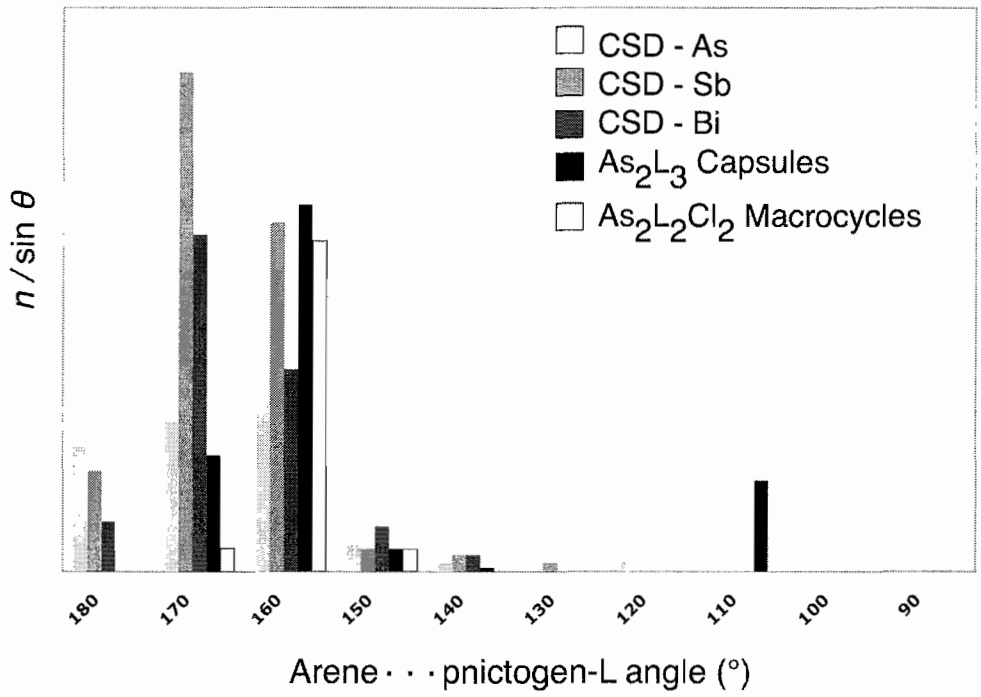

Chart 5.3. Angular preferences for pnictogen•••arene interactions as observed in the CSD. The angular distribution is weighted as $1/\sin(\theta)$.[121]

A second way to examine the angular data's distribution is shown in Figure 5.7. As reported by Steiner,[122] a noncovalent interaction's angle can be associated with the frequency at which it occurs in order to generate a distribution. The frequency is weighted by sin θ in order to properly observe angular preferences.[121] The angular distribution shows that there is a preference for this angle to lie between 150° and 170°. A more linear angle is preferred for antimony and bismuth in particular, which suggests that the interaction may have some increased degree of covalent character for these elements. Conversely, a more bent angle is more

frequently observed in the supramolecular assemblies reported by our laboratory. This is most likely due to the geometric constraints applied by the relatively short mercaptomethylene tether.

Are Interaction Distances and Angles Correlated?

While there does appear to be some preference for the angle between the pnictogen-ligand bond and the noncovalent pnictogen•••π interaction to approach a linear orientation (160° to 170° are the most frequently observed angles), comparison between distance/angle pairs is necessary to determine whether there is a relationship between the strength of the interaction and its approach to linearity.

If the orbital overlap model shown in Figure 5.3 is correct, there should be a strong correlation between the pnictogen•••π interaction distance *d* and the interaction angle: as *d* decreases, the angle should approach 180°. In fact, a plot of the distance/angle pairs (Figure 5.5) reveals an essentially random distribution of distances and angles.

The lack of correlation between *d* and θ suggests that the pnictogen•••arene interaction is primarily electrostatic in character, corroborating the studies that indicated that a charge transfer model is insufficient to describe this type of interaction. The slight decrease in *d* as the pnictogen's size is increased is likely due to decreased repulsions between the π system of the arene ring and the lone pair of

electrons on the pnictogen. This is likely the result of increased delocalization of these electrons.[108] The fact that this interaction is primarily electrostatic in character is actually quite useful for the design of supramolecular assemblies, as the interaction's geometric preferences are less likely to dominate the final structure as much as the primary coordination sphere and the structure of the chosen ligands.

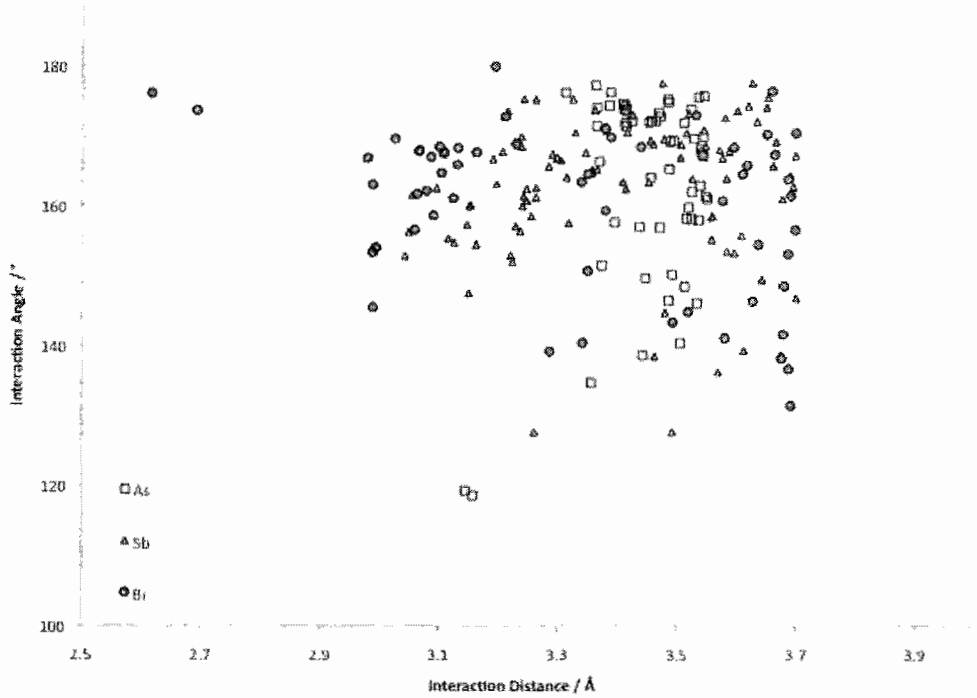

Figure 5.5. Scatter plot of interaction distance/angle pairs. No apparent correlation between the strength of the pnictogen•••π interaction and the interaction angle is observed.

How Does the Pnictogen•••π Interaction Influence Self-Assembly?

A closer look at the similarities and differences between the "adduct" pnictogen•••π structures and supramolecular pnictogen•••π structures provides a great deal of insight into both the likely pathway for self-assembly and how ligand properties may be adjusted to achieve desired structural outcomes.

Effects of Competing π-Stacking Interactions

In systems less constrained than rigid $M_2\mathbf{L}_3$ assemblies, the overall structure of pnictogen-based assemblies depends heavily on the nature of competing arene•••arene interactions, particularly edge-to-face CH•••π interactions. Compare, for example, the two structures shown in Figure 5.6. The first (Figure 5.6(*a*)), a mononuclear $As\mathbf{L}^2_3$ complex in which $H\mathbf{L}^2$ = 2-mercaptomethylnaphthalene, contains one As•••π interaction of moderate strength (3.53 Å). The naphthalene portions of all three ligands are simultaneously engaged in an extended network of edge-to-face arene interactions that appear to be the dominant feature of this structure.

In contrast, the $As_2\mathbf{L}^3_3$ assembly shown in Figure 5.6(*b*) bears the expected six As•••π contacts ($H_2\mathbf{L}^3$ = 2,7-bis(mercaptomethylanthracene)). These contacts vary slightly in magnitude, probably due to interactions between the assembly and cocrystallized benzene molecules (omitted for clarity). They are all, however, at least as strong as that found in the mononuclear naphthalene complex. These

ligands are structurally very similar – it is quite obvious that the bisfunctional ligand's structure is strongly influenced by macrocyclic and macrobicyclic effects.

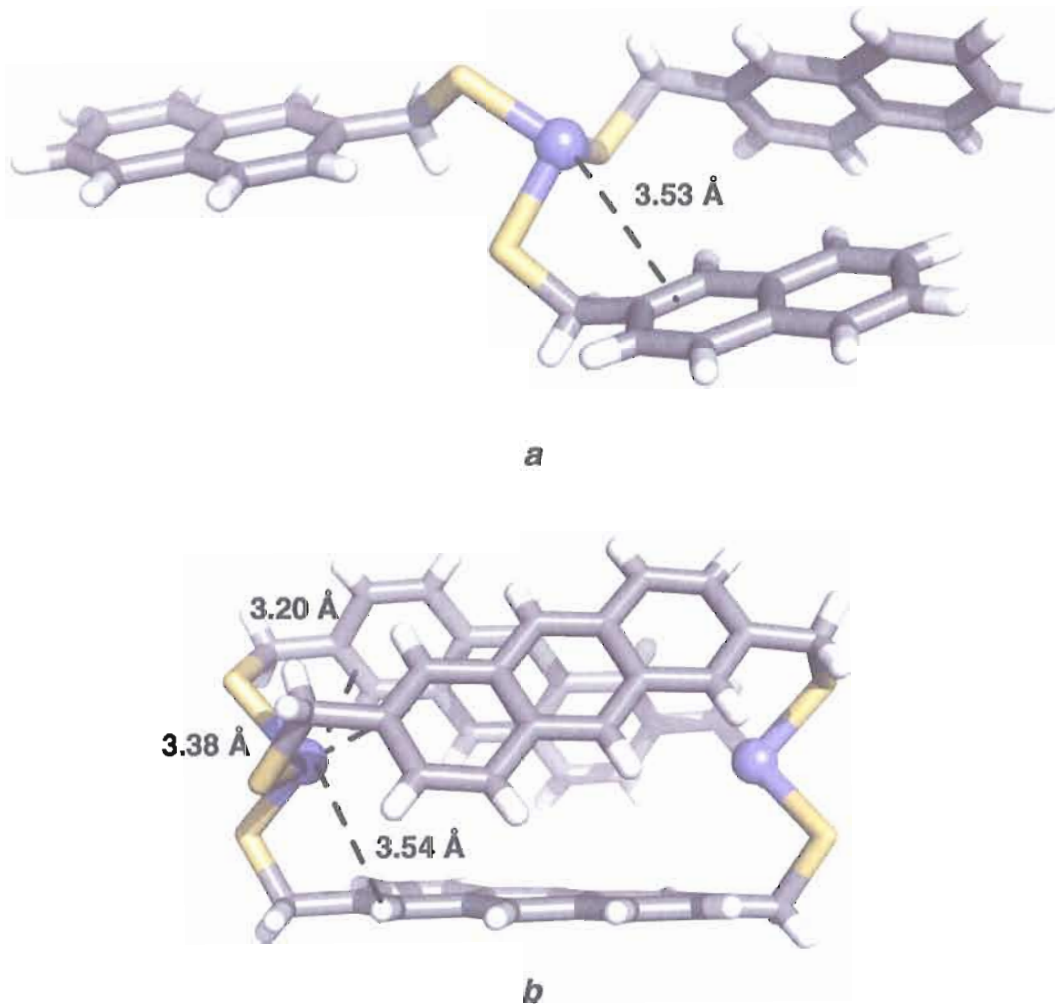

Figure 5.6. Macrocyclic effects and pnictogen•••arene interactions. Edge-to-face aromatic interactions dominate the packing of a mononuclear AsL^2_3 structure shown in (*a*). One As•••π interaction of moderate strength (3.53 Å) is found per assembly. The anthracene spaced $As_2L^3_3$ assembly shown in (*b*) contains six As•••π interactions per assembly (3.20, 3.38, and 3.54 Å); one benzene molecule cocrystallizes with the assembly and has been omitted for clarity.

Macrobicyclic Effects and Steric Strain

The intramolecular nature of the pnictogen•••arene interaction in these structures necessarily induces endohedral directionality in the stereochemically active lone pair found in the pnictogens. Analogous systems bearing nitrogen or C-H groups as a bridgehead are known to isomerize between "in-in," "in-out," and "out-out" isomers,[123] and the stability of any one of these isomers is directly related to the macrocycle's ring size and amount of steric stain on the system. An organic π-prismand bearing nitrogen bridgeheads covalently linked by a *p*-diethylbenzene spacer[124] is most stable in the "in-in" conformation, suggesting that relief of steric strain imposed by the macrobicyclic framework contributes to the exclusive formation of this isomer in our supramolecular systems.

Geometric Consequences of Chelate Ring Size

The restrictions imposed on the geometry of the interaction between the metal center and the neighboring arene ring by the effective size of the chelate ring may compete with the driving force toward forming a given pnictogen•••π interaction. The chelate ring formed by the mercaptomethyl(arene) system is effectively five-membered if the point of interaction between the metal and the arene is included in counting the ring system. The interaction angles observed for these structures are much more bent than would be expected for an As•••π interaction, given the typical angles found in the structural survey. These sharper

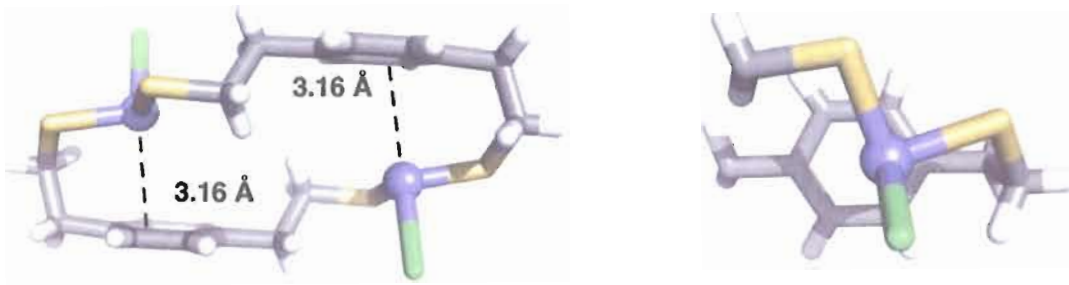

Figure 5.7. Effect of increased "chelate" ring size on an *anti*-$As_2L_2Cl_2$ macrocycle. Use of the ligand 1,4-dimercaptoethylenebenzene ($H_2\mathbf{L}^4$) increases the size of the "chelate" ring created when As(III) center interacts with the arene ring (*a*). An expanded view of one side of this complex (*b*) shows that the added conformational freedom afforded by this spacer allows the metal center to interact with the ring in an η^3 manner rather than η^2 as in the bis(mercaptomethyl) complex $As_2\mathbf{L}^1_3$. The preference of the ethylene spacer groups to minimize gauche interactions also contributes to the placement of the As(III) center over the arene ring.

angles are the result of the geometric constraints inherent in the short mercaptomethylene tether. The addition of one more methylene group to the spacer between the phenylene scaffold and the thiol group increases the effective size of the "chelate" ring, allowing the pnictogen center more freedom to adopt the most favorable interaction geometry (Figure 5.7). The increased length of the alkyl tether in $As_2\mathbf{L}^4{}_2Cl_2$ ($H_2\mathbf{L}^4$ = 1,4-bis(mercaptoethylbenzene)) gives the As(III) center the ability to seek out the most favorable orientation – this appears to be much closer to the "tilted" geometry frequently observed in crystalline adducts and in DFT calculations.[35,108] This "tilted" orientation has the effect of drawing the two As(III)

centers closer together; this proximity may encourage the formation of the *syn* macrocycle, which may prevent the coordination of a third ligand to form $As_2\mathbf{L}^4_3$.

Conclusions

Our $As_2\mathbf{L}_3$ and $As_2\mathbf{L}_2Cl_2$ assemblies showcase the remarkable power of self-assembly reactions and supramolecular chemistry in that geometric preferences and noncovalent interactions can be used to influence final structure types. The pnictogen•••arene interaction has been successfully employed in twofold symmetric dithiolate ligands as rigid and semirigid spacers. In particular, in a mononuclear $As\mathbf{L}_3$ structure, just one As•••π interaction is observed, despite the ready availability of electron-rich naphthalene rings. A similar bisfunctional ligand based on an anthracene spacer readily forms a supramolecular assembly bearing six close As•••π contacts, clearly showing that the steric constraints imposed during the formation of macrobicyclic assemblies contribute to the formation of pnictogen-arene interactions. This once again highlights the dramatic effects of multiple weak interactions working in concert to create sophisticated assemblies from very simple components.

As this design strategy grows in order to generate even larger and more sophisticated structures, the following factors may provide insight to guide this process. First, the choice of pnictogen can influence the overall structure: the interaction distance decreases slightly as the pnictogen size is increased, likely as a

result of increased delocalization of the "lone pair" of electrons and the resultant decreased repulsions between it and the neighboring arene ring. The range of possible interaction distances also increases significantly as the pnictogen increases in size, presenting additional opportunities to fine-tune supramolecular structures.

Second, the nature of the complex itself, influences the potential strength of the interaction. Macrocyclic structures tend to have somewhat stronger interactions when compared with capsules, and increasing the effective size of the chelate ring allows a stronger pnictoge•••arene interaction than does the mercaptomethyl spacer.

Finally, competition with edge-to-face aromatic interactions has an influence on the final structure of the assembly. One weaker pnictogen•••π interaction was observed in a mononuclear As(III) complex based on naphthalene ligands; the other two ligands were involved in an extended network of edge-to-face interactions that dominated the crystal structure. In contrast, the use of an analogous bifunctional ligand led to the formation of the triple helix, showing that a combination of macrocyclic effects and pnictogen•••π interactions can effectively compete with edge-to-face interactions that would otherwise dominate the overall packing of the structure.

Experimental Details

General Information

Starting materials and reagents were obtained from commercial sources and used without further purification unless otherwise noted. NMR spectra were obtained on Varian 300 MHz, 500 MHz, and 600 MHz spectrometers as noted; chemical shifts are reported in parts per million (ppm) downfield from tetramethylsilane and referenced to residual solvent as an internal standard. X-ray diffraction data were collected at 173 K on a Bruker Apex diffractometer using MOKα-radiation (λ=0.71073 Å). Absorption corrections were applied by SADABS. All structures were determined by direct methods and refined on F^2 by a full-matrix least-squares procedure. All non-H atoms were refined with anisotropic thermal parameters. H atoms were refined in calculated positions in a model of a rigid group. All calculations were performed by the Bruker SHELXTL 6.10 package (SHELXTL, version 6.10, Bruker AXS, Inc., Madison, WI, 2000).

Ligand and Complex Syntheses

1,4-bis(mercaptoethyl)benzene (H_2L^4): 1,4-bis(hydroxyethyl)benzene (0.967 g, 5.81 mmol) and thiourea (1.51 g, 19.78 mmol) were suspended in 48% hydrobromic acid (4 mL) and brought to reflux with stirring for 20 hours. The reaction mixture was cooled to room temperature and the reaction apparatus was placed under N_2 atmosphere. NaOH (1.2 g, 30 mmol) in water (3.6 mL) was quickly

added and the system degassed. The mixture was refluxed for 2 hours, cooled to room temperature, and acidified with concentrated HCl. The reaction mixture was extracted with $CHCl_3$ (3 x 10 mL); the pooled extracts were then washed with brine (2 x 10 mL) and dried over $MgSO_4$. Removal of the solvent under reduced pressure yielded a clear oil identified as the product in 77% yield.

Macrocycle $As_2L^4{}_2Cl_2$: H_2L^4 (0.116 g, 0.584 mmol) was dissolved in 10 mL $CHCl_3$ in a scintillation vial; $AsCl_3$ (49.8 uL, 0.584 mmol) was added and the mixture sonicated. Layering of hexanes over the reaction mixture yielded X-ray quality crystals of the desired macrocycle.

Crystal Structures Included in Survey

Table 5.2. Arsenic-containing crystal structures included in structural survey.

BRPHAS	EPSARS	KISWUE	QAFYIF	TAYTIX
CIGNIP10	ESEARS	KIWWOP	RARYIS	VABYAY
COPHAZ	FAPXAS	KUNSIV	SADDOQ	VAMGOF
COPHAZ01	GAHZIY	MUNWUN	SAFWEB	WEPXEU
DAFLOL	GESZAF	OPIMAS	SALCIR	WUFYOL
DAFLUR	HACTOV	PDASOB	TADFAF	XIQBEE
DAXLOD	HAVMEW	PELDUF	TAYSIW	ZALHEZ
DIYDAQ	HIHYOM	PHASOC	TAYSOC	ZAZDUZ
DOGNAO	HIHYUS	PHASOC01	TAYSUI	
DPASTS	IBUHAP	POXARS	TAYTAP	
DPASTS01	JUNPIR	POYROK	TAYTET	

Table 5.3. Antimony-containing crystal structures included in structural survey.

AFATIK	FOWYAR	LUWZIM	PYRABR	VELQUY
BIPHSB10	GEQBUZ	MAXGOI	PYRSBB10	VEMKED
BUMGEV	GOMWAG	MXBXSB10	QAFYEB	VOJTUJ
CECJEZ	HEFCOK	NAPSBC	QIVWUN	WANDAQ
CUDHOY	HIHZIH	NECLIR	QIVWUN01	XAQJEF
CUDHOY01	IREZOU	NEKJUI	SAVDUP	XAVLIP
DALLOR	ISOYAQ	OCEPAN	SAVFAX	XDPANT01
DBDSB01	JEWDEU	PGALSB	SAVFEB	ZAZYOO
DEJYAS	KIXSAL	PHENBS	STISBC	ZOCWUX
DEJYEW	KUJVAM	PITPEN	TADDOR	ZZZBAM10
DPASBC10	KUTXOM	POSWUP	TIDGOC	
FAFLUU	KUTXUS	POSXAW	TUMQOH	
FAGFAU	KUTYAZ	POSXEA	UGIHUN	
FOJKOE	LAFBUQ	PXYLSB	VABYEC	

Table 5.4. Bismuth-containing crystal structures included in structural survey.

ABOLIN	ECOKUC	ISOYEU	QEPXIS	XADQOI
ACUPIY	EYOSEQ	JEJPAP	QOWHIT	XATWOF
APUSOT	FAKMIN	JOLBAN	RADHAF	XATWUL
AVIKUL	FAPYOK	JUMZOG	REYYAV	YEGDUJ
BOBMUA	FAPYOK10	JUMZOG01	SAJSOM	YULYAF
BOZVER01	FAPYUK	KANKUG	TUQRUS	
CECWAJ	FAPYUK10	KAXYUD	VEFPUS	
DAZJAQ	FUNJUT	KISXEP	VUMZAE10	
EBIHED	GOMWEK	LOFZIP	WAMPAB	

CHAPTER VI

CONCLUSIONS AND OUTLOOK FOR FUTURE WORK

Supramolecular Design for Lead(II) and Mercury(II)

Lead(II) has been well established as a significant environmental concern based on the myriad toxic effects on human physiology. From the results obtained in this research and recent reports in the literature, it is clear that the preferred coordination geometry of lead(II) is that of a trigonal pyramid, particularly when sulfur donors are involved. These donors can come in the form of either arylthiolate ligands or cysteine residues of proteins. The fact that this preferred coordination geometry of lead(II) is easily accessible suggests that this is a viable candidate for the design of supramolecular structures. The key to obtaining discrete supramolecular structures rather than coordination oligomers appears to lie in minimizing the occurrence of secondary bridging interactions between the thiolate donors and neighboring lead(II) centers. This can be accomplished in several ways: the presence of a bulky countercation and the presence of sterically demanding ligands around the metal center both prevent additional undesirable secondary interactions. Several new ligand designs have been proposed that provide both a

scaffold of sufficient size to accommodate lead(II), as well as a coordination sphere that blocks secondary interactions to other metal centers.

Extended Supramolecular Assemblies of As(III)

In the process of expanding the established design strategy for As(III) assemblies, several new ligands incorporating flexible linkages and benzylic thiolates have been prepared which incorporate larger, more flexible ligand scaffolds such as diphenylmethane and diphenylethane. The flexibility of these ligand spacers give the resulting $As_2\mathbf{L}_3$ complexes increased conformational mobility in both the solid state and solution; the structure of these assemblies in solution is sensitive to both temperature and solvent. Thermodynamic data obtained from variable temperature NMR spectroscopy indicates the CH•••π interactions that cause flexible ligands to contract at lower temperatures are stronger in smaller solvents, which may be attributable to these solvents' improved ability to solvate the outward directed edges of the arene rings. The fact that these assemblies are more likely to be in the "open" conformation in larger solvents is quite desirable – studying these assemblies in large solvents such as $CDCl_2CDCl_2$ may encourage the formation of host-guest assemblies that have not yet been observed.

A promising avenue for future work in this area lies in the structures that are analogous to the cryptophane family[125] of supramolecular hosts. The $As(SCH_2Ph)_3$ unit has the same approximate dimensions as the cyclotriveratrylene cap that is ubiquitous in the cryptophanes. This research could be taken in several directions:

- Incorporation of other spacer units found in the cryptophane family[126-129] to create larger and more functional capsules
- Metallation of the exterior of the complexes is known to alter the electronic environment of the interior of cryptophanes[125,87,130,131] – this may have implications on host-guest activity or the pnictogen•••π interaction that directs the assembly of the structures
- The influence of the pnictogen lone pair on host-guest activity can be better probed when the $As_2\mathbf{L}_3$ assembly is sufficiently capacious to accommodate a guest molecule

Mechanical Coupling and Design Strategies for Higher-Order As_mL_n Assemblies

Chapter IV illustrated the manner in which mechanical coupling across ligand spacers can influence the final stereochemistry of $As_2\mathbf{L}_3$ assemblies. Ligands that can communicate this information either through their structure or conformation lead to the formation of homoconfigurational assemblies. Most of the higher-order coordination polyhedra in the literature are homoconfigurational, a prime example of this being supramolecular tetrahedral of the $M_4\mathbf{L}_6$ variety. This kind of implies that a design strategy for these higher-order structures based on secondary bonding interactions such as the As-π interaction will require ligands capable of this information transmission, and will probably also require some sort of offset to

prohibit the formation of smaller helicates instead; also appropriate guest encapsulation.

Proposed Design Requirements for Higher Order As_mL_n Assemblies

Taking into consideration the structural effects of pnictogen•••arene interactions and the ligand spacer itself, the following design criteria are proposed in order to provide greater access to higher order assemblies:

- Ligands must have some structural element that encourages coupling of configurations at the As(III) centers
- The ligand and metal should be chosen to maximize the strength of the secondary bonding interaction – homoconfigurational assemblies are observed when closer pnictogen•••arene interactions are present.
- Substituents that encourage or discourage the pnictogen•••arene interaction either through steric or electronic effects could prove useful in fine-tuning structures.
- The chelate donors should be offset if larger-order structures are desired.
- Larger order structures often require guests or templates; ligand spacers must be chosen in order to accommodate both the space requirements of the guest and that of the endohedral lone pair.

Pnictogen•••π Interactions as Supramolecular Design Elements

We have shown that the interaction between the pnictogens and the π electron systems of arene rings are an important component of main group supramolecular assembly design. This interaction mode frequently appears in cocrystals of pnictogen trihalides with arene rings and is ubiquitous in supramolecular stuctures of As(III) prepared from benzylic thiolate ligands. A study

of how this interaction changes with varying pnictogen size and Lewis acidity has shown that this interaction has most likely a strong electrostatic component, with minimal covalent character. The current standard for pnictogen ligand design in our laboratory is the benzylic thiol – increasing the length of the spacer unit has the effect of increasing the "chelate ring" size experienced by the metal center. In the case of 1,4-dimercaptoethylbenzene, this provided additional conformational flexibility to allow the As•••π interaction to reach a more optimal geometry than was previously observed in our structures. This suggests that the Ar-$(CH_2)_2$-SH based ligands will be promising for future assembly design.

APPENDIX

SPREADSHEET FOR THERMODYNAMIC PARAMETERS EXTRACTED FROM VARIABLE TEMPERATURE NMR DATA

The interconversion between the "skew" and "gable" conformations of diphenylmethane drives the forming and breaking on the aryl C-H•••π contact responsible for the upfield shift of H3 at lowered temperature. As previously described in this chapter, the equilibrium constant for this process can be defined in terms of the relative populations of the "closed" and "open" forms of the $As_2\mathbf{L}^2_3$ assembly:

$$K = \frac{P_{\text{open}}}{P_{\text{closed}}}$$

The observed chemical shift of an Ar-H proton involved in edge-to-face π interactions (in this case, H3) is the average chemical shift of the "open" (δ_o) and "closed" (δ_c) shifts weighted with their respective populations. Combined with the mass balance ($P_c + P_o = 1$), the following expression is obtained:

$$\delta_{obs} = \delta_c P_c + \delta_o P_o = \delta_c P_c + \delta_o (1 - P_c)$$

The crystal structure of $As_2\mathbf{L}^2_3$ provides a reasonable initial value for δ_c using Johnson-Bovey ring current tables.[132] The chemical shift of H3 from the free ligand

can be used as the initial estimate for the chemical shift of H3 in $As_2(dpm)_3$ when it is not directed to the interior of the assembly and is therefore free of anisotropic shielding effects. With reasonable initial estimates for $\Delta H°$ and $\Delta S°$, a curve can be fit to the data such that

$$\hat{P}_c = \frac{1}{1 + e^{\frac{-(\Delta H° - T\Delta S°)}{RT}}}$$

and

$$\hat{\delta} = \delta_c \hat{P}_c + \delta_o (1 - \hat{P}_c)$$

These parameters are varied until a suitable curve is obtained and the error is minimized.

Application of Model

The following pages include a template for extraction of thermodynamic parameters of a simple two-state equilibrium model through a nonlinear least-squares curve fitting technique using Microsoft Excel. The primary requirement for determination of thermodynamic parameters with this method is the installation of the Solver add-in package. The example given utilizes 12 data points and 4

parameters ($\Delta H°$, $\Delta S°$, δ_{open}, and δ_{closed}).** The gray-shaded cells are the only locations where user-entered data should be required, although the use of more data points will require that certain parts of the spreadsheet be moved. The basic workflow for using this spreadsheet is as follows:

- Enter raw NMR data from temperature and chemical shifts.
- Enter estimates for the four parameters ($\Delta H°$, $\Delta S°$, δ_{open}, and δ_{closed}).
- In Excel, click "Solver" in the "Tools" menu. Set the target cell to the sum of squared residuals, which in this case is F20, equal to "Min" by changing the cells corresponding to the parameter estimates (E2-E5). Click "Solve."
- If the calculated curve does not fit the data points well or the error estimates are too large, change initial guesses for the parameters and run the Solver again.
- If using a different number of data points, make sure to update n, the t value (from a Student's t table), and the matrix dimensions for matrices **D**, $\mathbf{D^T}$, **E**, and $\mathbf{E^{-1}}$.

Note that since the van't Hoff plot is generated from the parameterized $\Delta H°$ and $\Delta S°$, it is *necessarily* a straight line.

** If the chemical shifts for completely open and completely closed complex are known with reasonable certainty, they need not be included in the parameter set adjusted by the Solver function. If this is the case, the finite difference matrices (culminating in **D**) should only have two columns. Likewise, $\mathbf{D^T}$ should have two rows, and $\mathbf{D^TD}$ and $\mathbf{E^{-1}}$ should be 2 x 2 matrices. The t value chosen should be based on $n - 2$ degrees of freedom instead of $n - 4$.

Basic Data Entry and Output
NMR Curve Fitting - Fast Exchange

	A	B	C	D	E	F
1	**Sample Information**			**Parameter Estimates**		**±**
2	**Compound Name**		**Solvent**	**Δ*H*° (cal/mol)**	2124.72	425.87
3	As2(dpm)3		CD2Cl2	**Δ*S*° (cal/mol K)**	7.47	2.05
4	***n* (data points)**		**R**	**δ_open**	7.10	0.05
5	12		1.987	**δ_closed**	6.82	0.01
6		**Shift**				
7	**Temperature (K)**	**(ppm)**	***P*_hat**	**δ_hat**	**δ-δ_hat**	**(δ-δ_hat)^2**
8	193.15	6.859	0.855	6.859	-6.357E-04	4.041E-07
9	203.15	6.870	0.818	6.870	1.477E-04	2.181E-08
10	213.15	6.881	0.779	6.881	2.061E-04	4.249E-08
11	223.15	6.893	0.737	6.893	1.343E-04	1.802E-08
12	233.15	6.905	0.696	6.905	7.140E-04	5.098E-07
13	243.15	6.917	0.654	6.916	5.934E-04	3.521E-07
14	253.15	6.928	0.614	6.928	7.487E-05	5.606E-09
15	263.15	6.938	0.575	6.939	-3.889E-04	1.512E-07
16	273.15	6.948	0.539	6.949	-1.092E-03	1.193E-06
17	283.15	6.958	0.504	6.959	-1.171E-03	1.372E-06
18	293.15	6.969	0.472	6.968	5.043E-04	2.543E-07
19	303.15	6.977	0.442	6.976	9.394E-04	8.825E-07
20				**Σ[(δ-δ_hat)^2]**		**5.207E-06**
21						
22	*Enter estimates for the four parameters in E2-E5.*					
23	*Use the Solver function to minimize cell F20 by changing cells $E$2:$E$5.*					
24	*The black line below should be similar to the plotted points.*					
25	*If not, change your parameters!*					

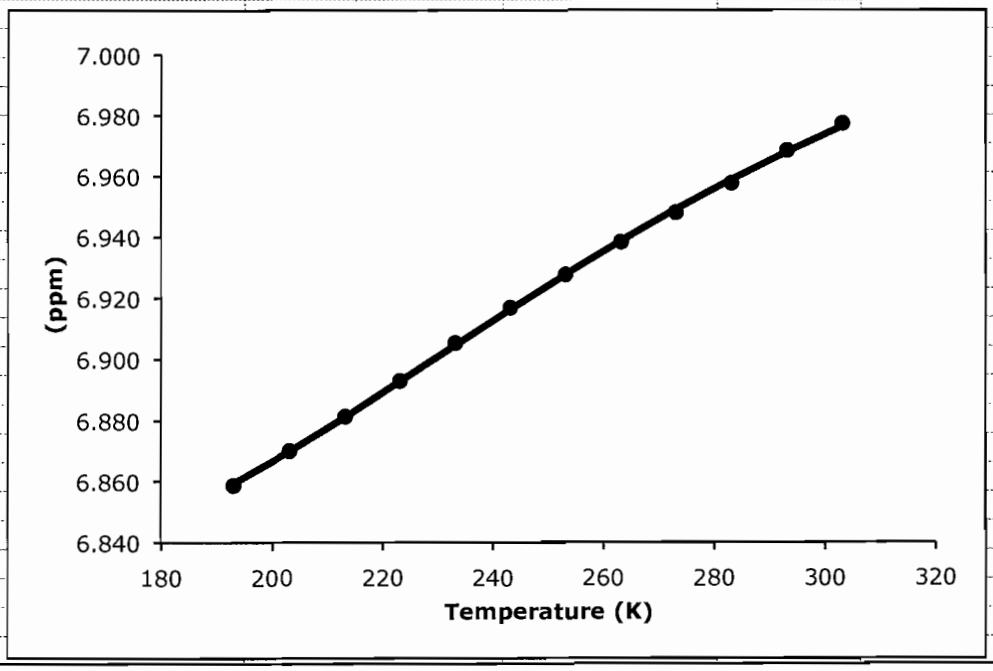

Basic Data Entry and Output
NMR Curve Fitting - Fast Exchange

	G	H	I	J	K	L
1	**P_hat = 1/(exp((-1*$E$2+A8*$E$3)/($F$2*A8))+1)**					
2	**δ_hat = $E$5*C8+$E$4*(1-C8)**					
3						
4						
5	**Error Analysis**			**Parameter Change**		
6	**Parameter Modification**			1.00E-06		
7		**From**				
8		**Solver**	**Modify ΔH°**	**Modify ΔS°**	**Modify δ_o**	**Modify δ_c**
9	**ΔH°**	2.125E+03	2.125E+03	2.125E+03	2.125E+03	2124.724258
10	**ΔS°**	7.470E+00	7.470E+00	7.470E+00	7.470E+00	7.469759
11	**δ_open**	7.102E+00	7.102E+00	7.102E+00	7.102E+00	7.101871
12	**δ_closed**	6.818E+00	6.818E+00	6.818E+00	6.818E+00	6.818313
13						
14						
15	**Modified P_hats**		8.553E-01	8.553E-01	8.553E-01	8.553E-01
16			8.182E-01	8.182E-01	8.182E-01	8.182E-01
17			7.786E-01	7.786E-01	7.786E-01	7.786E-01
18			7.374E-01	7.374E-01	7.374E-01	7.374E-01
19			6.957E-01	6.957E-01	6.957E-01	6.957E-01
20			6.544E-01	6.544E-01	6.544E-01	6.544E-01
21			6.141E-01	6.141E-01	6.141E-01	6.141E-01
22			5.755E-01	5.755E-01	5.755E-01	5.755E-01
23			5.388E-01	5.388E-01	5.388E-01	5.388E-01
24			5.043E-01	5.043E-01	5.043E-01	5.043E-01
25			4.721E-01	4.721E-01	4.721E-01	4.721E-01
26			4.423E-01	4.423E-01	4.423E-01	4.423E-01
27	**Modified δ_hats**		6.859E+00	6.859E+00	6.859E+00	6.859E+00
28			6.870E+00	6.870E+00	6.870E+00	6.870E+00
29			6.881E+00	6.881E+00	6.881E+00	6.881E+00
30			6.893E+00	6.893E+00	6.893E+00	6.893E+00
31			6.905E+00	6.905E+00	6.905E+00	6.905E+00
32			6.916E+00	6.916E+00	6.916E+00	6.916E+00
33			6.928E+00	6.928E+00	6.928E+00	6.928E+00
34			6.939E+00	6.939E+00	6.939E+00	6.939E+00
35			6.949E+00	6.949E+00	6.949E+00	6.949E+00
36			6.959E+00	6.959E+00	6.959E+00	6.959E+00
37			6.968E+00	6.968E+00	6.968E+00	6.968E+00
38			6.976E+00	6.976E+00	6.976E+00	6.976E+00
39						
40						
41						
42						
43						
44						
45						
46						
47						
48						

Basic Data Entry and Output
NMR Curve Fitting - Fast Exchange

	M	N	O	P	Q	R
1	**D Matrix**					
2	-9.144E-05	1.766E-02	1.447E-01	8.553E-01		
3	-1.045E-04	2.123E-02	1.818E-01	8.182E-01		
4	-1.154E-04	2.460E-02	2.214E-01	7.786E-01		
5	-1.238E-04	2.763E-02	2.626E-01	7.374E-01		
6	-1.296E-04	3.021E-02	3.043E-01	6.957E-01		
7	-1.327E-04	3.228E-02	3.456E-01	6.544E-01		
8	-1.336E-04	3.382E-02	3.859E-01	6.141E-01		
9	-1.325E-04	3.486E-02	4.245E-01	5.755E-01		
10	-1.298E-04	3.546E-02	4.612E-01	5.388E-01		
11	-1.260E-04	3.567E-02	4.957E-01	5.043E-01		
12	-1.213E-04	3.557E-02	5.279E-01	4.721E-01		
13	-1.161E-04	3.520E-02	5.577E-01	4.423E-01		
14						
15	**Transpose**					
16	-9.144E-05	-1.045E-04	-1.154E-04	-1.238E-04	-1.296E-04	-1.327E-04
17	1.766E-02	2.123E-02	2.460E-02	2.763E-02	3.021E-02	3.228E-02
18	1.447E-01	1.818E-01	2.214E-01	2.626E-01	3.043E-01	3.456E-01
19	8.553E-01	8.182E-01	7.786E-01	7.374E-01	6.957E-01	6.544E-01
20						
21	**E Matrix (DtD)**					
22	1.787E-07	-4.493E-05	-5.345E-04	-9.223E-04		
23	-4.493E-05	1.148E-02	1.398E-01	2.244E-01		
24	-5.345E-04	1.398E-01	1.761E+00	2.552E+00		
25	-9.223E-04	2.244E-01	2.552E+00	5.135E+00		
26						
27	**E-1 (Inverse)**					
28	1.428E+11	6.837E+08	-1.708E+07	4.252E+06		
29	6.837E+08	3.293E+06	-8.287E+04	2.008E+04		
30	-1.708E+07	-8.287E+04	2.107E+03	-4.937E+02		
31	4.252E+06	2.008E+04	-4.937E+02	1.316E+02		
32						
33						
34	**σ**					
35	0.000807					
36	**σ ΔH**	**σ ΔS**	**σ δ_o**	**σ δ_c**		
37	304.845	1.464	0.037	0.009		
38						
39	***t* Value for Your Number of Measurements (90% Confidence)**					
40	1.397					
41						
42						
43						
44						
45						
46						
47						
48						

Basic Data Entry and Output
NMR Curve Fitting - Fast Exchange

	S	T	U	V	W	X
1						
2						
3						
4						
5						
6						
7						
8						
9						
10						
11						
12						
13						
14						
15						
16	-1.336E-04	-1.325E-04	-1.298E-04	-1.260E-04	-1.213E-04	-1.161E-04
17	3.382E-02	3.486E-02	3.546E-02	3.567E-02	3.557E-02	3.520E-02
18	3.859E-01	4.245E-01	4.612E-01	4.957E-01	5.279E-01	5.577E-01
19	6.141E-01	5.755E-01	5.388E-01	5.043E-01	4.721E-01	4.423E-01
20						
21	**v'ant Hoff Plot**		**R24=(-1*$E$2+A8*$E$3)/($C$5*A8)**			
22			**T53=1/A8**			
23	**ln(K) = (-ΔH+TΔS)/RT**		**1/T**			
24	-1.7768621		0.00517732			
25	-1.5043454		0.00492247			
26	-1.257399		0.00469153			
27	-1.0325855		0.00448129			
28	-0.8270568		0.00428908			
29	-0.6384337		0.00411269			
30	-0.4647126		0.00395023			
31	-0.3041947		0.00380011			
32	-0.1554299		0.00366099			
33	-0.017173		0.0035317			
34	0.11165143		0.00341122			
35	0.23197681		0.0032987			
36						
37						
38						
39						
40						
41						
42						
43						
44						
45						
46						
47						
48						

Basic Data Entry and Output
NMR Curve Fitting - Fast Exchange

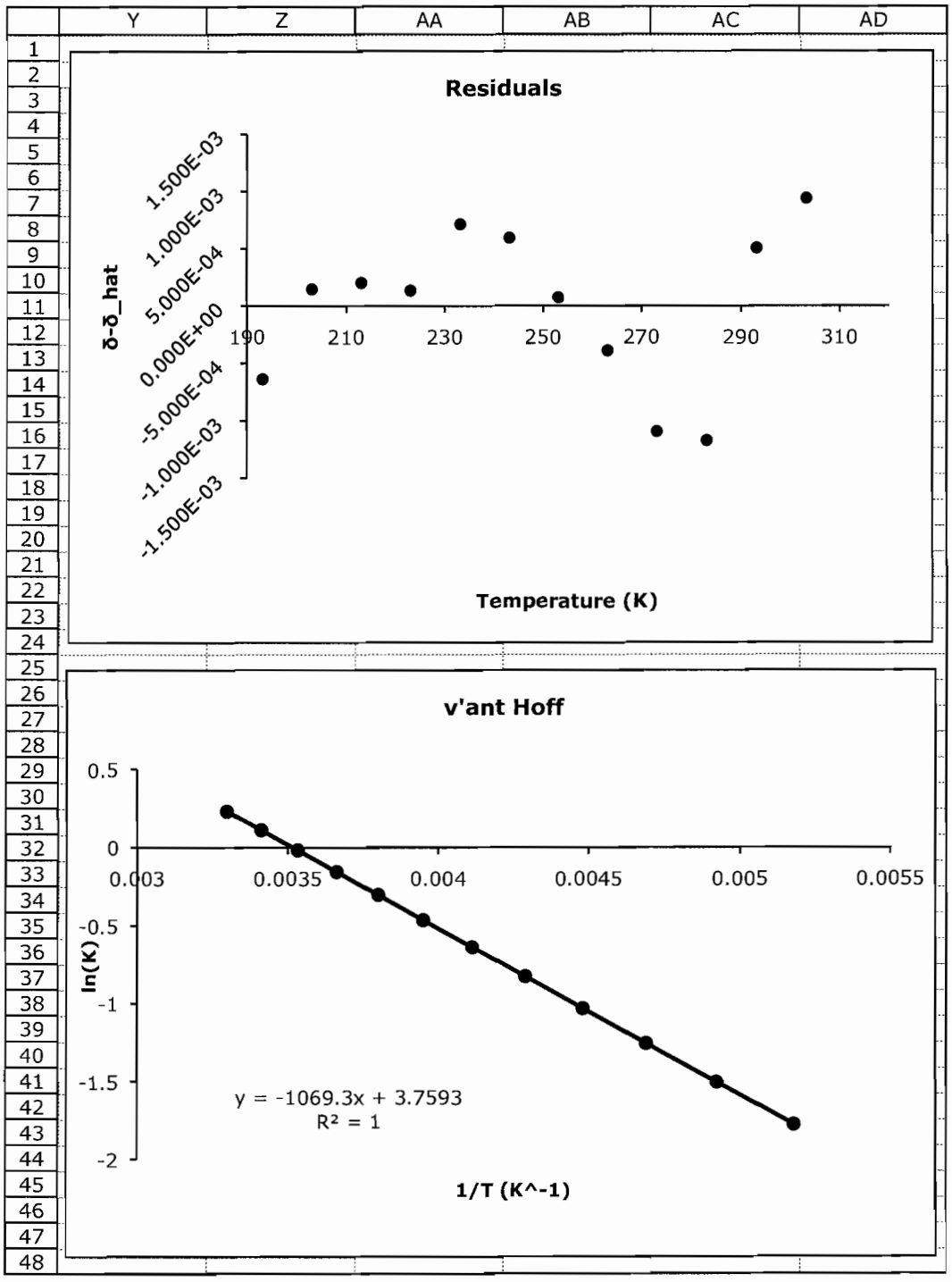

REFERENCES

(1) Pitt, M. A.; Johnson, D. W. "Main-Group Supramolecular Chemistry," *Chemical Society Reviews*, **2007**, *36*, 1441-1453.

(2) Leininger, S.; Olenyuk, B.; Stang, P. J. "Self-Assembly of Discrete Cyclic Nanostructures Mediated by Transition Metals," *Chemical Reviews*, **2000**, *100*, 853-908.

(3) Bouhadir, G.; Bourissou, D. "Unusual Geometries in Main Group Chemistry," *Chemical Society Reviews*, **2004**, *33*, 210-217.

(4) Cowley, A. H. "Some Past Achievements and Future Perspectives in Main Group Chemistry," *Journal of Organometallic Chemistry*, **2004**, *689*, 3866-3872.

(5) Baker, R. J.; Jones, C. ""GaI": A versatile reagent for the synthetic chemist," *Journal of the Chemical Society, Dalton Transactions*, **2005**, 1341-1348.

(6) Healey, E. R.; Vickaryous, W. J.; Berryman, O. B.; Johnson, D. W. In Bottom-Up Nanofabrication: Supramolecules, Self-Assemblies, and Organized Films; Ariga, K., Nalwa, H. S., Eds.; American Scientific Publishers: Stevenson Ranch, 2006.

(7) Jedinski, Z. "Alkali metal supramolecular complexes and their significance in organic chemistry," *Pure and Applied Chemistry*, **1992**, *65*, 483-488.

(8) Gale, P. A. "Supramolecular Chemistry: From Complexes to Complexity," *Philosophical Trnsactions of the Royal Society of London, Series A: Mathematical, Physical and Engineering Sciences*, **2000**, *358*, 431-453.

(9) Gokel, G. W.; Barbour, L. J.; Ferdani, R.; Hu, J. "Lariat ether receptor systems show experimental evidence for alkali metal cation-π interactions," *Accounts of Chemical Research*, **2002**, *35*, 878-886.

(10) Veggel, F. C. J. M. v.; Verboom, W.; Reinhoudt, D. N. "Metallomacrocycles: Supramolecular Chemistry with Hard and Soft Metal Cations in Action," *Chemical Reviews*, **1994**, *92*, 279-299.

(11) Albrecht, M. "From Molecular Diversity to Template-Directed Self-Assembly: New Trends in Metallo-Supramolecular Chemistry," *Journal of Inclusion Phenomena and Macrocyclic Chemistry*, **2000**, *36*, 127-151.

(12) Matzapetakis, M.; Farrer, B. T.; Weng, T.-C.; Hemmingsen, L.; Penner-Hahn, J. E.; Pecoraro, V. L. "Comparison of the Binding of Cadmium(II), Mercury(II), and Arsenic(III) to the de Novo Designed Peptides TRI L12C and TRI L16C," *Journal of the American Chemical Society*, **2002**, *124*, 8042-8054.

(13) Poojary, M. D.; Manohar, H. *Inorganica Chimica Acta*, **1984**, *93*, 153.

(14) Burchell, T. J.; Eisler, D. J.; Puddephatt, R. J. "Self-Assembly Using Dynamic Coordination Chemistry and Hydrogen Bonding: Mercury(II) Macrocycles, Polymers, and Sheets," *Inorganic Chemistry*, **2004**, *43*, 5550-5557.

(15) Henry, M.; Hosseini, M. W. "Molecular Tectonics: Geometry and Energy Based Analysis of Coordination Networks," *New Journal of Chemistry*, **2004**, *28*, 897-906.

(16) Haneline, M. R.; Taylor, R. E.; Gabbaï, F. P. "Trimeric Perfluoro-*o*-phenylene Mercury: A Versatile Lewis Acid Host," *Chemistry - A European Journal*, **2003**, *9*, 5188-5193.

(17) Wedge, T. J.; Hawthorne, M. F. "Multidentate Carborane-Containing Lewis Acids and Their Chemistry: Mercuracarborands," *Coordination Chemistry Reviews*, **2003**, 111-128.

(18) Bharara, M. S.; Parkin, S.; Atwood, D. A. "Mercury(II) 2-Aminoethanethiolate Clusters: Intramolecular Transformations and Mechanisms," *Inorganic Chemistry*, **2006**, *45*, 7261-7268.

(19) Bird, C. M.; Breheny, C.; Davidson, M. G.; Edwards, A. J.; Llewellyn, S. C.; Raithby, P. R.; Snaith, R. "Synthesis and Structure of a 16-Membered $(AlNCO)_4$ Ring," *Angewandte Chemie, International Edition in English*, **1993**, *32*, 1483-1484.

(20) Schalley, C. A.; Lutzen, A.; Albrecht, M. "Approaching supramolecular functionality," *Chemistry - A European Journal*, **2004**, *10*, 1072.

(21) Saalfrank, R. W.; Stark, A.; Peters, K.; Vonschnering, H. G. "Adamantoid Chelate Complexes. 1. The 1st Adamantoid Alkaline-Earth Metal Chelate Complex - Synthesis, Structure, and Reactivity," *Angewandte Chemie, International Edition in English*, **1988**, *27*, 851-853.

(22) Caulder, D. L.; Raymond, K. N. "Supermolecules by Design," *Accounts of Chemical Research*, **1999**, *32*, 975-982.

(23) Davis, A. V.; Fiedler, D.; Seeber, G.; Zahl, A.; Eldik, R. v.; Raymond, K. N. "Guest Exchange Dynamics in an M_4L_6 Tetrahedral Host," *Journal of the American Chemical Society*, **2006**, *128*, 1324.

(24) Janczak, J.; Kubiak, R., *Journal of Alloys and Compounds*, **1992**, *202*, 69.

(25) Kubiak, R.; Janczak, J. "Coordination Geometries Of Metal Ions In Metallophthalocyaninato Complexes," *Crystal Research and Technology*, **2001**, *36*, 1095-1104.

(26) Roesky, H. W.; Haiduc, I.; Hosmane, N. S. "Organometallic Oxides of Main Group and Transition Elements Downsizing Inorganic Solids to Small Molecular Fragments," *Chemical Reviews*, **2003**, *103*, 2579.

(27) Shimoni-Livny, L.; Glusker, J. P.; Bock, C. W. "Lone Pair Functionality in Divalent Lead Compounds," *Inorganic Chemistry*, **1998**, *37*, 1853-1867.

(28) Sun, X.; Johnson, D. W.; Caulder, D. L.; Raymond, K. N.; Wong, E. H. "Rational Design and Assembly of $M_2M'_3L_6$ Supramolecular Clusters with C_{3h} Symmetry by Exploiting Incommensurate Symmetry Numbers," *Journal of the American Chemical Society*, **2001**, *123*, 2752-2763.

(29) Garcia-Zarracino, R.; Höpfl, H. "Self-Assembly of Diorganotin(IV) Oxides (R = Me, *n*-Bu, Ph) and 2,5-Pyridinedicarboxylic Acid to Polymeric and Trinuclear Macrocyclic Hybrids with Porous Solid-State structures: Influence of Substituents and Solvent on the Supramolecular Structure," *Journal of the American Chemical Society*, **2005**, *127*, 3120.

(30) Ruben, M.; Rojo, J.; Romero-Salguero, F. J.; Uppadine, L. H.; Lehn, J.-M. "Grid-type metal ion architectures: Functional Metallosupramolecular Arrays," *Angewandte Chemie, International Edition in English*, **2004**, *43*, 3644-3662.

(31) Thompson, L. K.; Zhao, L.; Xu, Z.; Miller, D. O.; Reiff, W. M. "Self-Assembled Supramolecular M_9 (Mn(II), Fe(III), Zn(II)), M_5 (Fe(III)), and $[M_3]_2$ (Pb(II)) Complexes: Structural, Magnetic, and Mossbauer Properties," *Inorganic Chemistry*, **2003**, *42*, 128-139.

(32) Menger, F. M. "Supramolecular Chemistry and Self-Assembly," *Proceedings of the National Academy of Science*, **2002**, *99*, 4818-4822.

(33) Vickaryous, W. J.; Herges, R.; Johnson, D. W. "Arsenic-π Interactions Stabilize a Self-Assembled As_2L_3 Supramolecular Complex," *Angewandte Chemie, International Edition in English*, **2004**, *43*, 5831-5833.

(34) Vickaryous, W. J.; Healey, E. R.; Berryman, O. B.; Johnson, D. W. "Synthesis And Characterization Of Two Isomeric, Self-Assembled Arsenic-Thiolate Macrocycles," *Inorganic Chemistry*, **2005**, *44*, 9247-52.

(35) Vickaryous, W. J.; Zakharov, L. N.; Johnson, D. W. "Self-assembled antimony-thiolate Sb_2L_3 and $Sb_2L_2Cl_2$ complexes," *Main Group Chemistry*, **2006**, *5*, 51-59.

(36) Matsumoto, K.; Kawaguchi, H.; Kuroya, H.; Kawaguchi, S. *Bulletin of the Chemical Society of Japan*, **1973**, *46*, 2424-2428.

(37) Schmidt, H. *Angewandte Chemie*, **1930**, *43*, 963-970.

(38) Marcovich, D.; Tapscott, R. E. *Journal of the American Chemical Society*, **1980**, *102*, 5712-5717.

(39) Paver, M. A.; Joy, J. S.; Hursthouse, M. B. "A Twenty-Four Membered Mixed-Metal Macrocycle: Synthesis And Structure of *cyclo*-$[(3\text{-Me-}1,2\text{-}C_6H_3O_2)_2SbNa(THF)_2]_6$," *Journal of the Chemical Society, Chemical Communications*, **2002**, 2150-2151.

(40) Cowley, A. H.; Jones, R. A.; Kidd, K. B.; Nunn, C. M.; Westmoreland, D. L. *Journal of Organometallic Chemistry*, **1988**, *341*, C1-C5.

(41) Janik, J. F.; Wells, R. L.; Jr., V. G. Y.; Rheingold, A. L.; Guzei, I. A. *Journal of the American Chemical Society*, **1998**, *120*, 532-537.

(42) Asato, E.; Katsura, K.; Arakaki, T.; Mikuriya, M.; Kotera, T. *Chemical Letters*, **1994**, 2123-2126.

(43) Vaira, M. D.; Mani, F.; Stoppioni, P. *European Journal of Inorganic Chemistry*, **1999**, 833-837.

(44) Landrum, G. A.; Hoffmann, R. "Secondary Bonding Between Chalcogens or Pnictogens and Halogens," *Angewandte Chemie, International Edition in English*, **1998**, *37*, 1887.

(45) Kobayashi, K.; Izawa, H.; Yamaguchi, K.; Horn, E.; Furukawa, N. "Macrocylic Multi-Telluranes with Hypervalent Te-O Apical Linkages," *Journal of the Chemical Society, Chemical Communications*, **2001**, 1428-1429.

(46) Radhakrishnan, U.; Stang, P. J. "Synthesis and Characterization of Cationic Iodonium Macrocycles," *Journal of Organic Chemistry*, **2003**, *68*, 9209-9213.

(47) Godwin, H. A. "The Biological Chemistry of Lead," *Current Opinion in Chemical Biology*, **2001**, *5*, 223-227.

(48) Coolidge, G. In Boston Globe; Globe Newspaper Company: Boston, 2008.

(49) Claudio, E. S.; Godwin, H. A.; Magyar, J. S. "Fundamental Coordination Chemistry, Environmental Chemistry, and Biochemistry of Lead(II)," *Progress in Inorganic Chemistry*, **2003**, *51*, 1-144.

(50) Warren, C. Brush With Death: A Social History of Lead Poisoning; The Johns Hopkins University Press: Baltimore, 2003.

(51) Parkin, G. "Applications Of Tripodal [S-3] And [Se-3] L_2X Donor Ligands To Zinc, Cadmium And Mercury Chemistry: Organometallic And Bioinorganic Perspectives," *New Journal of Chemistry*, **2007**, *31*, 1996-2014.

(52) Parkin, G. "Synthetic Analogues Relevant to the Structure and Function of Zinc Enzymes," *Chemical Reviews*, **2004**, *104*, 699-767.

(53) Gourlaouen, C.; Parisel, O. "Is An Electronic Shield At The Molecular Origin Of Lead Poisoning? A Computational Modeling Experiment," *Angewandte Chemie*, **2007**, *46*, 553-6.

(54) Smirnov, I.; Shafer, R. H. "Lead Is Unusually Effective In Sequence-Specific Folding Of DNA," *Journal of Molecular Biology*, **2000**, *296*, 1-5.

(55) Farkas, V.; Biely, P.; Bauer, S. "Transglycosylic Reactions of Nucleotides of 2-Deoxy-Sugars .I. Biosynthesis of 2-Deoxysucrose," *Biochimica Et Biophysica Acta*, **1968**, *165*, 63-&.

(56) Farkas, W. R.; Welch, J. W.; Hewins, S. "Effects of Plumbous Ion on Some Functions of Transfer-Rna," *Chemico-Biological Interactions*, **1972**, *5*, 191-&.

(57) Caulder, D. L.; Raymond, K. N. "The Rational Design of High Symmetry Coordination Clusters," *Journal of the Chemical Society, Dalton Transactions*, **1999**, 1185-1200.

(58) Steed, J. W.; Atwood, J. L. Supramolecular Chemistry; Wiley, 2000.

(59) Carter, T. G.; Healy, E. R.; Pitt, M. A.; Johnson, D. W. "Secondary Bonding Interactions Observed in Two Arsenic-Thiolate Complexes," *Inorganic Chemistry*, **2005**, *44*, 9634-9636.

(60) Pitzer, K. S. "Relativistic Effects on Chemical Properties," *Accounts of Chemical Research*, **1979**, *12*, 271-276.

(61) McKelvey, D. R. "Relativistic Effects on Chemical Properties," *Journal of Chemical Education*, **1983**, *60*, 112-116.

(62) Banna, M. S. "Relativistic Effects at the Freshman Level," *Journal of Chemical Education*, **1985**, *62*, 197-198.

(63) Abu-Dari, K.; Hahn, F. E.; Raymond, K. N. "Lead Sequestering Agents. 1. Synthesis, Physical Properties, and Structures of Lead Thiohydroxamato Complexes," *Journal of the American Chemical Society*, **1990**, *112*, 1519-1524.

(64) Abu-Dari, K.; Karpishin, T. B.; Raymond, K. N. "Lead Sequestering Agents. 2. Synthesis of Mono- and Bis(hydroxypyridinethione) Ligands and Their Lead Complexes. Structure of Bis(6-(diethylcabamoyl)-1-hydroxy-2(1H)-pyridine-2-thionato-(O,S)lead(II)," *Inorganic Chemistry*, **1993**, *32*, 3052-3055.

(65) Lewis, J. A.; Cohen, S. M. "Addressing Lead Toxicity: Complexation of Lead(II) with Thiopyrone and Hydroxypyridinethione O,S Mixed Chelators," *Inorganic Chemistry*, **2004**, *43*, 6534-6536.

(66) Magyar, J. S.; Weng, T.-C.; Stern, C. M.; Dye, D. F.; Rous, B. W.; Payne, J. C.; Bridgewater, B. M.; Mijovilovich, A.; Parkin, G.; Zaleski, J. M.; Penner-Hahn, J. E.; Godwin, H. A. "Reexamination of Lead(II) Coordination Preferences in Sulfur-Rich Sites: Implications for a Critical Mechanism of Lead Poisoning," *Journal of the American Chemical Society*, **2005**, *127*, 9495-9505.

(67) Christou, G.; Folting, K.; Huffman, J. C. "Mononuclear, Three-Coordinate Metal Thiolates: Preparation and Crystal Structures of $[NBu_4][Hg(SPh)_3]$ and $[NPr_4][Pb(SPh_3]$," *Polyhedron*, **1984**, *3*, 1247-1253.

(68) Krebs, B.; Brommelhaus, A.; Kersting, B.; Nienhaus, M. "Novel Main Group Thiolates as Possible Sulfide Precursors in CVD - Preparation, Structures, and Properties of $Tl(SC_6H_{11})$ and $Pb(SC_6H_4\text{-}P\text{-}CH_3)_2$," *European Journal of Solid State and Inorganic Chemistry*, **1992**, *29*, 167-180.

(69) Hitchcock, P. B.; Lappert, M. F.; Samways, B. J.; Weinberg, E. L. "Metal (Li, Ge-II, Ge-III, Sn-II, and Pb-II) 2,6-Dialkylbenzenethiolates - X-Ray Crystal-Structures of $Sn(SAr)_2$ (Ar = C_6H_2-*t*Bu_3-2,4,6) and $[M(SAr')_2]_3$ (M = Sn or Pb, Ar' = C_6H_3-*i*-Pr_2-2,6)," *Journal of the Chemical Society, Chemical Communications*, **1983**, 1492-1494.

(70) Eichhofer, A.; Buth, G. "Synthesis and Structure of the Group 12 Pyrimidinethiolate Complexes (3) (infinity)[$Zn(S\text{-}2\text{-}N_2C_4H_3)(2)$], (2)(infinity)[$Cd(S\text{-}2\text{-}N_2C_4H_3)(2)$], [$Hg(S\text{-}2\text{-}N_2C_4H_3)(2)$] and [$Cd(S\text{-}2\text{-}N_2C_4H_3)(2)(tmeda)$]," *European Journal of Inorganic Chemistry*, **2005**, 4160-4167.

(71) Fleischer, H.; Heller, C.; Schollmeyer, D. "Poly[bis-(mu-pentafluorobenzenethiolato)lead(II)]," *Acta Crystallographica Section E-Structure Reports Online*, **2006**, *62*, M1365-M1367.

(72) Edelmann, F. T.; Buijink, J. K. F.; Brooker, S. A.; Herbst-Irmer, R.; Kilimann, U.; Bohnen, F. M. "Formation And Structure Of The Oxygen-Centered Lead Thiolate Cluster $Pb_5O(SRF)_8 \bullet 2C_7H_8$ [R-F=2,4,6-tris(trifluoromethyl)phenyl]," *Inorganic Chemistry*, **2000**, *39*, 6134.

(73) Pitt, M. A.; Zakharov, L. N.; Vanka, K.; Thompson, W.; Laird, B.; Johnson, D. W. "Multiple Weak Supramolecular Interactions Stabilize a Surprisingly Twisted $As_2\mathbf{L}_3$ Assembly," *Chemical Communications*, **2008**, 3936-3938.

(74) Hof, F.; Nuckolls, C.; Rebek Jr., J.; Craig, S. L. "Molecular Encapsulation," *Angewandte Chemie, International Edition in English*, **2002**, *41*, 1488-1508.

(75) Davis, A. V.; Yeh, R. M.; Raymond, K. N. "Supramolecular Assembly Dynamics," *Proceedings of the National Academy of Sciences, USA*, **2002**, *99*, 4793-4796.

(76) Pluth, M. D.; Raymond, K. N. "Reversible Guest Exchange Mechanisms in Supramolecular Host-Guest Assemblies," *Chemical Society Reviews*, **2007**, *36*, 161-71.

(77) Babíc, D.; Rabii, S.; Bernholc, J. "Structural and Electronic Properties of Arsenic Chalcogenide Molecules," *Physical Review B: Condensed Matter*, **1989**, *39*, 10831.

(78) Cangelosi, V. M.; Zakharov, L. N.; Fontenot, S. T.; Pitt, M. A.; Johnson, D. W. "Host–Guest Interactions in a Series of Self-Assembled $As_2\mathbf{L}_2Cl_2$ Macrocycles," *Journal of the Chemical Society, Dalton Transactions*, **2008**, 3447.

(79) Martínez, A. G.; Barcina, J. O. In Encyclopedia of Supramolecular Chemistry; Atwood, J., Steed, J. W., Eds.; CRC Press: 2004.

(80) Dong, G.; Ke-liang, P.; Chun-ying, D.; Cheng, H.; Qing-jon, M. "Design and Crystal Structures of Triple Helicates with Crystallographic Idealized D_3 Symmetry: The Role of Side Chain Effect on Crystal Packing," *Inorganic Chemistry*, **2002**, *41*, 5978-5985.

(81) Cram, D. J.; Steinberg, H. "Macro Rings. I. Preparation and Spectra of the Paracyclophanes," *Journal of the American Chemical Society*, **1951**, *73*, 5691-5704.

(82) Steinberg, H.; Cram, D. J. "Macro Rings. II. Polynuclear Paracyclophanes," *Journal of the American Chemical Society*, **1952**, *74*, 5388-5391.

(83) Albrecht, M.; Fröhlich, R. "Symmetry Driven Self-Assembly of Metallo-Supramolecular Architectures," *Bulletin of the Chemical Society of Japan*, **2007**, *80*, 797-808.

(84) Schaefer, T.; Niemczura, W.; Danchura, W.; Wildman, T. A. "Derivatives of Diphenylmethane. Preferred Conformations and Barriers to Internal Rotation by the J Method.," *Canadian Journal of Chemistry*, **1979**, *57*, 1881.

(85) Straßner, T. "Diphenylmethane and Diphenyl Ether - Experimental Conformations and Torsional Surfaces Calculated with AM1, MNDO, PM3, and Density Functional Theory (Becke3LYP)," *Canadian Journal of Chemistry*, **1997**, *75*, 1011-1022.

(86) Meyer, E. A.; Castellano, R. K.; Diederich, F. "Interactions With Aromatic Rings In Chemical And Biological Recognition," *Angewandte Chemie, International Edition in English*, **2003**, *42*, 1210-50.

(87) Mough, S. T.; Goeltz, J. C.; Holman, K. T. "Isolation and Structure of an "Imploded" Cryptophane," *Angewandte Chemie, International Edition in English*, **2004**, *43*, 5631-5.

(88) Frisch, M. J.; Trucks, G. W.; Schlegel, H. B.; Scuseria, G. E.; Robb, M. A.; Cheeseman, J. R.; J. A. Montgomery, J.; Vreven, T.; Kudin, K. N.; Burant, J. C.; Millam, J. M.; Iyengar, S. S.; Tomasi, J.; Barone, V.; Mennucci, B.; Cossi, M.; Scalmani, G.; Rega, N.; Petersson, G. A.; Nakatsuji, H.; Hada, M.; Ehara, M.; Toyota, K.; Fukuda, R.; Hasegawa, J.; Ishida, M.; Nakajima, T.; Honda, Y.; Kitao, O.; Nakai, H.; Klene, M.; Li, X.; Knox, J. E.; Hratchian, H. P.; Cross, J. B.; Bakken, V.; Adamo, C.; Jaramillo, J.; Gomperts, R.; Stratmann, R. E.; Yazyev, O.; Austin, A. J.; Cammi, R.; Pomelli, C.; Ochterski, J. W.; Ayala, P. Y.; Morokuma, K.; Voth, G. A.; Salvador, P.; Dannenberg, J. J.; Zakrzewski, V. G.; Dapprich, S.; Daniels, A. D.; Strain, M. C.; Farkas, O.; Malick, D. K.; Rabuck, A. D.; Raghavachari, K.; Foresman, J. B.; Ortiz, J. V.; Cui, Q.; Baboul, A. G.; Clifford, S.; Cioslowski, J.; Stefanov, B. B.; Liu, G.; Liashenko, A.; Piskorz, P.; Komaromi, I.; Martin, R. L.; Fox, D. J.; Keith, T.; Al-Laham, M. A.; Peng, C. Y.; Nanayakkara, A.; Challacombe, M.; Gill, P. M. W.; Johnson, B.; Chen, W.; Wong, M. W.; Gonzalez, C.; Pople, J. A.; Gaussian, Inc.: Wallingford, CT, 2004.

(89) Jennings, W. B.; Farrell, B. M.; Malone, J. F. "Attractive Intramolecular Edge-to-Face Aromatic Interactions in Flexible Organic Molecules," *Accounts of Chemical Research*, **2001**, *34*, 885-894.

(90) Hamor, T. A.; Jennings, W. B.; Proctor, L. D.; Tolley, M. S.; Boyd, D. R.; Mullan, T. "Imines and Derivatives. Part 23. Anomalous ^{1}H NMR Spectrum of N-[1-(1-Naphthyl)-ethylidene]-1-phenyl-2-propylamine: Conformation in Solution, Atropisomerism and an X-Ray Crystal Structure.," *Journal of the Chemical Society, Perkin Transactions 2.*, **1990**, 25-30.

(91) Slawin, A. M. Z.; Spencer, N.; Stoddart, J. F.; Williams, D. J. "The Dependence of the Solid-State Structures of Bisparaphenylene-(3n+4)-Crown-n Ethers Upon Macrocyclic Ring Size," *Journal of the Chemical Society, Chemical Communications*, **1987**, 1070-1072.

(92) Paliwal, S.; Geib, S.; Wilcox, C. S. "Chemistry of Synthetic Receptors and Functional-Group Arrays. 24. Molecular Torsion Balance for Weak Molecular Recognition Forces - Effects of Tilted-T Edge-to-Face Aromatic Interactions on Conformational Selection and Solid-State Structure.," *Journal of the American Chemical Society*, **1994**, *116*, 4497-4498.

(93) Hosseini, M. W. "Molecular Tectonics: From Simple Tectons to Complex Molecular Networks," *Accounts of Chemical Research*, **2005**, *38*, 313-323.

(94) Tranchemontagne, D. J. L.; Ni, Z.; O'Keeffe, M.; Yaghi, O. M. "Reticular chemistry of metal-organic polyhedra," *Angewandte Chemie, International Edition in English*, **2008**, *47*, 5136-5147.

(95) Wang, Z.; Cohen, S. M. "Tandem Modification of Metal–Organic Frameworks by a Postsynthetic
Approach," *Angewandte Chemie, International Edition in English*, **2008**, *47*, 4699-4702.

(96) Hutin, M.; Schultz, D.; Nitschke, J. R. "From Simplicity To Complexity Via Subcomponent Self-Assembly," *Chimia*, **2008**, *62*, 198-203.

(97) Sarma, R. J.; Nitschke, J. R. "Self-Assembly In Systems Of Subcomponents: Simple Rules, Subtle Consequences," *Angewandte Chemie, International Edition in English*, **2008**, *47*, 377-380.

(98) Fiedler, D.; Leung, D. H.; Bergman, R. G.; Raymond, K. N. "Selective Molecular Recognition, C-H Bond Activation, and Catalysis in Nanoscale Reaction Vessels," *Accounts of Chemical Research*, **2005**, *38*, 351-360.

(99) Albrecht, M. "Supramolecular Templating in the Formation of Helicates," *Topics in Current Chemistry*, **2004**, *248*, 105-139.

(100) Holliday, B. J.; Mirkin, C. A. "Strategies For The Construction Of Supramolecular Compounds Through Coordination Chemistry," *Angewandte Chemie, International Edition*, **2001**, *40*, 2002-2043.

(101) Gianneschi, N. C.; Masar, M. S.; Mirkin, C. A. "Development Of A Coordination Chemistry-Based Approach For Functional Supramolecular Structures," *Accounts of Chemical Research*, **2005**, *38*, 825-837.

(102) Schier, A.; Wallis, J. M.; Müller, G.; Schmidbaur, H. "$[C_6H_3(CH_3)_3][BiCl_3]$ and $[C_6(CH_3)_6][BiCl_3]_2$, Arene Complexes of Bismuth with Half-Sandwich and Inverted Sandwich Structures," *Angewandte Chemie, International Edition in English*, **1986**, *25*, 757-759.

(103) Schmidbaur, H.; Bublak, W.; Huber, B.; Müller, G. "Arene Adducts with Weak Interactions – Hexaethylbenzene-Bis(tribromoarsane)," *Angewandte Chemie*, **1987**, *99*, 248.

(104) Schmidbaur, H.; Nowak, R.; Huber, B.; Müller, G. "Hexaethylbenzene Trichloroantimony - a Menshutkin Complex with a Centroid Antimony Arene Coordination," *Organometallics*, **1987**, *6*, 2266-2267.

(105) Schmidbaur, H.; Nowak, R.; Schier, A.; Wallis, J. M.; Huber, B.; Müller, G. "Arene Complexes with an Inverse Sandwich Structure - the 1-2 Complexes of Hexamethylbenzene with $SbCl_3$, $SbBr_3$, $BiCl_3$, and $BiBr_3$," *Chemische Berichte-Recueil*, **1987**, *120*, 1829-1835.

(106) Schmidbaur, H.; Wallis, J. M.; Nowak, R.; Huber, B.; Müller, G. "Arene Complexes with Half-Sandwich Structure - the 1-1 Complexes of Mesitylene with $SbCl_3$, $SbBr_3$, $BiCl_3$, and $BiBr_3$," *Chemische Berichte-Recueil*, **1987**, *120*, 1837-1843.

(107) Schmidbaur, H.; Nowak, R.; Steigelmann, O.; Müller, G. "π-Complexes of p-Block Elements – Planar Dihydroanthracene in a Menshutkin Complex – Crystal Structure of $Br_3Sb{\bullet}C_6H_4(CH_2)_2C_6H_4{\bullet}SbBr_3$," *Chemische Berichte*, **1990**, *123*, 1221.

(108) Schmidbaur, H.; Schier, A. "π-Complexation of Post-Transition Metals by Neutral Aromatic Hydrocarbons" *Organometallics*, **2008**, *27*, 2361-2395.

(109) Cangelosi, V. M.; Zakharov, L. N.; Fontenot, S. T.; Pitt, M. A.; Johnson, D. W. "Host–Guest Interactions in a Series of Self-Assembled $As_2\mathbf{L}_2Cl_2$ Macrocycles," *Dalton Transactions*, **2008**, 3447.

(110) Schmidbaur, H.; Probst, T.; Huber, B.; Steigelmann, O.; Müller, G. "Arene Complexes of P-Block Elements - $[(\eta^6\text{-}C_6H_6)_2SnCl(AlCl_4)]_2$ - the 1st Bis(Arene) Coordination Compound of a Group-14 Element," *Organometallics*, **1989**, *8*, 1567-1569.

(111) Piguet, C.; Bernardinelli, G.; Hopfgartner, G. "Helicates As Versatile Supramolecular Complexes," *Chemical Reviews*, **1997**, *97*, 2005-2062.

(112) Hembury, G. A.; Borovkov, V. V.; Inoue, Y. "Chirality-Sensing Supramolecular Systems," *Chemical Reviews*, **2008**, *108*, 1-73.

(113) Albrecht, M. "How Do They Know? Influencing The Relative Stereochemistry Of The Complex Units Of Dinuclear Triple-Stranded Helicate-Type Complexes," *Chemistry - A European Journal*, **2000**, *6*, 3485-3489.

(114) Caulder, D. L.; Powers, R. E.; Parac, T. N.; Raymond, K. N. "The Self-Assembly Of A Predesigned Tetrahedral M_4L_6 Supramolecular Cluster," *Angewandte Chemie, International Edition in English*, **1998**, *37*, 1840-1843.

(115) Yeh, R. M.; Xu, J.; Seeber, G.; Raymond, K. N. "Large M_4L_4 (M = Al(III), Ga(III), In(III), Ti(IV)) Tetrahedral Coordination Cages: An Extension Of Symmetry-Based Design," *Inorganic Chemistry*, **2005**, *44*, 6228-39.

(116) Meyer, M.; Kersting, B.; Powers, R. E.; Raymond, K. N. "Coordination Incommensurate Cluster Formation .4. Rearrangement Reactions In Dinuclear Triple Helicates," *Inorganic Chemistry*, **1997**, *36*, 5179-5191.

(117) Xu, J.; Parac, T. N.; Raymond, K. N. "*meso* Myths: What Drives Assembly of Helical versus *meso* Supramolecular Assemblies" *Angewandte Chemie*, **1999**, *38*, 2878-2882.

(118) Lehn, J.-M. "Supramolecular Chemistry - Scope and Perspectives," *Angewandte Chemie, International Edition in English*, **1988**, *27*, 89-112.

(119) Bünzli, J.-C. G.; Piguet, C. "Lanthanide-Containing Molecular and Supramolecular Polymetallic Functional Assemblies," *Chemical Reviews*, **2002**, *102*, 1897-1928.

(120) Turner, D. R.; Pastor, A.; Alajarin, M.; Steed, J. W. In Structure and Bonding; Springer Berlin: Heidelberg, 2004; Vol. 108, p 97-168.

(121) Kroon, J.; Kanters, J. A. *Nature*, **1974**, *248*, 667-669.

(122) Steiner, T. "The Hydrogen Bond in the Solid State," *Angewandte Chemie, International Edition in English*, **2002**, *41*, 48-76.

(123) Alder, R. W.; East, S. P. "In/Out Isomerism.," *Chemical Reviews*, **1996**, *96*, 2097-2111.

(124) Kunze, A.; Bethke, S.; Gleiter, R.; Rominger, F. *Organic Letters*, **2000**, *2*, 609.

(125) Holman, K. T. In Encyclopedia of Supramolecular Chemisty; Atwood, J., Steed, J. W., Eds. 2004.

(126) Canceill, J.; Cesario, M.; Collet, A.; Guilhem, J.; Riche, C.; Pascard, C. "Selective Recognition of Neutral Molecules - ^{1}H-NMR Study of the Complexation of CH_2Cl_2 and CH_2Br_2 by Cryptophane-D in Solution and Crystal-Structure of Its CH_2Cl_2 Cavitate," *Journal of the Chemical Society, Chemical Communications*, **1986**, 339-341.

(127) Canceill, J.; Lacombe, L.; Collet, A. "New Cryptophane Forming Unusually Stable Inclusion Complexes with Neutral Guests in a Lipophilic Solvent," *Journal of the American Chemical Society*, **1986**, *108*, 4230-4232.

(128) Canceill, J.; Lacombe, L.; Collet, A. "Water-Soluble Cryptophane Binding Lipophilic Guests in Aqueous-Solution," *Journal of the Chemical Society, Chemical Communications*, **1987**, 219-221.

(129) Canceill, J.; Cesario, M.; Collet, A.; Guilhem, J.; Lacombe, L.; Lozach, B.; Pascard, C. "Structure and Properties of the Cryptophane-E $CHCl_3$ Complex, a Stable Van der waals Molecule," *Angewandte Chemie, International Edition in English*, **1989**, *28*, 1246-1248.

(130) Fairchild, R. M.; Holman, K. T. "Selective anion encapsulation by a metalated cryptophane with a π-acidic interior," *Journal of the American Chemical Society*, **2005**, *127*, 16364-16365.

(131) Fairchild, R. M.; Holman, K. T. "Facile, Near-Quantitative, Aqueous Routes To Nearly Any [Cp*Ru(η^6-Arene)]Cl Compound," *Organometallics*, **2007**, *26*, 3049-3053.

(132) Johnson Jr, C. E.; Bovey, F. A. "Calculation of Nuclear Magnetic Resonance Spectra of Aromatic Hydrocarbons," *The Journal of Chemical Physics*, **1958**, *29*, 1012-1014.